

Summer 2019

DOWNHOLE RF COMMUNICATION: CHARACTERIZATION AND MODELING OF WAVEGUIDE PROPAGATION IN A FLUID-FILLED DRILL PIPE

Patrick Cote

Follow this and additional works at: https://digitalcommons.mtech.edu/grad_rsch

 Part of the [Electrical and Computer Engineering Commons](#)

DOWNHOLE RF COMMUNICATION:
CHARACTERIZATION AND MODELING OF WAVEGUIDE
PROPAGATION IN A FLUID-FILLED DRILL PIPE

by
Patrick Cote

A thesis submitted in partial fulfillment of the
requirements for the degree of

Masters of Science Electrical Engineering

Montana Technological University

2019



Abstract

Current technologies for downhole communication in oil and gas drilling applications are severely limited in data rate and latency. This work proposes that a system based upon guided wave propagation could be designed to utilize a wireless, radio frequency (RF) signal to yield tens of megabits per second of data transfer. To determine the feasibility of the proposed system, a test setup was built to measure attenuation of RF signals transmitted through a pipe filled with various drilling fluids. A finite element analysis model was also built to further investigate waveguide propagation of electromagnetic signals in a fluid filled pipe. The measurement setup was validated using fluids of known dielectric properties. A number of a drilling base fluids and oil-based fluids were measured and their dielectric properties calculated. The feasibility of the proposed communication system is not promising for liquid based fluids. However, there is significant potential in an air-based system.

Keywords: Wireless communication, drilling telemetry, RF propagation modeling, Ansys HFSS, dielectric properties, loss tangent, drilling fluid permittivity

Dedication

This work is dedicated to anyone going back to school later in life.

Acknowledgements

I would like to thank my advisor Dr. Kevin Negus for all of his help and insight as well as providing the funding to allow me to work on this project. I would also like to thank Dr. Lee Richards and the entire Petroleum Engineering department for helping me with all of my oil and gas related questions. The Petroleum department also helped with purchasing supplies and allowed me to work in their brand new lab. I want to thank Dr. Bryce Hill not only for his advice on this project, but also for bringing me on to the pit boat project during my undergraduate studies. I also want to thank the entire Electrical Engineering department for their support and encouragement during my time at Montana Tech. Finally, I would like to thank Dr. Dan Trudnowski, who somehow convinced me it would only take six months to complete my master's degree.

Table of Contents

ABSTRACT	II
DEDICATION	III
ACKNOWLEDGEMENTS	IV
LIST OF TABLES.....	VIII
LIST OF FIGURES.....	IX
LIST OF EQUATIONS	XIII
GLOSSARY OF ACRONYMS.....	XVII
1. INTRODUCTION	1
2. LITERATURE REVIEW.....	4
3. DRILLING BACKGROUND.....	7
3.1. <i>Drilling Basics</i>	7
3.2. <i>Downhole Communication Applications</i>	9
3.3. <i>Communication Technologies</i>	11
4. ELECTRICAL BACKGROUND.....	16
4.1. <i>Waveguides</i>	16
4.2. <i>Permittivity and Dielectric Losses</i>	31
4.3. <i>Scattering Parameters</i>	36
5. EXPERIMENTAL SETUP AND MODEL DESIGN.....	39
5.1. <i>Measurement Setup Design</i>	39
5.2. <i>Safety Precautions</i>	47
5.3. <i>Network Analyzer</i>	48
5.4. <i>Finite Element Analysis Simulation</i>	54
5.4.1. <i>Simple Pipe Model</i>	55

5.4.2.	Detailed Model.....	57
6.	MEASUREMENTS AND SIMULATIONS	62
6.1.	<i>Air-filled Pipe</i>	62
6.1.1.	Pipe Characterization	62
6.1.2.	Simulations.....	71
6.2.	<i>Water Based Fluids</i>	75
6.2.1.	Distilled Water.....	75
6.2.2.	Salt Water 5% by Weight.....	81
6.3.	<i>Oil-Based Fluids</i>	85
6.3.1.	Pure Diesel	86
6.3.2.	OBF Mixing Procedure.....	90
6.3.3.	90:10 OBF	92
6.3.4.	80:20 OBF	95
6.3.5.	70:30 OBF	98
6.3.6.	90:10 OBF – Distilled Water	100
6.3.1.	Mineral Oil.....	103
6.3.2.	Escaid™ 110.....	106
7.	CONCLUSIONS.....	108
8.	FUTURE WORK.....	111
	REFERENCES	112
	APPENDIX A: KIRKBY 3.5MM CAL KIT STANDARDS COEFFICIENTS.....	119
	APPENDIX B: PIPE CONDUCTIVITY MEASUREMENTS.....	120
	APPENDIX C: AIR S-PARAMETER PLOTS.....	121
	APPENDIX D: WATER S-PARAMETER PLOTS	126
	APPENDIX E: DIESEL S-PARAMETER PLOTS.....	129
	APPENDIX F: OBF S-PARAMETER PLOTS	132
	APPENDIX G: MINERAL OIL S-PARAMETER PLOTS	140
	APPENDIX H: ESCAID™ 110 S-PARAMETER PLOTS	143

APPENDIX I: MATLAB SCRIPTS 144

List of Tables

Table I: n^{th} zeros of the derivative of the m^{th} -order Bessel Functions	23
Table II: n^{th} zeros of m^{th} -order Bessel Functions.....	24
Table III: Dielectric Constants and Loss Tangents [36], [50], [54].....	35
Table IV: Pipe Combination Lengths and Approximate Volumes	40
Table V: OBF 90:10 Parameters.....	93
Table VI: OBF 80:20 Parameters	96
Table VII: OBF 70:30 Parameters	98
Table VIII: OBF 90:10 Distilled Parameters	101
Table IX: Summary of Results	108

List of Figures

Figure 1. Flow of drilling fluid	8
Figure 2. Mud Pulse Telemetry, Positive Pulse Pressure Wave	12
Figure 3. Coaxial cable cutaway [66]	16
Figure 4. TEM Propagation [67].....	17
Figure 5. E-Fields of Rectangular Waveguide TE modes	18
Figure 6. Circular waveguide.....	19
Figure 7. Un-polarized and Polarized dielectric [69].....	32
Figure 8. Out-of-phase polarization.....	34
Figure 9. Generalized Complex Permittivity Values [70]	35
Figure 10. Scattering Parameters components.....	36
Figure 11. Device under test with and without a matching network	37
Figure 12. Multiple sections of Pipe	40
Figure 13. SMA Connector, left, and SMA Connector with copper extension	41
Figure 14. Detailed Model Probe parametric sweep simulation.....	43
Figure 15. Probe Plate CAD drawing, left, and modified pipe.....	44
Figure 16. Probe positions 1-4, left to right	44
Figure 17. S_{11} comparison of modified probes	45
Figure 18. End cap valve modification	46
Figure 19. S_{11} comparison of pre and post valve modification.....	47
Figure 20. Spill containment setup	48
Figure 21. VectorVu main display	50
Figure 22. Two-port SOLT calibration dialog box.....	51

Figure 23. S_{21} and S_{11} measurement of the “Thru” standard after calibration.....	52
Figure 24. Long section of pipe being measured with the VNA	53
Figure 25. Simple Two Probe model	56
Figure 26. Simulated S_{11} of Simple Two-Port Model.....	57
Figure 27. Detailed Two Probe model.....	58
Figure 28. Detailed probe and rounded cap	58
Figure 29. Wave port with defined integration line	59
Figure 30. Simulated scattering parameters of the Detail Two Port model.....	60
Figure 31. Calculated MAG of the Detailed Two Port simulation	61
Figure 32. Three Pipe Section model.....	61
Figure 33. S_{11} measurements of the probe tuning position tests.....	62
Figure 34. S_{21} measurement of the probe orientation tests	63
Figure 35. MAG calculation and possible field configurations of an air-filed pipe	64
Figure 36. Calculated MAG of the Joint Gap Tests.....	66
Figure 37. Conductivity measurement experiment setup	68
Figure 38. Maximum available gain calculate for various lengths of air filed pipe	69
Figure 39. Measured and Curve Fit losses in air at 2.082 GHz	70
Figure 40. Comparison of simulated and measured S-Parameters of an Air Filed Pipe (short-short)	71
Figure 41. Comparison of simulated and measured S-Parameters of Air Filed Pipe (short-short-short)	72
Figure 42. Comparison of simulated and measured S-Parameters of Air Filed Pipe (short-long-short)	73

Figure 43. Updated simulation comparison of Air Filled Pipe (short-long-short).....	74
Figure 44. Comparison of simulated and measured S-Parameters of Air Filled Pipe (short-long-long-short).....	75
Figure 45. Calculated MAG of Distilled Water.....	76
Figure 46. Normalized MAG of Distilled Water.....	77
Figure 47. Measured and curve fit losses in distilled water.....	78
Figure 48. Relaxation Parameters of Water.....	79
Figure 49. Comparison of simulated and measured S-Parameters of Distilled Water (short-short).....	80
Figure 50. Comparison of simulated and measured S-Parameters of Distilled Water (short-short-short).....	81
Figure 51. Maximum available gain of 5% NaCl by weight brine solution.....	82
Figure 52. Scattering Parameters of 5% NaCl by weight brine solution.....	83
Figure 53. Smith Plot – Calibration standard “short”.....	84
Figure 54. Smith Plot of S_{11} Parameter of 5% NaCl by weight brine solution.....	85
Figure 55. Maximum available gain of red-dyed diesel.....	86
Figure 56. Measured and curve fit losses of red-dyed diesel.....	87
Figure 57. Comparison of simulated and measured S-Parameters of Diesel Fuel (short-short).....	88
Figure 58. Comparison of simulated and measured S-Parameters of Diesel Fuel (short-short-short).....	89
Figure 59. Comparison of simulated and measured S-Parameters of Diesel Fuel (short-long-short).....	90

Figure 60. Four stages of emulsions [73].....	91
Figure 61. Maximum available gain of an Oil-based fluid ratio of 90:10.	94
Figure 62. Measured and curve fit losses of an Oil-based fluid ratio of 90:10.....	95
Figure 63. Maximum available gain of an Oil-based fluid ratio of 80:20.	96
Figure 64. Measured and curve fit losses of an Oil-based fluid ratio of 80:20.....	97
Figure 65. Maximum available gain of an Oil-based fluid ratio of 70:30.	99
Figure 66. Measured and curve fit losses of an Oil-based fluid ratio of 70:30.....	100
Figure 67. MAG of 90:10 OBF using distilled water.	101
Figure 68. Measured and curve fit losses of an Oil-based fluid ratio of 90:10 using distilled water.....	102
Figure 69. Maximum available gain of Mineral Oil.....	103
Figure 70. Measured losses in Mineral Oil.....	104
Figure 71. Comparison of simulated and measured S-Parameters of Mineral Oil (short-short)	105
Figure 72. Comparison of simulated and measured S-Parameters of Mineral Oil (short-short- short).....	106
Figure 73. Maximum available gain of Escaid™ 110	107

List of Equations

Equation

(1)	20
(2)	20
(3)	20
(4)	20
(5)	20
(6)	20
(7)	20
(8)	20
(9)	20
(10)	21
(11)	21
(12)	21
(13)	21
(14)	21
(15)	21
(16)	21
(17)	21
(18)	21
(19)	22
(20)	22
(21)	22

(22)	22
(23)	22
(24)	22
(25)	23
(26)	23
(27)	23
(28)	24
(29)	24
(30)	24
(31)	25
(32)	26
(33)	26
(34)	27
(35)	27
(36)	27
(37)	28
(38)	28
(39)	28
(40)	28
(41)	28
(42)	28
(43)	29
(44)	29

(45)	29
(46)	29
(47)	30
(48)	30
(49)	30
(50)	30
(51)	31
(52)	31
(53)	34
(54)	34
(55)	36
(56)	36
(57)	37
(58)	38
(59)	38
(60)	38
(61)	38
(62)	38
(63)	67
(64)	67
(65)	78
(66)	79
(67)	81

(68)109

Glossary of Acronyms

Term	Definition
BHA	Bottom hole assembly
bps	Bits per second
DUT	Device under test
LWD	Logging While Drilling
MPT	Mud Pulse Telemetry
MWD	Measurement While Drilling
OBF	Oil-based Fluid
RF	Radio Frequency
RSS	Rotary Steerable System
TE	Transverse Electric
TM	Transverse Magnetic
VNA	Vector Network Analyzer
WBF	Water-based Fluid
WDP	Wired Drill Pipe

1. Introduction

As oil and gas exploration operations expand the reach and complexity of wells being drilled, the need for real-time, downhole information becomes increasingly important. The telemetry systems currently being used commercially suffer from extremely low data rates and high latency, thereby leading to delays in drill times. This work proposes that a system based upon guided wave propagation could be designed to utilize a wireless, radio frequency (RF) signal to yield tens of megabits per second of data transfer.

The low data rates and high latency of current systems means the data being transferred from downhole must be prioritized, limiting the amount of real time information sent to the surface. Data that is deemed less critical is stored in an internal memory and is only read after the drill string is removed from the hole. The data that is sent to the surface also must be compressed, resulting in a low resolution picture of the downhole conditions. Higher data throughput would enable access to all of the available data in high-resolution in nearly real time. The increased data through also has the potential to enable system monitoring using real-time video and enough data to run full reservoir simulations.

Telemetry systems in use today also lose communication with downhole sensors when the drill pipe is being moved in or out of the hole, known as tripping. During tripping the fluid pressures in the hole are fluctuating. In wells where the hydrostatic pressure must be maintained in a critical region, the fluctuations caused by tripping pipe can lead to dangerous kicks [1]. In the proposed system, a surface antenna could be designed to receive the guided waves propagating from the open end of the drill string, enabling a communication link with downhole sensors. Constant, real-time measurement of wellbore dynamics could help detect kicks sooner.

Existing research into downhole RF communication systems propose using the drill string as a conducting path with either the earth or a conductive drilling fluid as the return path for the signal. Neither return path is very conductive resulting in very high signal attenuation, especially at RF. Waveguides, on the other hand, are systems that direct high frequency energy with minimal losses. Conveniently, the structure of the drill string, a hollow metal pipe, can be looked at as an electrical waveguide. If the structure of the pipe could be leveraged into a waveguide communication channel then a high-speed link could be built, provided the addition of drilling fluids does not induce significant loss.

With well lengths exceeding 30,000 feet, a single link is potentially unrealistic so a system of signal repeaters would need to be utilized to reliably send information up and down the drill string. The critical factor in determining feasibility of a potential system then becomes the maximum allowable distance between signal repeaters that would still yield a usable signal. To calculate the maximum distance the total signal attenuation per length of pipe must first be determined.

The signal attenuation in waveguide propagation is a result of ohmic losses in the walls of the waveguide and dielectric losses in the medium filling the waveguide. As discussed in Section 4.1, the dominating propagation loss is due to the dielectric properties of the medium, specifically the loss tangent. Unfortunately, dielectric properties of drilling fluid mixtures are unknown so a numerical analysis cannot immediately be performed. Therefore, to determine the maximum repeater distance the dielectric properties of the fluids to be used in the system must be measured.

A series of experiments were designed to measure the waveguide propagation losses in a fluid filled pipe of various lengths. By measuring losses in multiple lengths of a pipe, a loss per

meter value could be determined and the maximum distance between repeaters can be directly calculated. However, the direct loss per meter calculation is only applicable to the exact steel type and inner diameter of the pipe used to make the measurements. Fortunately, the dielectric properties of the fluids under test can be back calculated using the loss per meter value and known properties of waveguide propagation. Theoretical signal loss calculations for different types of pipe can then be determined using the calculated dielectric properties.

The measurement setup was also modelled using a finite element analysis software package called Ansys HFSS. First, the model was validated using the materials with known electrical characteristics: air and distilled water. Then the fluid properties derived from measurements in the pipe were applied to the model and the measured and simulated results were compared.

The goal of this work was to determine the feasibility of using the inner diameter of drill pipe as a waveguide to propagate radio frequency (RF) signals for downhole communication in oil and gas drilling applications by characterizing the propagation loss and dielectric properties of various drilling fluids. Furthermore, the work developed a test setup to make precise measurements of unknown fluids and as well as a finite element analysis simulation model to further analyze the electromagnetic wave propagation.

2. Literature Review

Significant research into various communication systems for downhole telemetry applications is available [2]–[22] and the four main systems currently in commercial use are described in detail in Section 3.3. Minimal literature, however, is available on systems designed to use electromagnetic signals in the radio frequency (RF) spectrum. Much of the research into RF communication links utilizes the outer face of the pipe as the main conductor for the signal with either the earth or the drilling fluid as the return path [23]–[28].

Only three patents filed with the US Patent and Trademark Office [29]–[31] were found that specifically address using waveguide propagation inside a drill pipe for a downhole telemetry link. No other literature was found describing the use of the drill string as a waveguide for downhole communication.

Described in [29] is a system to monitor downhole pressure and temperature of a reservoir using the well tubing as a waveguide. Effects of tubing size and material properties of the fluid are considered for determination of an optimal operating frequency but there is no discussion of signal attenuation.

A measurement-while-drilling telemetry system using electromagnetic transmissions through the drill string as a waveguide is described in [30]. Theoretical values of signal attenuation are calculated but only for an air-filled waveguide with various water vapor concentrations. The proposed propagation mode, TE_{01} , is potentially unsuitable for any type of direction drilling due to the potential of coupling with other propagation modes as the longitudinal curvature of the pipe changes.

Experimental data for signal attenuation in a drill pipe waveguide is provided in [31]. Using commercial-off-the-shelf wireless transceivers, received signal strength was measured in

varying lengths of up to 540 feet of pipe. The results of the experiments show significantly higher attenuation than the expected attenuation calculations. After reviewing the author's derivation of the attenuation constant, it appears the magnetic permeability of the pipe may have been neglected.

Fortunately, there is a wealth of information related to generic waveguides that can aid in the analysis of theoretical signal propagation and losses [32]–[43].

The attenuation of signals propagating through a nonconductive material, such as drilling fluid, is due to the electrical properties of the material, specifically the dielectric constant and the dielectric loss factor. Dielectric properties of wide range of materials are well known,[44]–[55], but information of fluids specific to drilling systems is relatively unknown.

Many fluids, such as diesel fuel, a common base fluid in oil-based fluids, have a known dielectric constant but the loss factor is unknown. While other base fluids, such as mineral oil, paraffin oils, H₂O, or salt water have well known dielectric constants and loss factors. A problem arises when trying to determine theoretical dielectric properties of actual mixtures because of the non-standardized nature of drilling fluids. For each formation drilled the drilling fluid can be a combination of base fluid, dispersed fluid, emulsifier, and additives. All of which will influence the dielectric properties affecting the propagation losses.

Another challenge of finding the needed dielectric properties to make proper estimations is the proprietary nature of specialized fluids. ExxonMobil produces a synthetic-based fluid called Escaid 110 developed for extended reach wells and offshore use. Information of the chemical makeup of Escaid 110 is limited to safety data sheets, one of which lists the “Chemical Family” as a paraffin, [56]. Now, it is possible to make rough estimations of the propagation

losses using known properties of paraffin oils but the estimate should not be used to make a prediction of the feasibility of a communication system.

3. Drilling Background

To better understand the applications and benefits of an RF communication link for downhole telemetry, as well as the scope of potential research, a brief overview of drilling practices, current technologies, and communication applications will now be discussed.

3.1. Drilling Basics

Oil and gas wells are drilled by rotating sections of drill pipe with a drill bit attached to the bottom. The full length of drill pipe is called the drill string. As the well gets deeper, additional sections, or “joints”, of drill pipe added to the drill string. A joint of Range 2 drill pipe is typically nine meters in length. When joints are removed from the hole, or “tripped out”, they are sometimes removed in groups, known as a “stand”, to facilitate more efficient removal of the drill string. Stands are typically a group of three joints, but can be two or four joints. Near the bottom of the drill string is the bottom hole assembly (BHA) which can include the drill bit, drill collars, measurement tools, and communication hardware.

While drilling a well, fluid is pumped down the center of the drill string and then returned to the surface through the annulus of the wellbore as shown in Figure 1, [57]. The drilling fluid, sometimes referred to as drilling “mud”, has several essential functions in the drilling process.

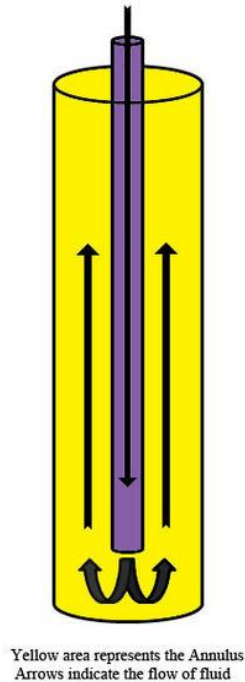


Figure 1. Flow of drilling fluid

Broken pieces of rock and earth, called cuttings, are produced while drilling and need to be cleared from the hole to avoid damaging equipment or getting the bottom hole assembly stuck. The drilling fluids help to flush cuttings from downhole to the surface where they are separated from the fluid, which is then recirculated back into the fluid system.

During drilling operations, the bit and drill string are rotating at rates of up to hundreds of revolutions per minute. Friction from the rotation of the drill bit on the formation and the drill string on the well bore can result in a substantial amount of the heat. The drilling fluid provides cooling and lubrication at the drill bit as well as lubrication for the drill string in the well bore to minimize wear on equipment.

Oil and gas reservoirs are typically highly pressurized due to the weight of the formations trapping the hydrocarbons. When the drill enters the reservoir formation pressure will try to force fluids into the well bore unless there is an equal pressure acting against the reservoir. The

column of drilling fluid provides hydrostatic pressure that helps maintain a balanced pressure with the formation. Loss of that balanced pressure can result in dangerous “kicks” or “blowouts.”

The flow of fluid can also provide hydraulic energy to downhole tools such as mud motors that will turn the drill bit even when the drill string itself is not rotating. Turbines in the BHA can also convert the fluid flow into electrical energy and provide power to measurement and logging while drilling systems.

The three common categories of drilling fluids are water based, oil based, and gas based. The type of fluid used is dependent on the formation being drilled as well as cost and environmental impact. Water-based fluids (WBFs) use a base of fresh water, seawater, or brine and is one of the more widely used drilling fluids due to the low cost compared to oil-based fluids. Oil-based fluids (OBFs) can use diesel or mineral oils and are used in wells that could potentially swell or slough with that addition of any WBF. Increased lubrication and the ability to tolerate higher downhole temperatures are another reason OBFs are used. Gas-based fluids use air, nitrogen, or aerated fluids to remove cuttings from the well bore and are used in what is called “underbalanced drilling.” Underbalanced refers to the hydrostatic head of the drilling fluid is less than the formation pressure. Air drilling has the benefit of increased rate of penetration compared to oil-based and water-based drilling but can only be used for specific formations. Formations not suited for air drilling are those with large volumes of water, high-pressure formations, and high-permeability formations [58]–[60].

3.2. Downhole Communication Applications

Downhole communication in drilling operations has three main applications: Logging While Drilling to produce a well log; Measurement While Drilling to monitor drilling mechanics; and Rotary Steerable Systems to control the directional drilling bit. Logging and

Measurement While Drilling serve as telemetry link to receive information at the surface from various sensors downhole. While Rotary Steerable Systems are more of a control link to send commands from the surface to tools downhole.

In directional or horizontal wells it is necessary to change the angle at which the wellbore is being drilled. Early directional wells were drilled using the slide technique, where a short, angled section of pipe is attached to the BHA, changing the angle the drill bit is pointed. During “sliding” the downhole mud motor, powered by the flow of fluid, rotates the drill bit while the drill string is stationary. Newer systems use Rotary Steerable Systems which let the driller send commands to the BHA and change the angle of the bit. The RSS allows for the continuous rotation of the drill string resulting in more precise and smoother boreholes. The real-time well log and drilling mechanics information received from MWD and LWD aid the driller in the process of geosteering to ensure the well is accurately placed.

A well log is a set of detailed measurements of the geological formations the borehole cuts through. Measurements in a well log can include resistivity, density, permeability, gamma ray, and wellbore dimensions. Traditionally, a well log was made using wireline logging techniques in which the entire drill string was removed from the well and a sensor array was lowered into the borehole. Wireline logging not only puts a halt to drilling but also allows the possibility of drilling fluids invading the formation. Any fluid penetrating the formation will affect measurements and give an inaccurate picture of the well.

Logging While Drilling (LWD) delivers real-time time measurements while the drill string is still in the well. Instead of pulling the entire drill string out to make measurements, the sensor array is a part of the bottom hole assembly and transmits the information to the surface via one of the communication techniques outlined in Section 3.3. Along with real-time

information, LWD has the added benefit of measuring a formation before the drilling fluid has time to permeate the formations, giving a more accurate measurement [61], [62].

Measurement While Drilling (MWD) is similar to LWD but monitors information related to mechanics of the drilling process. Azimuth and inclination of the wellbore, as well as tool information such as weight on the bit, downhole pressures, temperatures, drilling fluid flow, and torque are just a few of the measurements that can be made in a MWD system [63], [64]. The measurements taken through MWD are used to analyze the trajectory of the well bore to determine if directional steering adjustments need to be made.

3.3. Communication Technologies

There are four main systems used for downhole communication during the drilling of a well. Two of the systems, mud pulse telemetry and acoustic signaling, use pressure waves to transmit information. While the other two, wired drill pipe and electromagnetic telemetry, use electromagnetic waves. Current communication systems for drilling systems suffer from very low data rates with most systems only delivering up to 100 bits per second (bps) and the fastest system available delivering 57,000 bps. For comparison, data rates for dial-up internet modems are nominally 56,600 bps.

Mud Pulse Telemetry (MPT) utilizes the drilling fluid, or “mud”, within the drill string as the transmission medium. By modulating the fluid pressure at the bottom of the hole, pressure waves are sent up the column of fluid that can then be detected and decoded by a surface transducer. Three different pulse types are used in MPT systems: positive pulse, negative pulse, and continuous wave. A positive pulse system uses a valve to temporarily restrict the flow of fluid within the pipe, sending a wave of increased pressure up the column of fluid. Figure 2 shows a valve actuating upwards to temporarily impede the downward fluid flow rate and

thereby transmitting a positive pressure wave. Negative pulse systems operate in similar fashion but instead temporarily divert fluid from inside the drill pipe to the annulus, creating a decrease in pressure that will propagate [19].

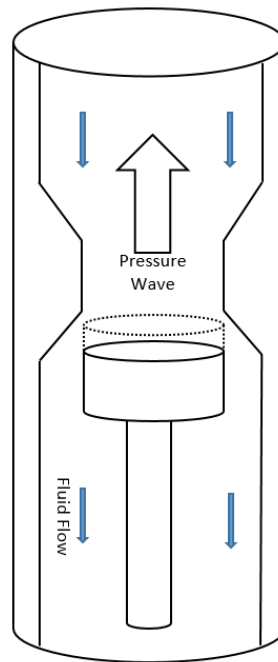


Figure 2. Mud Pulse Telemetry, Positive Pulse Pressure Wave

Continuous-wave systems use a motor to vary the amount of fluid allowed to flow between the rotor and stator. The constant rotation of the motor results in a continuous fluctuation of the fluid pressure within the pipe. Digital data can then be modulated onto the continuous pressure wave. The frequency of continuous wave is typically in the range of 10-30Hz. Continuous-wave systems allow for more complex modulation compared to the discrete signaling techniques implemented in the positive and negative pulse systems. Schemes such as binary phase shift keying (BPSK), frequency shift keying (FSK), and quadrature phase shift keying (QPSK) are possible with continuous-wave MPT systems [13].

Though it is one of the most widely used downhole communication systems, MPT has the lowest data throughput of any of the other systems. With no way to repeat the pressure waves within in the drill string, MPT throughput is limited by the overall length of the well. As length increases, the total attenuation of pulsed signals also increases, so to reliably receive signals in longer wells the pulse length must be increased, which in turn decreases the data throughput of the system. In shallower wells (<10,000 feet), data rates can be as high as 30 bps but in deeper wells (>30,000 feet) rates drop to around 3 bps [3]. Signal interference can also occur caused by vibrations in the drill string from mud motors or turning of the drill string which also reduces the data rates. Another disadvantage of MPT is latency due to propagation through the drilling fluid. The signal can only travel as fast as the speed of sound in the fluid. Sea water, for instance, has a sound wave propagation speed of 1,531 meters per second, which would results in multiple second delays for single direction transmissions in shallow wells.

Acoustic signaling also uses pressure waves to transmit information, however, instead of using the drilling fluid as the medium of transmission, acoustic pulses are transmitted through the metal of the drill string. Like MPT, acoustic signaling is limited by the speed of sound in the medium through which the pressure waves are propagating, resulting in high latency for longer wells. The speed of sound in carbon steel, for example, is 3,230 meters per second, [65], leading to at least a full second delay for a one way transmission in a shallow well. While, acoustic signaling does have the benefit of signal repeaters enabling up to 100 bps, the addition of more hardware increases the complexity, implementation costs, and points of failure of the overall system [5], [16], [18].

Electromagnetic telemetry systems transmit extremely low frequency EM waves from downhole to the surface by alternating a voltage across an insulated gap in the drill string near

the BHA, creating a dipole antenna. At the surface, the data is received by measuring a voltage between cables connected to the drill rig and a spike driven into the ground several hundred feet from the rig. With operational frequencies in the 20-30 Hz range there is not enough bandwidth to enable any sort of high-speed throughput limiting EMT to data rates similar to MPT, on the order of 10-20 bits per second [7], [22].

A large disadvantage of EMT is the signal must propagate through the earth, which will have different formation types at every drill site. Conductivity and permittivity affect signal propagation from downhole to the surface and, depending on the material properties of the formations, the signal attenuation may be too high to yield any useful signal at the surface. For examples, the high conductivity of saltwater prevents the use of EMT in off-shore applications. Even in the absence of a highly conductive formation, the signal attenuation of propagating through the earth still severely limits the maximum depth to around 9,000 feet [12].

Wired drill pipe (WDP) is one of the newest drill string communication technologies and is also one of the most promising in terms of total data throughput. The initial paper published by IntelliServe demonstrated data rates of up to two million bits per second, though in practice data rates are limited to around 57,000 bits per second. Wired drill pipe achieves the high data throughput by embedding a shielded cable in the wall of the drill pipe itself. At each joint the cable is terminated in a loop which is then inductively coupled to the adjacent joint, providing a direct connection from downhole to the surface [9], [15].

In long reach wells the length of the drill string can be upwards of 30,000 feet, which corresponds to roughly 1,000 coupling joints. Each coupling induces a loss that cumulatively require signal repeaters to overcome. If the inductive coupling is damaged at even one joint then the whole communication network will be disabled and the entire string must be tripped out until

the broken joint is found. The biggest drawback of WDP is cost due to the specialized drill pipe required to implement the system.

4. Electrical Background

To provide a basic understanding of electrical concepts utilized in the research transmission line propagation, waveguide propagation, electrical permittivity, and electrical measurements will now be discussed.

4.1. Waveguides

A waveguide is a structure that directs RF electromagnetic energy with minimal losses. Typical applications of waveguides are high frequency and high power systems such as antenna feeds for radar systems and microwave ovens. Rectangular waveguides are the most common waveguides in commercial use but circular structures are also used, primarily in rotating systems.

Traditional electrical transmission lines, such as coaxial cable, microstrip, or parallel lines, are made up of at least two conductors. Coaxial cables, for example, have an inner conductor and an outer conducting shield with a dielectric insulator separating the conductors, see Figure 3.

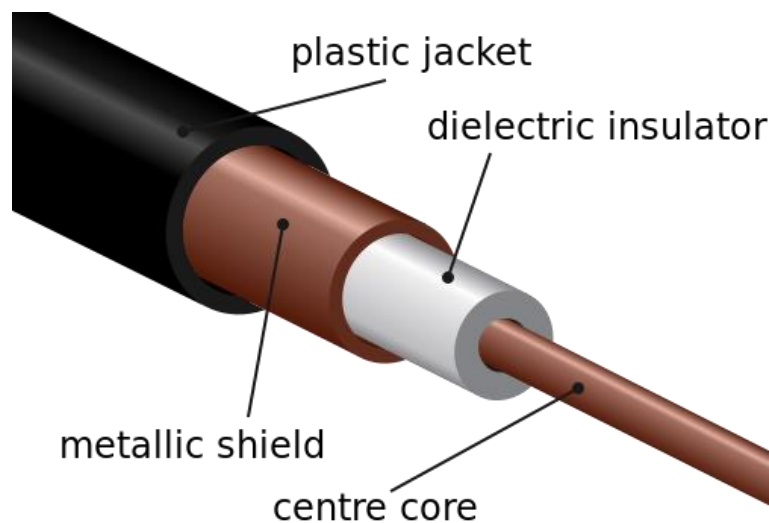


Figure 3. Coaxial cable cutaway [66]

In two conductor transmission lines, the dominant mode of electromagnetic wave propagation is transverse electromagnetic (TEM), where there is no electrical field component or magnetic field component in the direction of propagation. As seen Figure 4, a TEM wave propagating in the z direction has an electric field, \mathbf{E} , pointing in the x direction and a magnetic field, \mathbf{B} , pointing in the y direction. In the coaxial cable example, a TEM wave traveling longitudinally down the cable will have an electric field between the inner and outer conductor as well as a magnetic field encircling the inner conductor but neither of these fields will be pointed down the length of the cable [36].

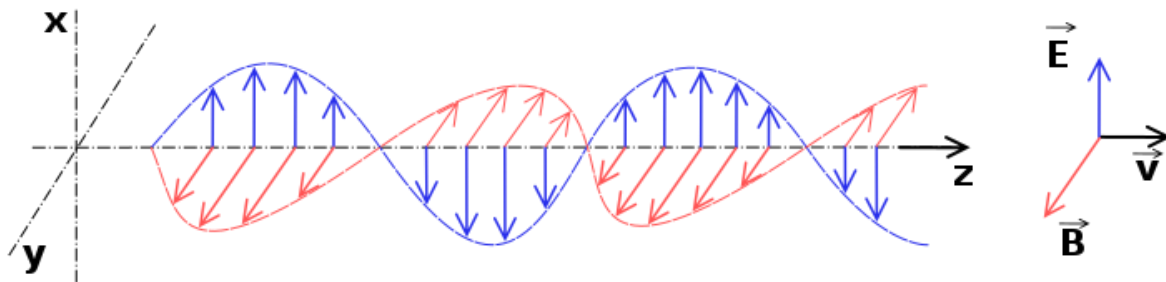


Figure 4. TEM Propagation [67]

Waveguides, however, are comprised of only a single conductor and so the propagation of TEM waves is not supported. Only transverse electric (TE) mode, where there is no electric field component in the direction of propagation but some component of magnetic field, and transverse magnetic (TM) modes, with no magnetic field in the direction of propagation but there is an electric field component. The inability to support TEM mode propagation is caused by boundary conditions of the electric and magnetic fields at the surfaces of the waveguide. The result is a maximum wavelength that is able to propagate in the waveguide. In other words, there is a minimum, or “cutoff”, frequency and so waveguides act as high pass filters.

Conceptually, the boundary conditions leading to a cutoff frequency effect can be most easily seen in the lower order, transverse electric modes of a rectangular waveguide. Consider

the rectangular waveguide at the top of Figure 5, with the x direction defined as horizontal, the y direction as vertical, and the z direction as out of the page. A TE mode traveling wave propagating in the z direction is bounded by the walls of the waveguide in the x and y directions. When boundary conditions are satisfied the result is a standing wave in the x - y plane. The wavelength of the standing wave is, in the case of the rectangular dominant TE_{10} mode, twice the width of the waveguide. The standing wave wavelength corresponds to the lowest frequency capable of propagating in the waveguide. The next transverse electric mode, TE_{20} , has a cutoff frequency that corresponds to a wavelength equal to exactly the width of the waveguide. For each successive TE_{m0} mode, the wavelength will be equal to twice the width divided by m . Rectangular transverse electric modes of the form TE_{0n} follow the same pattern but the wavelengths are set by the height of the waveguide.

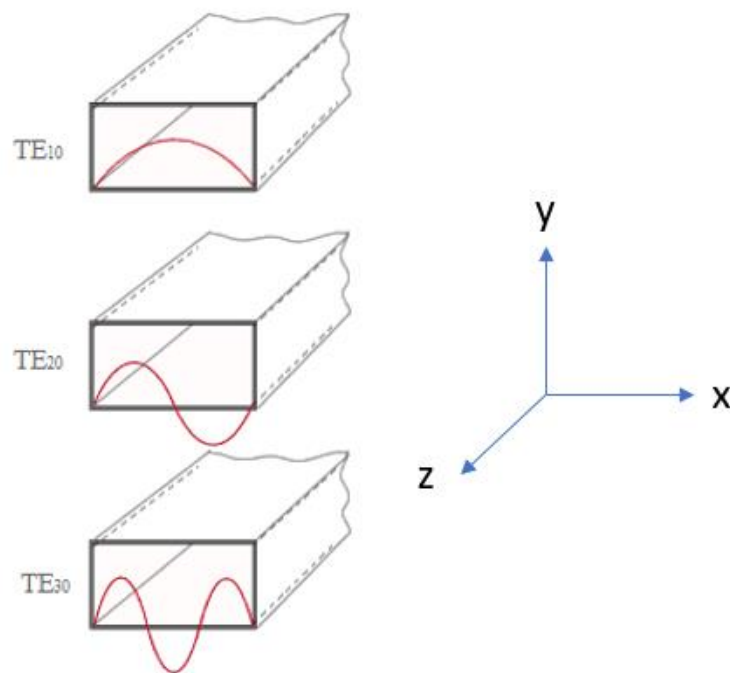


Figure 5. E-Fields of Rectangular Waveguide TE modes

The boundary conditions of the wave equation for Rectangular waveguides are solved using Cartesian coordinates leading to field solutions in terms of trigonometric functions and cutoff frequencies determined by the ratio of the dimensions of the structure and the mode numbers m and n . Whereas, circular waveguides are solved using cylindrical coordinates resulting in solutions involving Bessel functions, with the boundary conditions being met at either the zeros of a Bessel function or at the zeros of the derivative of the Bessel function.

Now, a derivation of the circular waveguide cutoff frequency for TE modes in circular waveguides will be discussed. Full derivations for both TE and TM modes in rectangular and circular waveguides can be found in [36], [39]. The following derivation uses the coordinate system of the circular waveguide show in Figure 6.

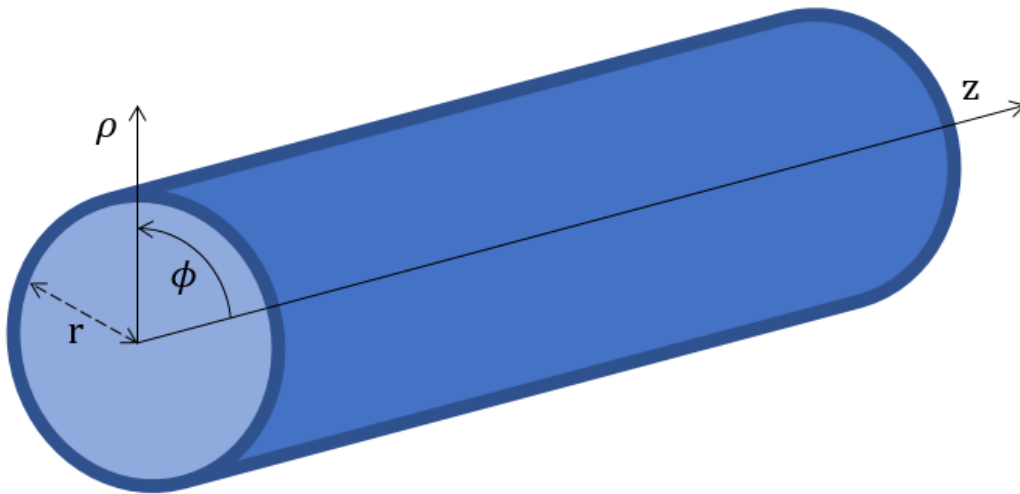


Figure 6. Circular waveguide

Any discussion of electromagnetic wave propagation starts with Maxwell's Equations. In a non-conducting, source free material, the time-harmonic, differential form of Maxwell's equations are given by:

$$\nabla \times \mathbf{E} = -j\omega\mu\mathbf{H} \quad (1)$$

$$\nabla \times \mathbf{H} = j\omega\varepsilon\mathbf{E} \quad (2)$$

$$\nabla \cdot \mathbf{E} = 0 \quad (3)$$

$$\nabla \cdot \mathbf{H} = 0 \quad (4)$$

where: \mathbf{E} is electric field intensity in volts per meter, \mathbf{H} is magnetic field intensity in amps per meter, ω is angular frequency in radians per second, μ is magnetic permeability in Henry's per meter, and ε is electric permittivity in Farads per meter.

By taking the curl of the Equation (1) and substituting in the right half of Equation (2):

$$\nabla \times \nabla \times \mathbf{E} = -j\omega\mu\nabla \times \mathbf{H} = \omega^2\mu\varepsilon\mathbf{E} \quad (5)$$

applying the vector identity:

$$\nabla \times \nabla \times \mathbf{A} = \nabla(\nabla \cdot \mathbf{A}) - \nabla^2\mathbf{A} \quad (6)$$

and recognizing, $\nabla \cdot \mathbf{E} = 0$, Equation (1) becomes the Helmholtz Equation:

$$\nabla^2\mathbf{E} + \omega^2\mu\varepsilon\mathbf{E} = 0 \quad (7)$$

Also known as wave equation. It is often written as:

$$\nabla^2\mathbf{E} + k^2\mathbf{E} = 0 \quad (8)$$

where k is the wavenumber, with units of 1/m, defined as the constant:

$$k = \omega\sqrt{\mu\varepsilon} \quad (9)$$

Now, consider a wave with electric and magnetic fields, given in cylindrical coordinates, of the form:

$$\mathbf{E}(\rho, \phi, z) = (\mathbf{e}(\rho, \phi) + \hat{z}e_z(\rho, \phi)) e^{-j\beta z} \quad (10)$$

$$\mathbf{H}(\rho, \phi, z) = (\mathbf{h}(\rho, \phi) + \hat{z}h_z(\rho, \phi)) e^{-j\beta z} \quad (11)$$

traveling in the longitudinal z direction of a cylindrical waveguide. Equations (1) and (2) can be reduced into the transverse components in terms of the longitudinal components, E_z and H_z , giving the following four equations:

$$E_\rho = \frac{-j}{k_c^2} \left(\beta \frac{\partial E_z}{\partial \rho} + \frac{\omega\mu}{\rho} \frac{\partial H_z}{\partial \phi} \right) \quad (12)$$

$$E_\phi = \frac{-j}{k_c^2} \left(\frac{\beta}{\rho} \frac{\partial E_z}{\partial \phi} + \omega\mu \frac{\partial H_z}{\partial \rho} \right) \quad (13)$$

$$H_\rho = \frac{j}{k_c^2} \left(\frac{\omega\varepsilon}{\rho} \frac{\partial E_z}{\partial \phi} - \beta \frac{\partial H_z}{\partial \rho} \right) \quad (14)$$

$$H_\phi = \frac{-j}{k_c^2} \left(\omega\varepsilon \frac{\partial E_z}{\partial \rho} + \frac{\beta}{\rho} \frac{\partial H_z}{\partial \phi} \right) \quad (15)$$

where the phase constant, β , defined as

$$\beta = \sqrt{k^2 - k_c^2} \quad (16)$$

with k_c defined as the cut off wavenumber. Now only the longitudinal components, E_z and H_z , need to be solved to completely describe the fields within a cylindrical waveguide.

For a transverse electric wave the solution for the longitudinal z component of the electric field, E_z , is simply zero, by definition. So only a solution for H_z must be derived from the wave equation:

$$\nabla^2 H_z + k^2 H_z = 0 \quad (17)$$

From Equation (11), the z component of the magnetic field is

$$H_z(\rho, \phi, z) = h_z(\rho, \phi) e^{-j\beta z}, \quad (18)$$

and so Equation (17) can then be written as

$$\left(\frac{\partial^2}{\partial \rho^2} + \frac{1}{\rho} \frac{\partial}{\partial \rho} + \frac{1}{\rho^2} \frac{\partial^2}{\partial \phi^2} + k_c^2 \right) h_z(\rho, \phi) = 0 \quad (19)$$

To solve the second order partial differential equation by separation of variables, Equation (19) is rewritten as two independent functions, in terms of ρ and ϕ :

$$h_z(\rho, \phi) = R(\rho)P(\phi) \quad (20)$$

and substituting back into Equation (19) and rearranging yields:

$$\frac{\rho^2 d^2 R}{R d\rho^2} + \frac{\rho dR}{R d\rho} + \rho^2 k_c^2 = \frac{-1 d^2 P}{P d\phi^2} \quad (21)$$

The left side and right side are independent of each other in terms of their variables ρ and ϕ so both sides must be equal to a constant. To aid in the differential solution, the constant will be defined as m^2 . So, solving for the right side of Equation (22) gives

$$\frac{d^2 P}{d\phi^2} + m^2 P = 0 \quad (22)$$

with the general solution of:

$$P(\phi) = A \sin(m\phi) + B \cos(m\phi) \quad (23)$$

The field solution must be periodic such that $h_z(\rho, \phi) = h_z(\rho, \phi \pm 2m\pi)$. So it can be seen that m must be an integer value. Substituting m^2 for the right side of Equation (21) and rearranging gives the following:

$$\rho^2 \frac{d^2 R}{d\rho^2} + \rho \frac{dR}{d\rho} + (\rho^2 k_c^2 + m^2)R = 0 \quad (24)$$

When m is an integer value, Equation (24) is in the form of Bessel's equation, which has the known solution of

$$R(\rho) = CJ_m(\rho k_c) + DY_m(\rho k_c) \quad (25)$$

where J_m and Y_m are Bessel Functions of the first and second kind, respectively, of the m^{th} order and C and D are arbitrary constants. An important property of Bessel functions of the second kind, Y_m , is the value becomes infinite as the argument goes to zero. Since a real solution at the radial center of the waveguide, $\rho = 0$, cannot be an infinite field, the constant D must equal zero. Then absorbing the arbitrary constant C into the constants A and B, the full solution becomes:

$$h_z(\rho, \phi) = J_m(\rho k_c)(A\sin(m\phi) + B\cos(m\phi)) \quad (26)$$

Substituting Equations (26) and (18) into Equation (13), the electric field component in the ϕ direction can be solved by

$$E_\phi(\rho, \phi, z) = \frac{\partial}{\partial(\rho k_c)}(J_m(\rho k_c)) \frac{j\omega\mu}{k_c}(A\sin(m\phi) + B\cos(m\phi)) e^{-j\beta z} \quad (27)$$

One boundary condition of electric fields is a tangential field cannot exist at the interface of conducting and dielectric materials. Therefore, E_ϕ must be zero when ρ is equal to the radius, r , of the waveguide, for all values of ϕ and z . It can be seen this will only occur when the derivative of the Bessel function equals zero, $J'_m(\rho k_c) = 0$. For each derivative of a non-negative, m^{th} order Bessel function there are infinite zeros. To distinguish between solutions, the n^{th} root of an m^{th} order Bessel function derivative is given by χ'_{mn} . Values for the first 12 zeros are given in Table I.

Table I: n^{th} zeros of the derivative of the m^{th} -order Bessel Functions

	m =0	m =1	m =2	m =3
n=1	3.8318	1.8412	3.0542	4.2012
n=2	70.156	5.3315	6.7062	8.0153
n=3	10.1735	8.5363	9.9695	11.3459

So, in order for the Bessel derivative to equal zero, ρk_c must equal a root, χ'_{mn} , when ρ is equal to the radius, r :

$$J'_m(rk_c) = J'_m(\chi'_{mn}) = 0 \quad (28)$$

As a result the cutoff wavenumber can be calculated from the radius and Bessel solution:

$$k_c = \frac{\chi'_{mn}}{r} \quad (29)$$

and the cutoff frequency for a circular waveguide operating in a transverse electric mode can be calculated by:

$$f_c = \frac{\chi'_{mn}}{2\pi * r * \sqrt{\mu\epsilon}} = \frac{\chi'_{mn} * c}{2\pi * r * \sqrt{\epsilon_{r_{medium}}}} \quad (30)$$

where c is the free-space speed of light, 3×10^8 m/s, and $\epsilon_{r_{medium}}$ is the dielectric constant of the medium filling the waveguide.

A similar derivation can be performed for TM_{mn} modes, however the boundary conditions are satisfied at zeros of the Bessel function, rather than at the derivative. The n^{th} root of an m^{th} order Bessel function is given by χ_{mn} , values for the first 12 solutions are given in Table II.

Table II: n^{th} zeros of m^{th} -order Bessel Functions

	m =0	m =1	m =2	m =3
n=1	2.4049	3.8318	5.1357	6.3802
n=2	5.5201	7.0156	8.4173	9.7610
n=3	8.6537	10.1735	11.36199	13.0152

Attenuation of a signal propagating in a waveguide is caused by ohmic losses and dielectric losses. Ohmic losses, also called conductor losses, are a result of current being conducted along a surface of finite conductivity. In the case of a waveguide the conductor is the internal walls of the structure. Dielectric losses are a result of electromagnetic waves propagating through the medium within the waveguide. The mechanism of dielectric loss is affected by the specific material properties and is further discussed in Section 4.2.

Conductor and dielectric losses are both affected by the propagation mode, due to the change in operating frequency as well as the different field configurations of the modes affecting the amount of current conduction in the walls of the waveguide. TE₀₁ mode, for example, has decreasing conductor losses as the operating frequency increases, making it an attractive mode to operate in using air filled waveguides. Though if the medium filling the waveguide is a lossy dielectric an increase in frequency will result in an increase in losses. The TE₀₁ mode is also more susceptible to coupling with other modes when there are discontinuities in the waveguide, such as changes in dimension or curvature [33]. If a transmitted signal couples with another mode it potentially would not be able to be detected by the receiver.

Losses in waveguides can be described by an attenuation constant, α , which is a summation of the dielectric losses, α_d , and conductor losses, α_c . The attenuation constant due to conductor loss operating in a transverse electric mode, from [39], is given by:

$$\alpha_c = \frac{R_s}{r\eta} * \frac{1}{\sqrt{1 - \left(\frac{f_c}{f}\right)^2}} * \left(\left(\frac{f_c}{f}\right)^2 + \frac{m^2}{\chi'_{mn}{}^2 - m^2} \right) \quad \text{Np/m} \quad (31)$$

and is a function of the surface resistance of the waveguide, R_s , the radius of the waveguide, r , and the dielectric wave impedance of the medium filling the waveguide, η . The center term can

be called the guided wave scaling factor, as the wavelength in the waveguide is the free space wavelength multiplied by the factor. The third term can be called the TE mode scaling factor because the conductor attenuation in TM modes is given by the same formula just without this factor. The units of the attenuation constants are Nepers per meter, where Nepers are a logarithmic ratio of the field strengths [39].

The wave impedance of the dielectric, or intrinsic impedance, can be approximated by:

$$\eta = \sqrt{\frac{\mu_{medium}}{\epsilon_{medium}}} = \sqrt{\frac{\mu_0 \mu_{r_{medium}}}{\epsilon_0 \epsilon_{r_{medium}}}} \cong \frac{377}{\sqrt{\epsilon_{r_{medium}}}} \quad \Omega \quad (32)$$

where μ is magnetic permeability and ϵ is the electric permittivity. Relative permittivity, ϵ_r , and relative permeability, μ_r , is defined as a ratio relative to the respective values in free space. Permittivity in free space, ϵ_0 , is approximately 8.85×10^{-12} farads per meter (F/m) and free space permeability, μ_0 , is approximately $4\pi \times 10^{-7}$ Henry per meter (H/m). Dielectrics tend to have negligible magnetic response so the relative permeability is assumed to be unity.

Surface resistance of the waveguide is given by:

$$R_s = \sqrt{\frac{2\pi f \mu_{pipe}}{2\sigma_{pipe}}} \quad \Omega \quad (33)$$

where operating frequency, f , magnetic permeability, μ , and bulk conductivity, σ , [39].

To better see the main components affecting propagation losses in a waveguide the attenuation constant will now be reduced and approximated. To determine a potential operating frequency, the proposed propagation mode can be looked at and compared to the next excitable

propagation mode. By comparing the cutoff frequencies of the two modes a potential range for the operating frequency can be calculated.

From Table I, the dominate propagating mode, TE₁₁, has a Bessel solution of $\chi'_{11} = 1.8412$. The next lowest order mode is TM₀₁ with $\chi_{01} = 2.4049$, from Table II. All other factors being equal, the cutoff frequencies are related by the ratio of the Bessel solutions of the two modes and the cutoff of TM₀₁ can be written in terms of the cutoff of TE₁₁:

$$f_{c_{TM01}} = f_{c_{TE11}} * \frac{2.4049}{1.8412} = 1.306 f_{c_{TE11}} \quad (34)$$

Consequently, operating frequencies capable of operating in the TE₁₁ mode can be described by a range from the dominant mode cutoff frequency to the cutoff frequency multiplied by the ratio of the Bessel solutions:

$$f_{c_{TE11}} < f < 1.306 f_{c_{TE11}} \quad (35)$$

Selecting a frequency roughly in the middle of range of valid frequencies supporting propagation mode TE₁₁ gives an operating frequency of:

$$f = 1.15 * f_{c_{TE11}} \quad (36)$$

Using the known propagation mode solution of $\chi'_{11} = 1.8412$ and substituting Equation (36) in for, f , into Equation (33), the surface resistance of the waveguide at the selected operating frequency can then be approximated as:

$$R_s = \sqrt{\frac{2\pi * 1.15 * 1.8412 * c * \mu_0 * \mu_{r_{pipe}}}{2 * \sigma_{pipe} * 2\pi * r * \sqrt{\epsilon_{r_{medium}}}}} \cong 20 * \sqrt{\frac{\mu_{r_{pipe}}}{\sigma_{pipe} * r * \sqrt{\epsilon_{r_{medium}}}}} \Omega \quad (37)$$

Continuing the approximation for the TE and guided wave scaling factors at the chosen operating frequency result in the scalar values:

$$\left(\left(\frac{f_{c_{TE11}}}{f} \right)^2 + \frac{m^2}{\chi'_{mn}{}^2 - m^2} \right) = \left(\left(\frac{1}{1.15} \right)^2 + \frac{1^2}{1.8412^2 - 1^2} \right) \cong 1.17 \quad (38)$$

$$\frac{1}{\sqrt{1 - \left(\frac{f_{c_{TE11}}}{f} \right)^2}} = \frac{1}{\sqrt{1 - \left(\frac{1}{1.15} \right)^2}} \cong 2 \quad (39)$$

Substituting the approximations from Equations (36) - (39) into Equation (31) yields a conductor attenuation constant of:

$$\alpha_c \cong 20 * \sqrt{\frac{\mu_{r_{pipe}}}{\sigma * r * \sqrt{\epsilon_{r_{medium}}}}} * \frac{2}{r\eta} * 1.17 \quad Np/m \quad (40)$$

$$\alpha_c \cong 46.9 * \sqrt{\frac{\mu_{r_{pipe}}}{\sigma * r * \sqrt{\epsilon_{r_{medium}}}}} * \frac{\sqrt{\epsilon_{r_{medium}}}}{r * 377} \quad Np/m \quad (41)$$

$$\alpha_c \cong \frac{0.124}{r} * \sqrt{\frac{\mu_{r_{pipe}} * \sqrt{\epsilon_{r_{medium}}}}{\sigma_{pipe} * r}} \quad Np/m \quad (42)$$

where Np/m is Nepers per meter. Nepers are a field, or voltage, ratio using the natural log, with a logarithmic base of e . RF engineers prefer to discuss losses in terms of decibels, a power ratio using log base 10. Nepers can be converted to decibels using the following formula:

$$1 \text{ Np} = 20 \log_{10} e \text{ dB} \cong 8.686 \text{ dB} \quad (43)$$

where e is Euler's number, equal to approximately 2.71828. The conversion can be used to convert (42) into decibels per meter:

$$\alpha_c \cong \frac{1.08}{r} * \sqrt{\frac{\mu_{r_{pipe}} * \sqrt{\epsilon_{r_{medium}}}}{\sigma_{pipe} * r}} \text{ dB/m} \quad (44)$$

Still assuming a non-magnetic medium filling the waveguide, the attenuation due to dielectric losses, from [40], is given by:

$$\alpha_d = \frac{\pi f \tan \delta}{\frac{c}{\sqrt{\epsilon_{r_{medium}}}} \sqrt{1 - \left(\frac{f_c}{f}\right)^2}} \text{ Np/m} \quad (45)$$

where $\tan \delta$ is the loss tangent of the dielectric medium filling the pipe. Loss tangent and dielectric loss is discussed more in depth in Section 4.2.

Substituting in the same operating frequency used in the conductor loss approximation of 1.15 times the cutoff, the dielectric attenuation constant can be approximated by:

$$\alpha_d \cong \frac{\pi * 1.15 * \frac{1.18412 * c}{2\pi * r * \sqrt{\epsilon_{r_{medium}}}} * \tan \delta}{\frac{c}{\sqrt{\epsilon_{r_{medium}}}} \sqrt{1 - \left(\frac{f_c}{f}\right)^2}} \text{ Np/m} \quad (46)$$

$$\alpha_d \cong \frac{1.36 * \tan \delta}{r} \quad Np/m \quad (47)$$

$$\alpha_d \cong \frac{11.81 * \tan \delta}{r} \quad dB/m \quad (48)$$

Resulting in a total attenuation constant loss per meter approximation of:

$$\alpha \cong \frac{1.08}{r} * \sqrt{\frac{\mu_{r_{pipe}} * \sqrt{\epsilon_{r_{medium}}}}{\sigma_{pipe} * r}} + \frac{11.81 * \tan \delta}{r} \quad dB/m \quad (49)$$

It can be seen that propagation losses, when operating in the middle of the pass band range of frequencies that support the TE₁₁ mode, are a function of the radius of the pipe, r , the electromagnetic properties of the pipe, $\mu_{r_{pipe}}$ and σ_{pipe} , and the dielectric properties of the medium filling the pipe, $\sqrt{\epsilon_{r_{medium}}}$ and $\tan \delta$. Typical values of conductivity for steel on the order of 10^6 S/m and permeability in the range of 10 to 100. So for materials with $\tan \delta > 10^{-5}$ the dominating parameter affecting attenuation will be the loss tangent.

Using current battery powered transceiver technologies it is reasonable to assume allowable transmission power of 1-100 milliwatt, or 0-20 dBm, where dBm is a power ratio in decibels relative to 1 milliwatt. The noise floor, or the minimum detectable signal is given by:

$$Noise\ floor_{dBm} = 10 \log_{10}(kT_0 \times 1000) + NF + 10 \log_{10} BW \quad (50)$$

where k is Boltzmann's constant (1.38×10^{-23} joules per kelvin), T_0 is the receiver temperature in kelvins, NF is the noise figure of the receiver in dB, and BW is the channel bandwidth in Hertz [68].

At room temperature, with a receiver noise figure of 4 dB, and a channel bandwidth of 10 MHz the noise floor is -100 dBm. To be able to send data reliably with no errors, a signal to noise ratio of around 10 dB would be adequate. In other words, the received signal power must be at least 10 dB higher than the noise floor, meaning the minimum signal power at the receiver must be -90 dBm. So, if the transmit power is 10 dBm an allowable path losses between signal repeaters is on the order of 100 dB and the distance between repeaters can be calculated by:

$$d_{max} \cong \frac{100 \text{ dB}}{\alpha \text{ dB/m}} \quad (51)$$

Petroleum engineers prefer to talk about distances in terms of pipe lengths. To convert the units of d_{max} to either joints or stands, divide by 9 meters or 27 meters, respectively. For a practical system to be implemented, the minimum distance between repeaters would need be at least three joints. This would allow the drill string to be tripped out in stands.

4.2. Permittivity and Dielectric Losses

Dielectric permittivity is a metric used to characterize the charge storing capacity of an insulator. It is usually given as a value relative to the permittivity of free space, ϵ_0 , which is approximately equal to 8.85×10^{-12} farads per meter (F/m). The total permittivity is equal to:

$$\epsilon = \epsilon_0 \epsilon_r \quad (52)$$

and, ϵ_r , is relative permeability, also known as the dielectric constant.

Take for instance, the two parallel, conducting plates in Figure 7, with a dielectric material separating the plates. When a DC voltage is applied, because the dielectric insulator prevents the flow of current, free charges build up on the plates. The result is a net surface charge density and an applied electric field through the dielectric. Bound charges in the dielectric react

to the applied electric field by slightly shifting their orientation, with positive charges moving in the direction of the applied field and negative charges tending away. The slight shift in orientation is called dielectric polarization, and results in an internal electric field that opposes the applied field. A reduction of the net electric field means it will require a larger surface charge density on the plates to maintain the same voltage. Thus, materials with higher dielectric polarization properties will store more energy.

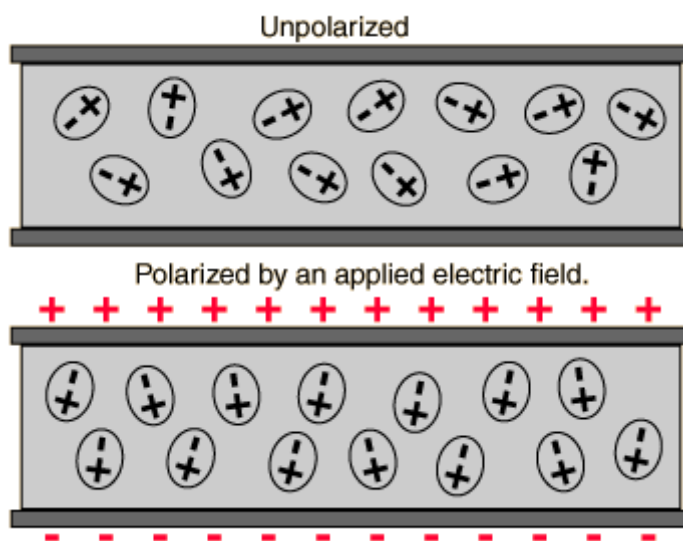


Figure 7. Un-polarized and Polarized dielectric [69]

Dielectric mechanisms can be broken down into four separate factors: dipole or orientational polarization, ionic conduction, atomic polarization, and electronic polarization. Dipole polarization occurs in what are called polar materials where, due to nature of their physical structure, a permanent electrical dipole moment is present without any applied field. When an external field is applied to the polar molecule permanent dipole moment will align with the field. Water is the classic example of a polar molecule, where a natural electrical dipole exists from the two hydrogen atoms to the more electronegative oxygen. Ionic conduction, usually only a factor at lower frequencies, is the movement of ions through a material resulting

in electric current, but the charge carriers are ions rather than electrons. Atomic polarization occurs in materials that are composed of bound positive and negative ions, such as sodium chloride. When a field is applied, the positively charged sodium ions will slightly displace in the direction of the field and the negatively charged chloride ions. Finally, electronic polarization is a displacement of the electron cloud relative the nucleus of the atom and is apparent in most materials. Electronic and atomic polarizations are more of a factor at higher frequencies, [39].

The parallel plate instance is an example of what is called static permittivity because the field being applied is not time varying. With a static field the dielectric polarization has enough time to reach an equilibrium. When the field is no longer applied to the material, the dipole moments caused by dielectric polarization will decrease to zero over time, also known as dielectric relaxation.

If an alternating field is applied to the dielectric, the dielectric polarization will try to follow the oscillations of the field. As the frequencies increase, the mechanisms of dielectric polarization and relaxation cannot keep up with the oscillations of the electric field and consequently will have less effect on the overall permittivity. The time delay between the oscillating field and the dielectric polarization can be described by a phase delay, as seen in Figure 8.

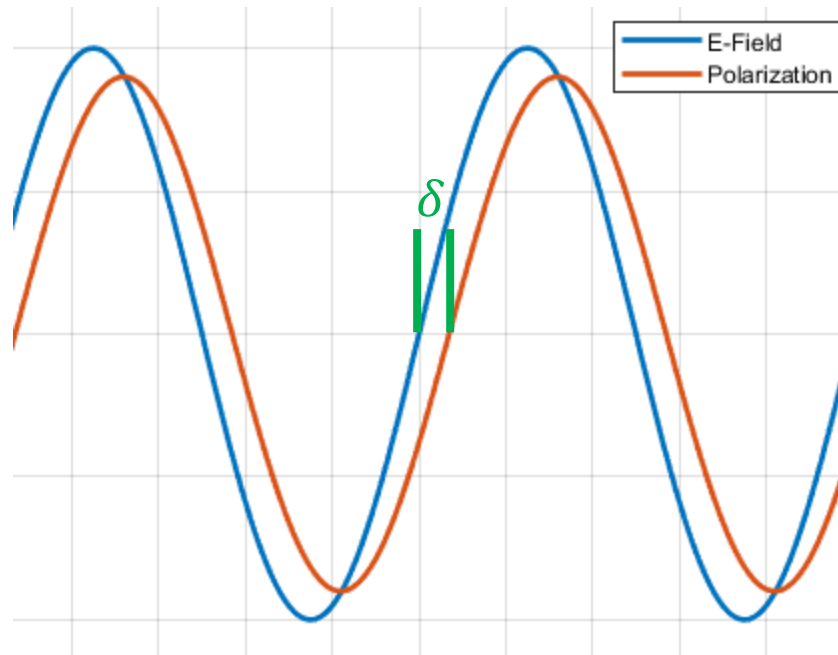


Figure 8. Out-of-phase polarization

The phase angle, δ , between the applied field and the resulting polarization is used to calculate the loss tangent, a metric characterizing losses in a system due to dielectrics. It is a simple ratio of the imaginary and real parts of the complex permittivity:

$$\tan \delta = \frac{\varepsilon''}{\varepsilon'} \quad (53)$$

Where complex permittivity, ε^* , given by:

$$\varepsilon^* = \varepsilon' - j\varepsilon'' \quad (54)$$

with ε' is the static permittivity (dielectric constant), and ε'' is imaginary part of the permittivity that results in dielectric loss. The dielectric loss is caused by a frictional damping factor due to the inertia of the charged particles [37]. Figure 9 shows the frequency dependence of both the real and imaginary parts of complex permittivity and where different types of dielectric mechanisms occur for a generic dielectric material.

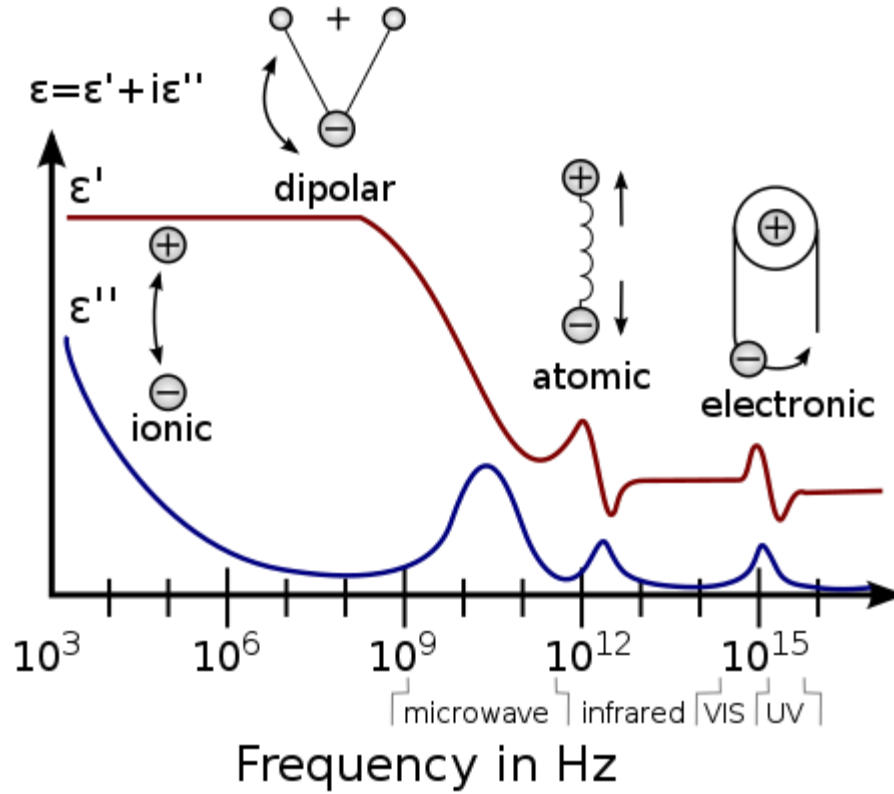


Figure 9. Generalized Complex Permittivity Values [70]

Values for dielectric properties of various materials are given in Table III, note the frequency dependence of both values for water.

Table III: Dielectric Constants and Loss Tangents [36], [50], [54]

	ϵ_r	$\tan \delta \times 10^{-3}$
Air	1.0	~0.00
Water (2.45 GHz)	78.0	160.00
Water (1 MHz)	88.0	40.00
Ice (2.44 GHz)	3.2	0.90
Silicon (10 GHz)	11.9	4.00
Teflon (10 GHz)	2.0	0.28
Paraffin (10 GHz)	2.24	0.20

4.3. Scattering Parameters

Scattering parameters, or S-Parameters, are a measure of the ratio of voltages sent and received from different ports of a system. System characteristics such as impedance match, return loss, and insertion loss can be described using S-Parameters.

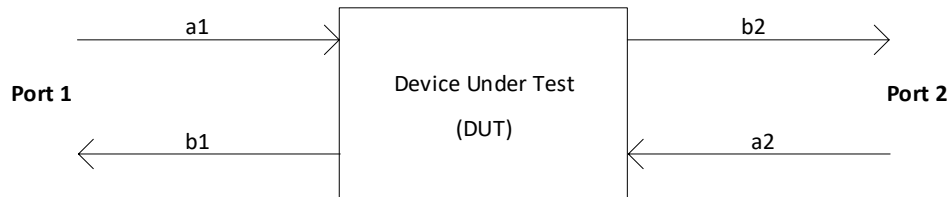


Figure 10. Scattering Parameters components

S-Parameters are given in the form S_{mn} where m is the receiving port and n is the sending port:

$$S_{mn} = \frac{b_m}{a_n} = \frac{V_m^-}{V_n^+} \quad (55)$$

where V^+ is the wave incident on the port and V^- is the reflected wave from the port. For example, S_{21} is the ratio of voltage received at Port 2 with respect to the voltage transmitted from Port 1 [36].

The S_{11} measurement is also known as the reflection coefficient and is used to calculate return loss, the power loss due to reflections caused by an impedance mismatch between the source and the device under test. Return loss is a power ratio given in decibels:

$$\text{Return Loss} = -20 \log_{10} |S_{11}| \quad (56)$$

Another loss metric calculated from S-parameters is called insertion loss and is a measure of the reduction of signal power from source to load due to the insertion of a device. For

measurements made with the same reference impedance on both ports, the insertion loss can be given by the power ratio in decibels:

$$\text{Insertion Loss} = -20 \log_{10} |S_{21}| \quad (57)$$

An ideal transmission line would have infinite return loss (no reflections) and zero insertion loss such that there would be no attenuation of the signal it is transmitting.

It can be tempting to look at the insertion loss as the total power lost in the device. However, that assumption is only true for devices with infinite return loss, i.e., the source, device under test, and load are all perfectly matched. If there is any power reflected back to the source due to impedance mismatches it will be seen as a reduction in signal power delivered through the device. Now, if conjugate matching networks are used on both sides of the device to transform the source and load impedances to match the impedance of the DUT there will no longer be mismatches and so the maximum available gain could be achieved [36].

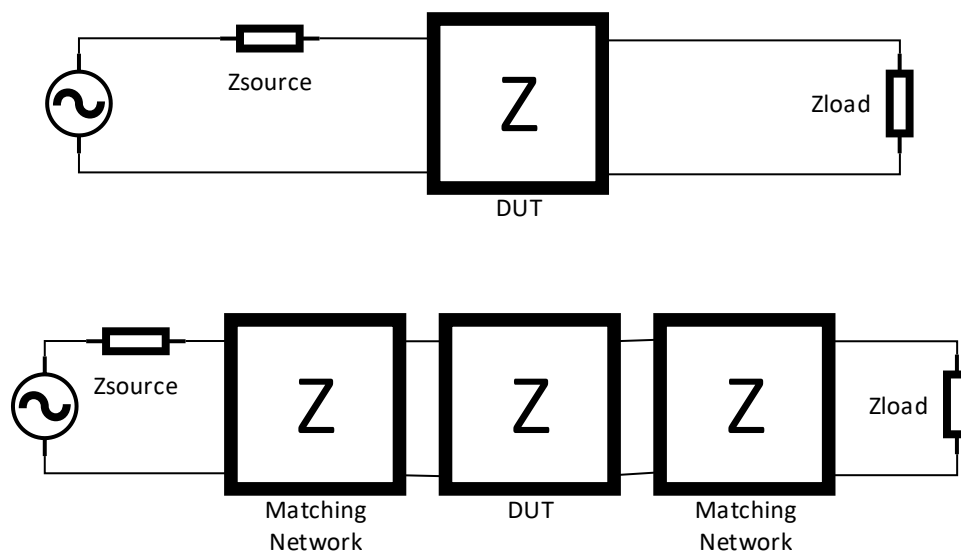


Figure 11. Device under test with and without a matching network

Given the S-parameters measured by an unmatched system, the following equations can be used to determine the maximum available gain (MAG) of a system that has been conjugately matched:

$$\Delta = S_{11}S_{22} - S_{12}S_{21} \quad (58)$$

$$K = \frac{1 - |S_{11}|^2 - |S_{22}|^2 + |\Delta|^2}{2|S_{12}S_{21}|} \quad (59)$$

$$G_{max} = \frac{|S_{21}|}{|S_{12}|} \left(K - \sqrt{K^2 - 1} \right) \quad (60)$$

where K is the Rollet's stability factor and Δ is the determinant of the scattering matrix. The maximum available gain, G_{max} , calculated in Equation (60) is only valid for unconditionally stable systems; stability is defined where K is greater than unity and the magnitude of Δ is less than unity [36]. Stability is a concern for active devices such as transistors and amplifiers but for passive devices, such as a waveguide, the magnitude of the S-parameters cannot be greater than unity due to conservation of energy. Consequently, the unconditional stability criteria will always be satisfied. The maximum available gain for passive devices can never be greater than unity and any value of MAG below unity will be a result of real losses can be defined as

$$Total\ Real\ Loss = 1 - MAG \quad (61)$$

Thus, by making a scattering parameter measurement of a waveguide and calculating the MAG the total signal attenuation due to waveguide propagation can be determined. The above equations are all given in a linear format. To look at gains in terms of decibels where a MAG below unity will be a result of real losses can be defined as

$$G_{dB} = 10 * \log_{10} G_{linear} \quad (62)$$

5. Experimental Setup and Model Design

5.1. Measurement Setup Design

Drill pipe is expensive and can be difficult to source on a small scale so instead “black pipe”, typically used for low-pressure plumbing, was used to build a measurement setup. Since the primary focus is the propagation losses caused by the different fluids, as long as the losses caused by the material properties of the pipe are accounted for, it is straightforward to isolate the losses due to the fluids.

The dominant propagation mode frequency of a waveguide is determined by the internal radius so it was important to select a pipe that would closely represent a realistic drill string. Drill pipe comes in a wide range of sizes suitable for all types of applications with typical values of internal diameter ranging from 2-6 inches. To fall inside that range, a pipe with an internal diameter of 4 inches was selected. Four 3.2 meter sections were purchased allowing for up to 42 feet of pipe to be measured. One of the sections of pipe was cut into fourths to yield smaller sections allowing for different combinations of length of pipe and easily managed lengths for the probes. The pipe selected is nominally listed as 4” inner diameter but was measured using digital calipers at 4.03”, or for the purposes of making calculations using the equations previous derived, a radius of 51.2 mm. The resulting cutoff frequency, in air, is 1.717 GHz.

One challenge of using “black pipe” steel is the unknown makeup of the actual steel used in the production of the pipe. So an initial theoretical analysis of expected losses is difficult but, as seen in Section 6, the critical electromagnetic properties of the metal can be measured.



Figure 12. Multiple sections of Pipe

For ease of description and documentation in measurement file names, the two different lengths of pipe were termed “shorts” (0.8 meters) and “longs” (3.2 meters). The total length and approximate volume of the different combinations of pipe sections used are listed in Table IV. Short sections of pipe referenced by “S” and long sections of pipe referenced as “L.”

Table IV: Pipe Combination Lengths and Approximate Volumes

	Length (m)	Volume (liter)
S-S	1.6	14.76
S-S-S	2.4	22.33
S-L-S	4.8	44.29
S-L-L-S	8.0	73.82
S-L-L-L-S	11.2	103.34

To get energy into the pipe a waveguide launcher had to be designed. Waveguide launchers can be designed with the intention of either exciting the electric field, known as an E-Plane launcher, or the magnetic field, known as an H-Plane launcher. Since the dominant mode trying to be excited is a Transverse Electric wave, it was desirable to have an E-Plane launcher. An easily implemented E-Plane launcher is a coaxial cable to straight jack connector, where the center pin extends into the pipe. SMA connectors were selected because the cables available for the vector network analyzer also use SMA. The Amphenol straight jack connectors purchased did not have a center pin long enough to reach all the way into the pipe so 3 mm diameter copper rods were also purchased and modified to extend the length of the pin. The original connector and modified probe are shown in Figure 13.



Figure 13. SMA Connector, left, and SMA Connector with copper extension

With a probe designed, determining the placement inside the pipe was the critical next critical step in creating an effective waveguide launcher. The location of the probe with respect

to the closed end, also known as the back short, will set the impedance of the waveguide launcher. Distance from the back-short in a rectangular waveguides is typically a straightforward design of one quarter wavelength of the desired operating frequency. Cylindrical waveguides, however, are a little more complicated. The test setup being used also has the added difficulties of a rounded end cap as well as a discontinuity in the waveguide radius where the pipe ends and the cap begins.

An HFSS model, discussed in further detail in Section 5.4, was built to examine the placement of the probe and a parametric sweep simulation run to test a range of distances from 0.2λ (60 mm) to 0.377λ (116 mm). From the simulation results, shown in Figure 14, a back-short distance near 108 mm looked to yield the highest return loss indicating the best placement to optimize the impedance match.

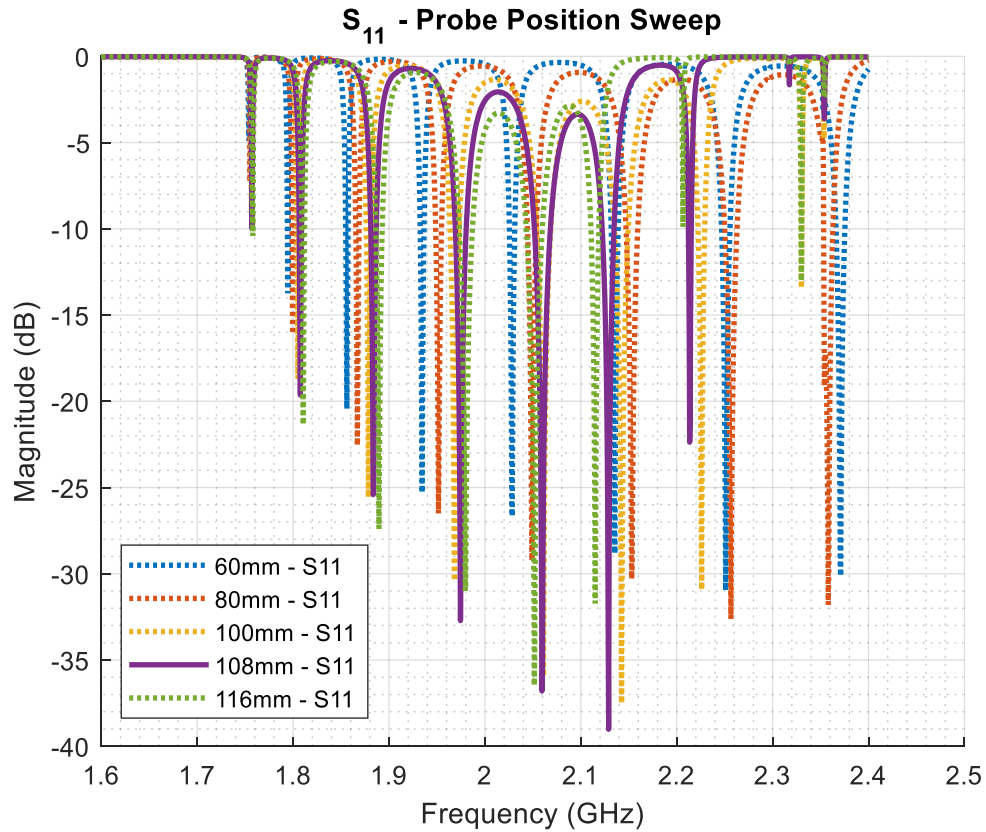


Figure 14. Detailed Model Probe parametric sweep simulation

Though because the model had not been fully validated the parametric sweep was only a reference. To be able to tune the distance of the probe to the back-short a slotted system was designed.

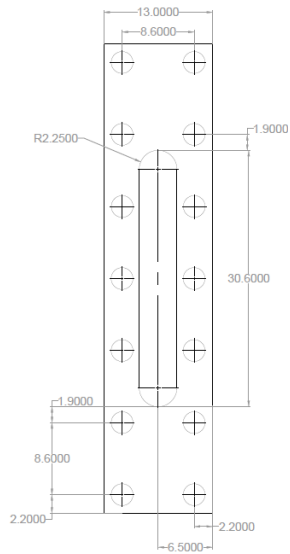


Figure 15. Probe Plate CAD drawing, left, and modified pipe

The slot machined in the pipe allows the probe to slide forward and backward with tapped holes at intervals matching the dimensions of the SMA connector plate, creating four individual probe locations.



Figure 16. Probe positions 1-4, left to right

A single section of pipe was modified initially and only after determining the probe placement system would work as designed was the second section of pipe modified. With the second modification complete, the S_{11} of both probe setups were measured and compared in

Figure 17. The nearly perfect overlap of the S_{11} measurements of each probe indicates a good impedance match.

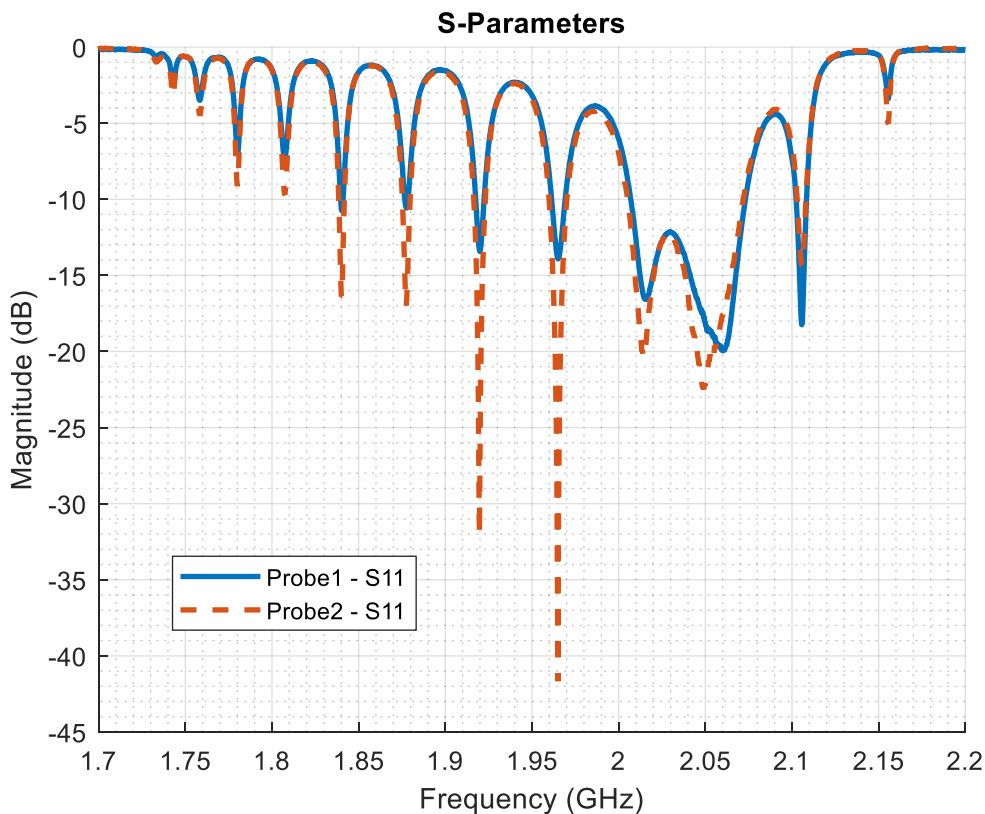


Figure 17. S_{11} comparison of modified probes

To facilitate filling the pipe with fluids, holes were drilled and tapped for $\frac{1}{2}$ " NPT pipe in the center of both end caps. A valve was placed on one end cap and a funnel/hose was attached to the other end. The end of the pipe with the funnel was elevated above the valve to allow any air in the pipe to escape out a bleed hole drilled in the funnel cap.

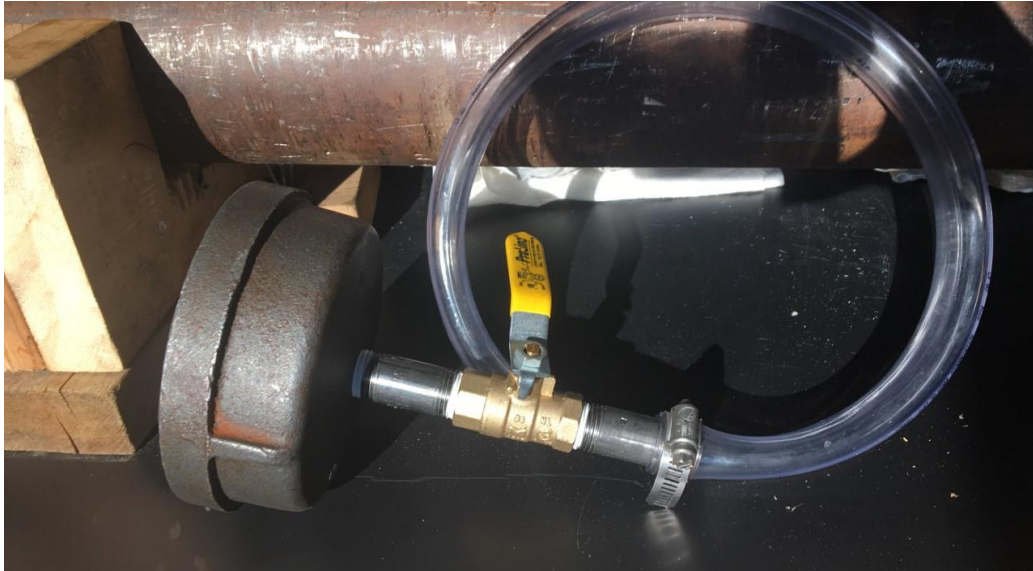


Figure 18. End cap valve modification

A measurement with only air filling the pipe was made to determine the effect of the modifications. Figure 19 shows the results of the comparison where “PreValves” is the unmodified end caps and “PostValves” is the drilled and tapped end caps.

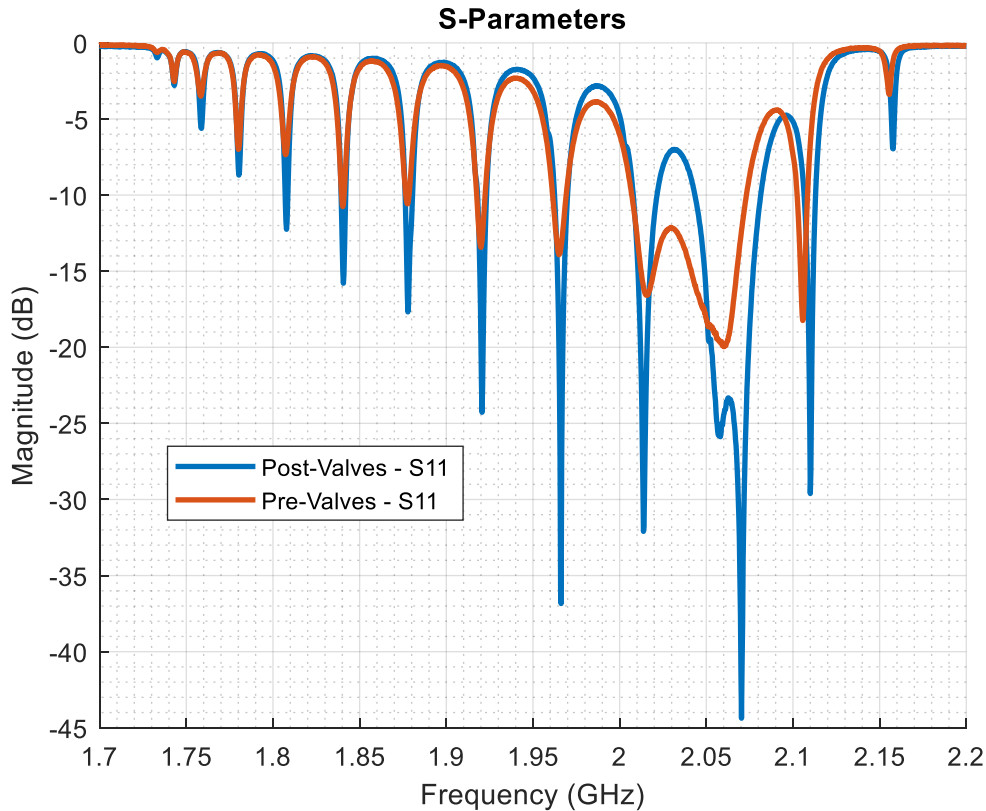


Figure 19. S₁₁ comparison of pre and post valve modification

The added holes on the end caps electrically look like a waveguide to waveguide transition but the radius of the valve is roughly eight times smaller than the pipe. Therefore the cutoff frequency will be eight times higher, and so no energy will be able to propagate in the valve section of the pipe.

5.2. Safety Precautions

Since the main base fluid used in the following experiments was diesel fuel, the inherent risks of flammability needed to be taken into consideration. All diesel fuel was stored in standard yellow fuel canisters with proper labeling. Those canisters, when not in use, were stored in a flammable materials storage cabinet. To prevent any buildup of static electricity that could lead

to an igniting spark during transfer of fuel into the pipe, a grounding clamp was attached to the pipe.

In the event of a spill, any amount of oil in the waste water system would be unacceptable so a two-layer containment system was built using black PVC lining, seen in Figure 20. A wood frame covered in lining created a basin the full length of the setup. Each section of pipe was then individually wrapped with PVC lining and towels placed near the potential leak spots, such as couplings, endcaps, and probe locations. Multiple 5-gallon buckets were on hand with enough empty to contain at least two times the volume of fluid held in the pipe. Floor drains were also covered with plastic lining. A bentonite clay-based cat litter and several dry towels were also on hand to absorb any oil spills. The additional materials used to create the oil-based fluids also have minor health risks so vinyl gloves and eye protection were used during the mixing and handling of any of the oil based fluids.



Figure 20. Spill containment setup

5.3. Network Analyzer

A Tektronix TTR500 vector network analyzer was used for all scattering parameter measurements. The TTR500 is capable of sweeping frequencies in the range of 100 kHz to 6 GHz with an output power range of -50 to +7 dBm, where dBm is a power ratio in decibels

relative to 1 milliwatt. A software interface called VectorVu is used to setup and control the network analyzer.

Before any measurements of a device are made, the VNA needs to be calibrated using a calibration kit of electrical standards: short circuit, open circuit, 50 ohm load, and through connection. Each specialized standard has known RF characteristics including inductance, capacitance, and electrical delay. The calibration sequence provides a measurement of electrical reflections and losses incurred by the cables, ensuring the scattering parameters measured are of the device under test (DUT) and not affected by the cables or connectors used to attach the VNA to the device. To perform a calibration sequence, measurements are made on Port 1 and Port 2 using each electrical standard. The software can then calculate and apply a calibration to any subsequent measurements, effectively subtracting any effects caused by the cables and moving what is called the “calibration plane” to the DUT.

The Kirkby Microwave 3.5mm Calibration Kit was used to perform a calibration of the TTR500 VNA before every measurement. Calibration coefficients for the Kirkby Cal standards were supplied in a format designed to be read by an older model VNA and weren't in a format the VectorVu software was capable of reading. The founder of Kirkby Microwave, Dr. David Kirkby, provided the necessary data, which can be found in Appendix A: Kirkby 3.5mm Cal Kit Standards Coefficients. Using the supplied coefficients a “Kirkby Cal State” was programmed into the VectorVu software and saved as an .xml file which can be recalled anytime a calibration is performed. Systems states in the VectorVu allow the user to store for future use the current settings of the program, including calibration, responses being measured, and display scales.

To start a full two-port calibration process the “base_state.cstate” was recalled. The “base state” is a system state that was created at the beginning of the research to include the Kirkby

Calibration coefficients as well as set up the stimulus range from 1.7 GHz to 2.2 GHz, the frequency range for the air-filled pipe. The base state also sets the displayed measurements to be S_{11} and S_{21} as well as sets the number of division displayed to 10 and the scale to 5 dB per division.

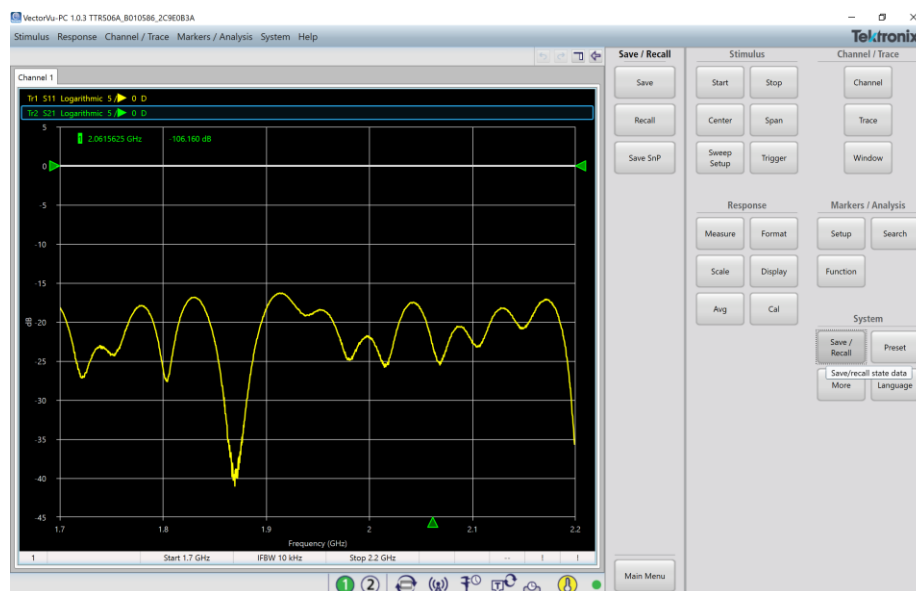


Figure 21. VectorVu main display

With the stimulus set to the desired frequency range, the calibration process is initiated by clicking “Cal” under the “Responses” menu. Clicking “Calibrate” and “Two-port Calibration” will bring up a dialog box shown in Figure 22. Attach a standard to the desired port and press the corresponding button in the VectorVu software. When making the single port calibration standards measurements it is a good idea to keep a 50 Ω load on the other port to prevent accidental radiation that could influence the calibration measurement or violate FCC regulations. A calibration measurement is made for all four standards on both ports.

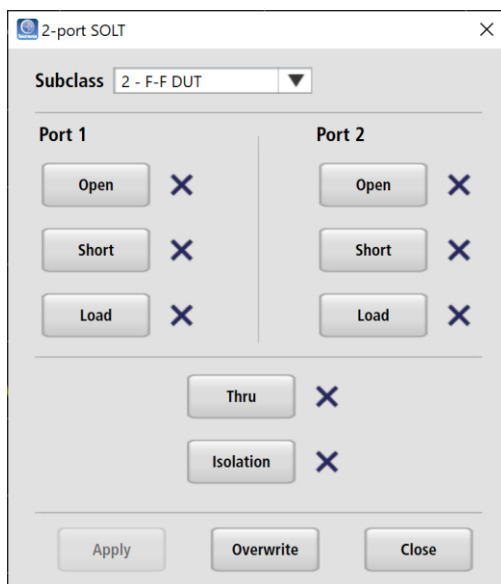


Figure 22. Two-port SOLT calibration dialog box

When every calibration standard has been measured, clicking the “Apply” button calculates the calibration parameters the software will use to correct any future measurements. After the calibration has been completed and applied it is always a good idea to verify the correction is accurate. One easy way to check the calibration is to view the S_{21} measurement of the “thru” standard. If properly calibrated, there should be virtually no loss across the entire frequency range. Figure 23 shows the results of an S_{21} measurement of the thru standard after calibration, notice the nearly flat response with a value of only -0.05 dB.

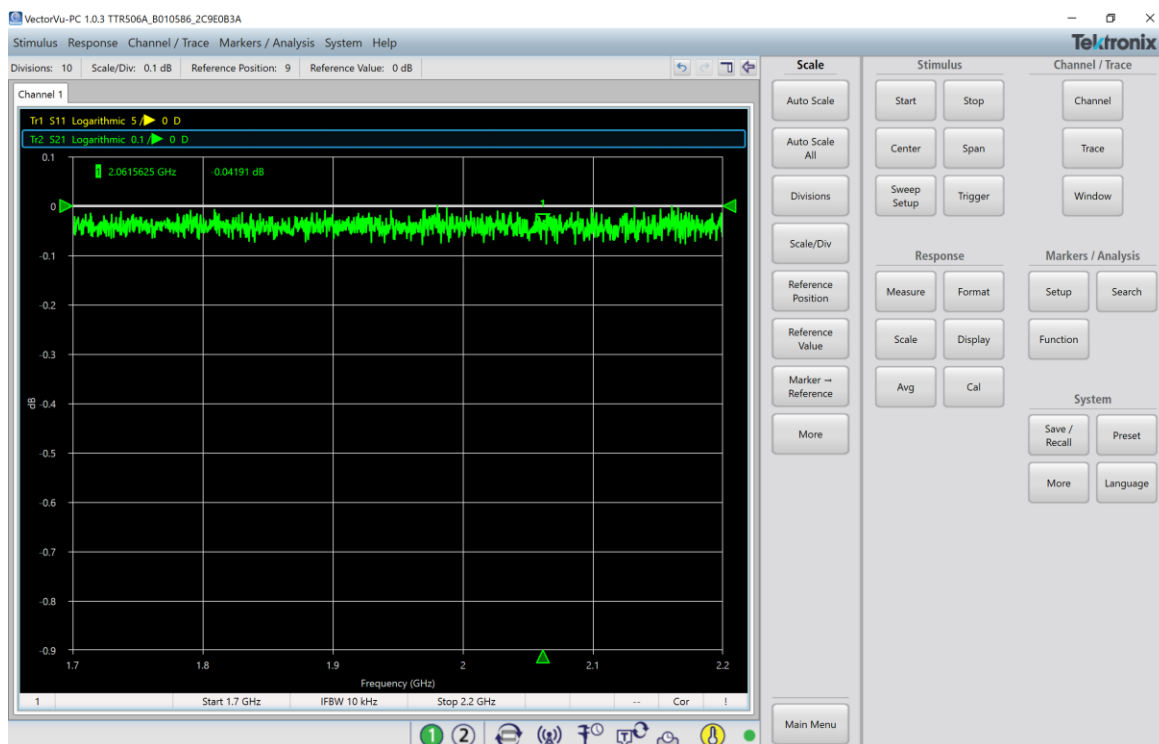


Figure 23. S_{21} and S_{11} measurement of the “Thru” standard after calibration

If the calibration was determined to be accurate it is then saved as a system state to be recalled later. The entire calibration process needs to be repeated for any frequency range of interest. Before each fluid measurement was performed, a calibration state was built for the range of 1.7 GHz to 2.2 GHz and the air-filled pipe was measured and compared with previous air measurements to verify a consistent starting point for each experiment. Then a calibration state was built for a frequency range based on expected dielectric constants.

After the VNA is calibrated, measuring scattering parameters is a straightforward procedure. The device under test is connected to the VNA, taking care to keep the cables connecting the two devices in the same positions as during the calibration. The scattering parameters can be seen on the visual display of the VectorVu software and the data can be saved as “Touchstone Files” by going to the menu under the System>Save/Recall and clicking “SnP”.

Touchstone files are a standard file format designed for saving data for a wide range of measurement equipment including frequency, reference impedance, scattering parameters, and other port data.

One significant challenge of making RF measurements on long sections of pipe is the VNA calibration process. Typical VNA measurements are on small filters or printed circuit board transmission lines where the dimensions the device under test are similar in size to the standards used for calibration so the position of the cables can be fixed during both calibration and measurement. With pipe lengths up to 11.2 meters there was no way to make the thru calibration measurement with the cables in the same position. During the short, open, and load standard measurements cables were placed as close as possible to the ports on the pipe. The location, orientation, and curvature of cables were also noted so the positioning of the cables could be replicated as closely as possible when making measurement. For the thru calibration the long cable, always Port 2 of the VNA, was circled back to the VNA with radius as wide and consistent as possible, to minimize any change of impedance due to self-coupling.



Figure 24. Long section of pipe being measured with the VNA

5.4. Finite Element Analysis Simulation

To confirm measurements made and dielectric properties calculated, as well as to further explore the electromagnetic wave propagation, the full test setup was modeled using finite element analysis software. ANSYS engineering simulation software is a full finite element analysis (FEA) suite used to model and analyze an extensive range of systems. One package in the ANSYS Electromagnetics suite is the High Frequency Structure Simulator (HFSS), built to aid in the design of high-frequency electromagnetic products such as antenna, RF components, and printed circuit boards. HFSS allows the designer to create three-dimensional structures, apply material properties, define radiation boundaries, set input and output ports, and measure various electromagnetic properties, such as S-parameters.

In finite element analysis, complex three-dimensional models are broken down into smaller components called meshes that are geometric shapes, such as cubes, tetrahedra, or pyramids, allowing the software to perform calculations on a known geometry. Most FEA packages require a mesh size, or minimum mesh size, to be defined by the user prior to simulation. Decreasing the mesh size will increase the complexity of the simulation and in turn increase the total time required to perform the simulation. If the mesh size is too large the calculations will be inaccurate, so a delicate balance between accuracy and efficiency is needed. HFSS, however, has the benefit of using adaptive meshing where the software begins by creating a default mesh based on the dimensions of the modeled geometries and then solves the electromagnetic fields for the entire model. Field solutions are analyzed for potential errors, and the meshes are refined in locations where an error is detected. The model is repetitively refined until the difference between S-Parameters of consecutive adaptive passes converges to a user defined threshold. So, instead of requiring the user to define a range of mesh parameters, HFSS allows the user to specify only a maximum delta in S-parameters [71].

5.4.1. Simple Pipe Model

A three-foot section of steel pipe was relatively easily modeled using two cylinders: an “outer” cylinder with a 4.5 inch diameter and an “inner” cylinder, 4 inches in diameter. The length of the inner cylinder was 0.5 inches shorter than the outer cylinder to build the capped end of the pipe. “Stainless Steel” was selected in the Assign Material properties dialog, thereby defining the outer cylinder with a conductivity of 1.1×10^6 S/m and a relative permeability of unity. A clone and subtract operation with both geometries selected subtracted the inner cylinder from the outer cylinder leaving a hollow cylinder with one open end. The cloned inner cylinder was then given the material properties of “Vacuum,” defined in the standard Materials Library with a dielectric constant of unity and a loss tangent of zero.

A launching probe was designed in a similar fashion using cylinders to create a center pin made of copper that extended halfway into the pipe. An outer dielectric made of Teflon was built to insulate the center pin from the pipe. The software reported geometry overlap issues when trying to make the dielectric flush with the surface of the pipe so it was extended 1 mm into the pipe and a 2mm tall conductor surrounds the dielectric outside the pipe. Dimensions for the center pin and dielectric were designed to model a 50Ω coaxial cable.

Electrical excitations in HFSS can be defined in a number of ways depending on what is being simulated and what are the measurements of interest. Types of excitations include wave port, lumped port, voltage, and current. A wave port excitation was the ideal choice as they are used to excite electromagnetic fields at the boundaries of a modeled structure and can be used to measure S-parameters. Wave ports can also be used to excite multiple modes so they are ideal for waveguide excitations.[71].

A full two-port pipe model was then designed using the single port model as the base. By decreasing the length of the internal “vacuum” cylinder the outer pipe became a fully enclosed

pipe. The probe geometry was then duplicated and mirrored across the center of the pipe and a new wave port excitation defined on the second port.

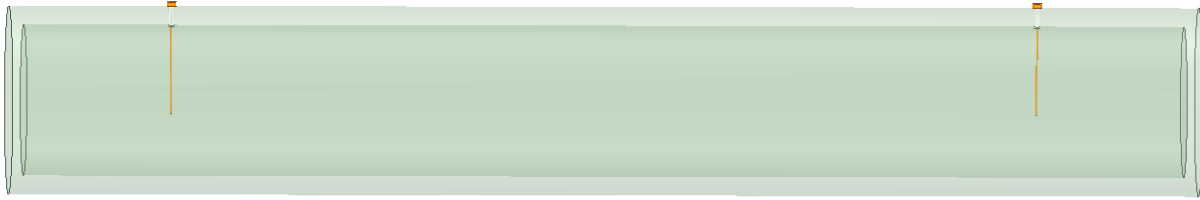


Figure 25. Simple Two Probe model

Simulation solutions have a great degree of configurability but for the first simulations all parameters were left at default. A single adaptive solution was set up to solve 1.7 GHz and a frequency sweep solution was added to solve for 1-5 GHz. The single adaptive solution is used to solve the mesh and the frequency sweep solves the scattering parameters using that mesh.

The scattering parameters measured using the simple two-port model are consistent with waveguide theory. As seen in Figure 26, all energy is reflected back below the cutoff frequency and as the frequency gets further in to the ideal range of the TE_{11} mode, less and less energy is being reflected. Though the results are still not a great representation of the real system, the simple two-port model was successful progression in understanding how to model waveguides in HFSS.

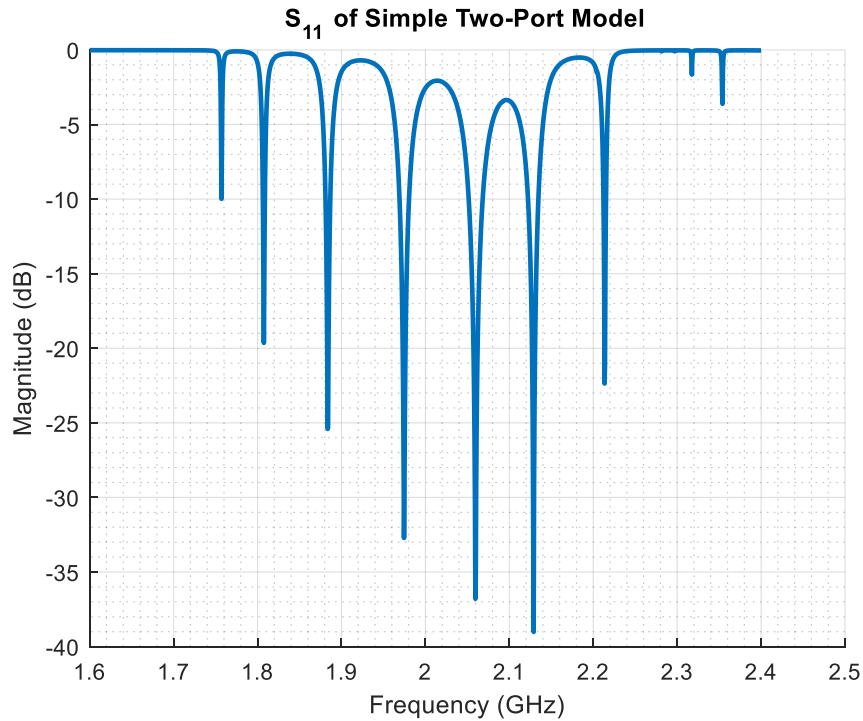


Figure 26. Simulated S_{11} of Simple Two-Port Model

5.4.2. Detailed Model

To create a more detailed model of the test setup, precision measurements of each piece of hardware were made and defined in HFSS. The SMA probe plate was modeled using the built in “Gold” material properties and the extensions of the probes used the “Copper” material. End caps were designed with the rounded inside. Two separate sections of pipe were built with a 1 mm air gap surrounded by a coupling piece in the middle.

Physical features not modeled that could affect propagation are the threads of the coupling and end pipe as well as any surface roughness of any of the metals, but because these features are all small ($< 1\text{mm}$) compared to the expected wavelength ($\sim 30\text{mm}$) their effect should be minimal. The additional complexity of the model would also unacceptably increase simulation time.

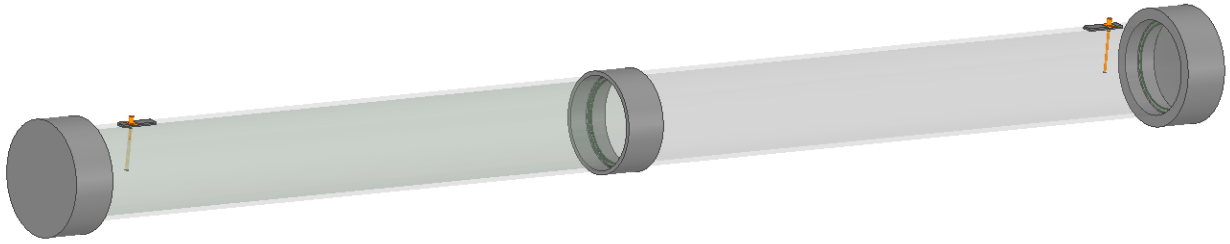


Figure 27. Detailed Two Probe model

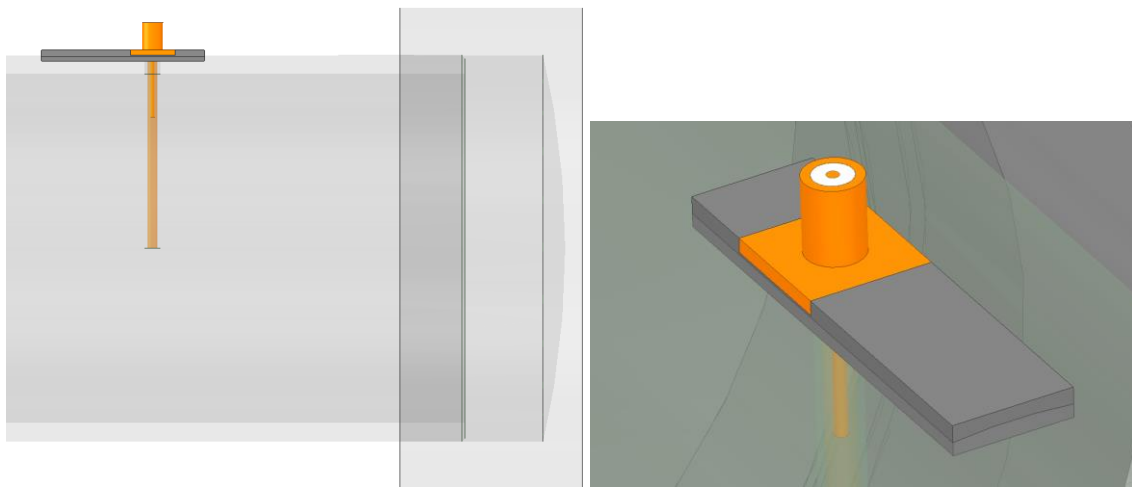


Figure 28. Detailed probe and rounded cap

Wave ports at each coaxial probe were defined and integration lines were drawn between the center conductor and the outer conductor, see Figure 29. Integration lines tell the program the direction and location of the largest field potentials for a given excitation. The settings of the single adaptive solution were also updated to use a First Order Iterative Solver from the default Direct Solver solution to reduce RAM usage.

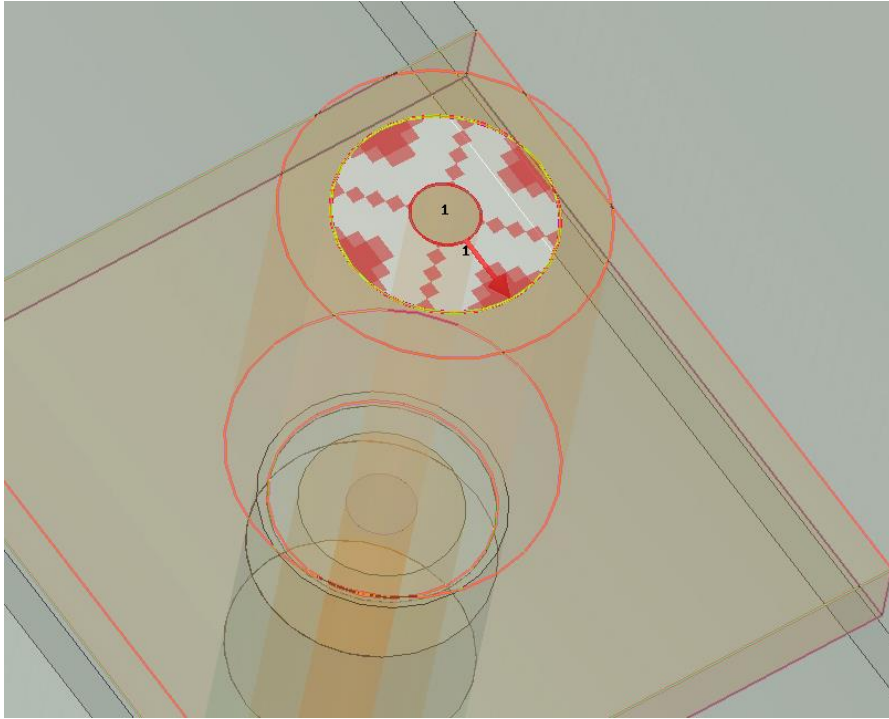


Figure 29. Wave port with defined integration line

With two ports modeled it was now possible to do a full scattering parameters measurement, plotted in Figure 30. The nulls in the S_{11} measurement, and the peaks in the S_{21} measurement, are a result of impedance mismatches between the wave impedance of the waveguide and the $50\ \Omega$ impedance of the probes. The mismatch causes reflections that lead to longitudinal standing waves in the waveguide.

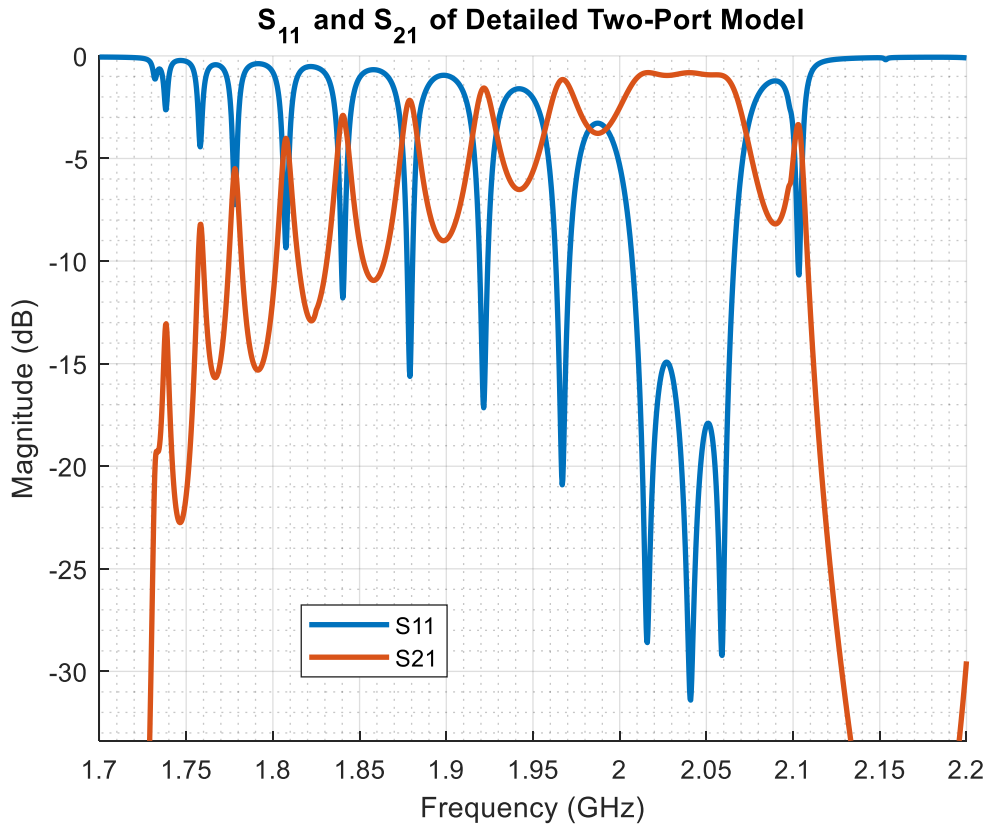


Figure 30. Simulated scattering parameters of the Detail Two Port model

The spacing of the nulls is a function of the length of the waveguide and the guided wavelength of that frequency. Take for instance, the null at 1.966 GHz the guided wavelength is 0.3133 meters and the total distance between probes is 1.410 meters. A wave sent from Probe 1 that is reflected back will travel 2.82 meters, nine full wavelengths. A standing wave that results from the reflection has a node exactly at Probe 1 and the VNA sees no reflection. As the length of the pipe increases, the frequency separation between these nulls should decrease.

The maximum available gain was then calculated using Equation (60), plotted in Figure 31, and clearly shows the benefit of the MAG calculation. If the probes feeding the waveguide were conjugately matched, there would be no reflections and a flat response across the TE₁₁ operating frequency range is seen.

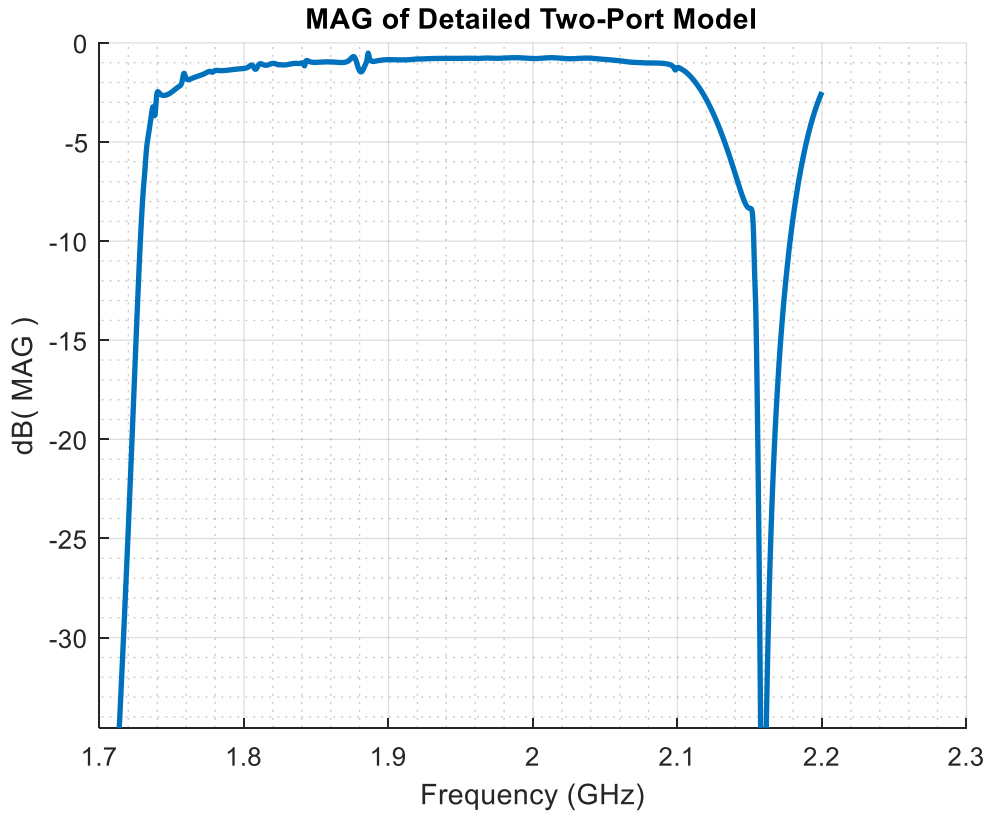


Figure 31. Calculated MAG of the Detailed Two Port simulation

A second detailed model was also built with three sections of pipe. The length of the middle section of was pipe defined using a “Project Variable” allowing for easy adjustment of the total pipe length for simulation of the longer sections to be measured.



Figure 32. Three Pipe Section model

6. Measurements and Simulations

6.1. Air-filed Pipe

6.1.1. Pipe Characterization

Before any measurements of unknown fluids were made it was critical to understand to a number of variables that may influence the propagation and or measurements of an air-filed pipe.

To test the four possible probe positions the S_{11} was measured in each position and compared in Figure 33. The first position (blue trace) gives the best match with the widest bandwidth, roughly 50 MHz of below 10 dB.

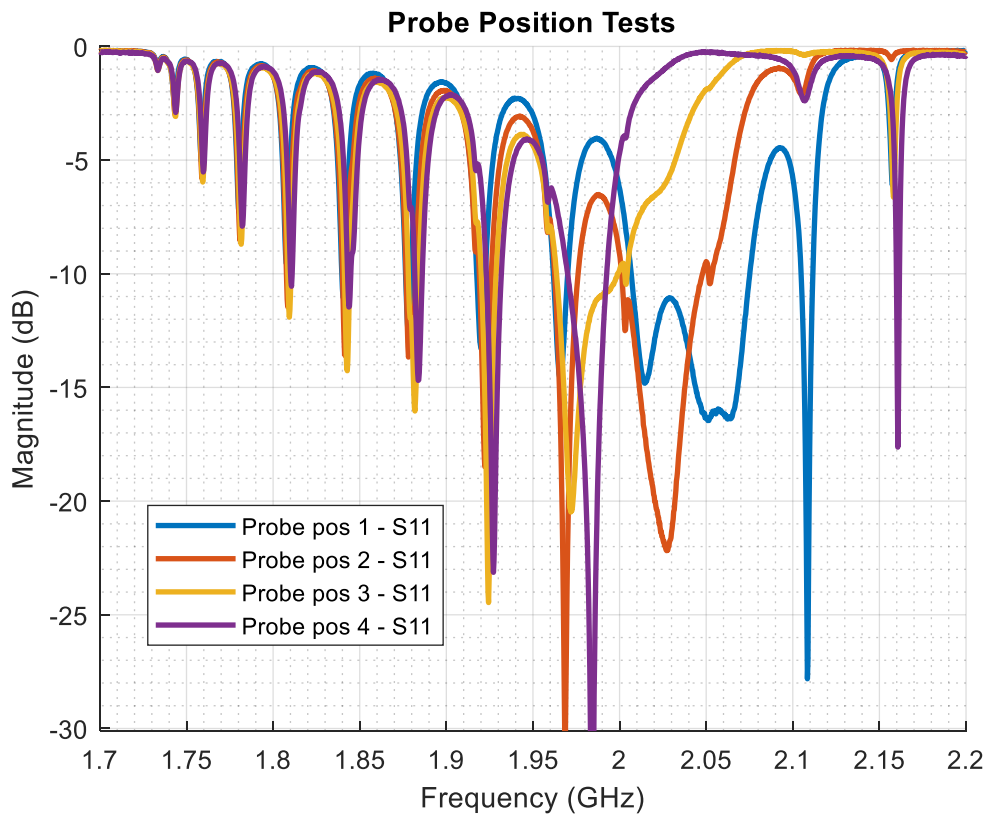


Figure 33. S_{11} measurements of the probe tuning position tests

The TE_{11} propagation mode is effectively a vertically polarized wave. Hence, if the receiving probe is not vertically aligned with the sending probe the electric field will not be able

to properly excite the probe and the signal will hit the receiving end back-short and be reflected back to the source. A series of measurements were made to determine the effect of the vertical orientation of the probes relative to one another, seen in Figure 34. Keeping Probe 1 positioned vertically, the S_{21} was measured with Probe 2 offset 0, 45, 90, and 180 degrees from vertical. The insertion loss is greatest when Probe 2 is horizontal, 90 degree offset (purple trace), at 45 degrees a large portion of the energy is transferred but larger reflections occur. At 0 degrees and 180 degrees the probe is vertically aligned, allowing maximum power transfer.

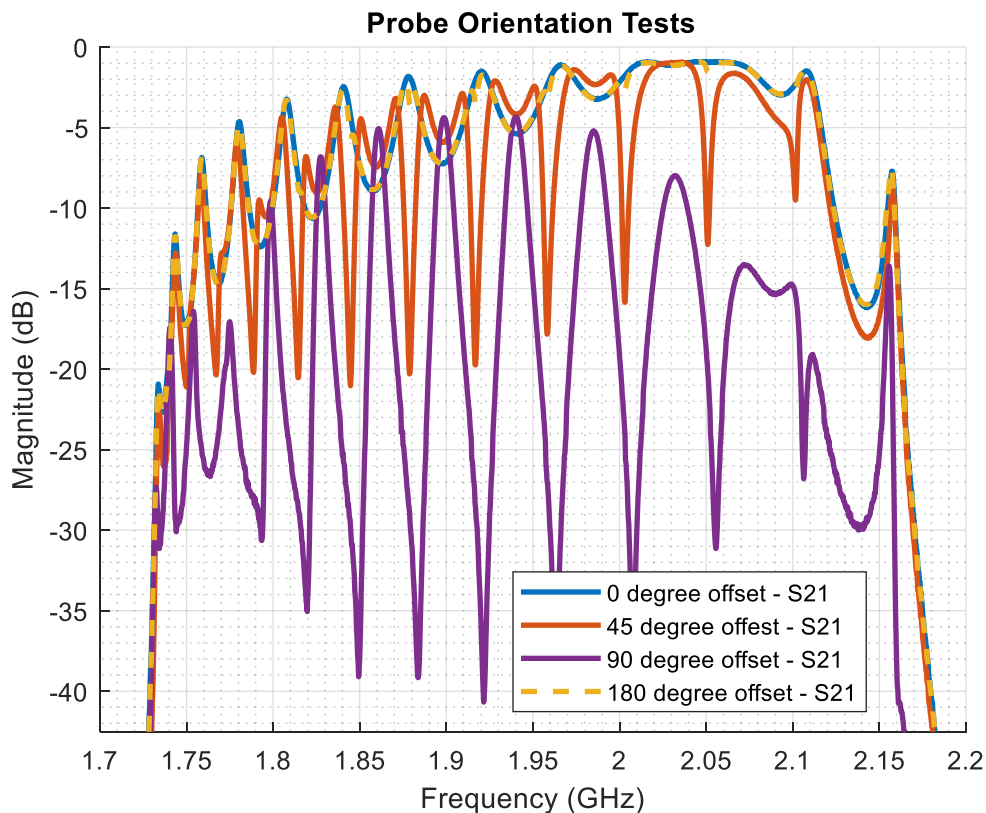


Figure 34. S_{21} measurement of the probe orientation tests

The primary mode of interest is TE_{11} but to test the propagation of higher order modes a sweep from 1.5 GHz to 6 GHz was measured. The first nine modes of waveguide propagation are seen in the MAG plotted in Figure 35. The theoretical cutoff frequencies for TE modes are

marked with a red 'x.' A red circle indicates cutoff frequencies of the TM modes. Depictions of the electric (solid) and magnetic (dashed) field lines of each propagation mode are seen near the bottom of the graph. Around 3.6 GHz there is a circle and an 'x' overlapping. This is due to the TE_{01} and TM_{11} modes having the same cutoff frequencies. However, because the electric field in TE_{01} mode is circularly polarized and a vertically polarized probe was used to launch the waves it is unlikely the energy propagating in the 3.5 to 3.9 GHz frequency range is propagating in the TE_{01} mode.

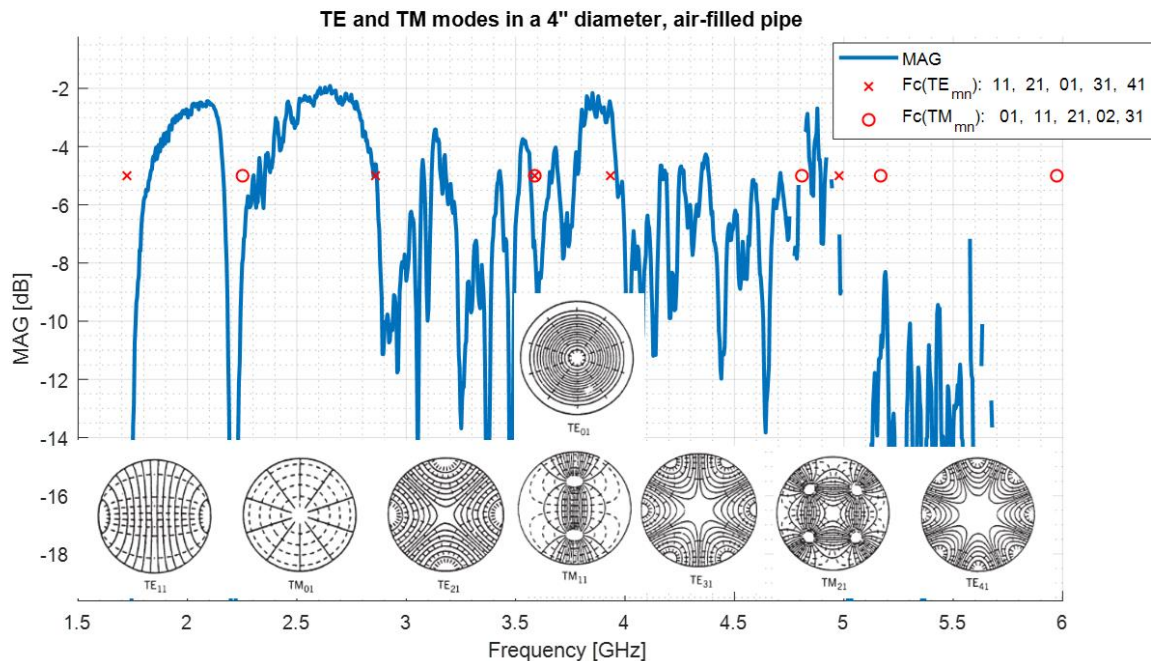


Figure 35. MAG calculation and possible field configurations of an air-filled pipe

One potential for loss in the measurement setup that is not described by the attenuation constant is in the transition between sections of pipe. If the pipe faces are not perfectly square or fully tightened such that the faces of the pipes are not touching there will be a discontinuity in the waveguide. At each joint there is a metal coupling on the outside of pipe, so the inner diameter of the coupling is the roughly the same as the outer diameter of a pipe. Increasing the

diameter of a waveguide increases the impedance seen by a wave propagating in the guide, and so the transition between the pipes to the coupling will simply look like a small impedance mismatch.

Several tests were performed to determine the effect of any gap between sections of pipe. Using the two short sections, measurements were first made with the faces of the pipe touching. Then the pipe was unscrewed by one full rotation leaving a small gap between the faces of the pipe but the pipes were still connected with the coupling and another measurement taken. This was repeated until the pipe was no longer touching the coupling. Three more measurements were taken with an air gap of 2, 5, and 10 centimeters between the pipe and the coupling. A selection of the maximum available gain results of the measurements are plotted in Figure 36.

Moving from no gap to nine rotations unscrewed changes the overall length of the system. The increase in length shifts the frequencies where the ripples in the response occur but the real, total loss is negligible.

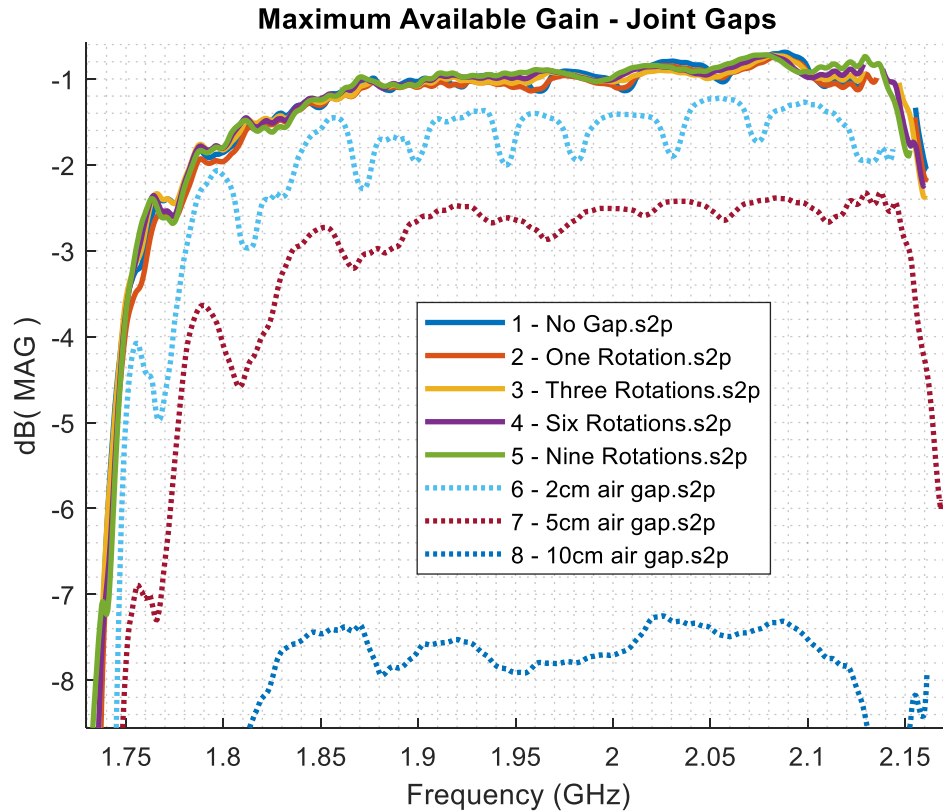


Figure 36. Calculated MAG of the Joint Gap Tests

The first step in understanding propagation losses in a waveguide filled with an unknown fluid is to determine the losses caused by current conduction in the pipe. Since the pipe being used is a steel of unknown make up it is essential to characterize the significant electrical properties of the pipe before any meaningful fluid measurements can be made.

Air is considered a lossless dielectric with $\tan \delta$ equal to zero, [39], so, going back to Equation (49), any losses measured in an air-filled waveguide will be due entirely to conduction of current in the pipe. From Equation (42), at the proposed operating frequency of 1.15 times the cutoff frequency, the factors affecting the conduction losses are: magnetic permeability of the pipe, $\mu_{r_{pipe}}$; conductivity of the pipe, σ ; radius of the pipe, r ; and the dielectric constant of the

medium filling the pipe, $\epsilon_{r_{medium}}$. The radius of the pipe is a fixed 51.2 mm and the dielectric constant of air is unity. The only unknowns are the conductivity and permeability of the pipe.

Conductivity of steel is highly dependent on the type but values are generally on the order of 10^6 S/m. The conductivity, σ , of a material can be calculated by

$$\sigma = \frac{\ell}{R * A} \quad (63)$$

where ℓ is the length of the material in meters, A is the surface area in square meters, and R is the electrical resistance in ohms.

An experiment, depicted in Figure 37, was designed to measure the conductivity of the pipe to be used in the research. By forcing a DC current through the pipe and measuring a voltage drop across a length of the pipe, ℓ , the resistance, R , was calculated using Ohm's law:

$$R = \frac{V}{I} \quad (64)$$

where V is the voltage drop measured and I is the current forced through the pipe. The inner and outer diameters of the pipe were measured using digital calipers and the surface area was calculated to be 0.0029 m^2 . With measurements for the length, surface area, and resistance the conductivity can be calculated from Equation (63).

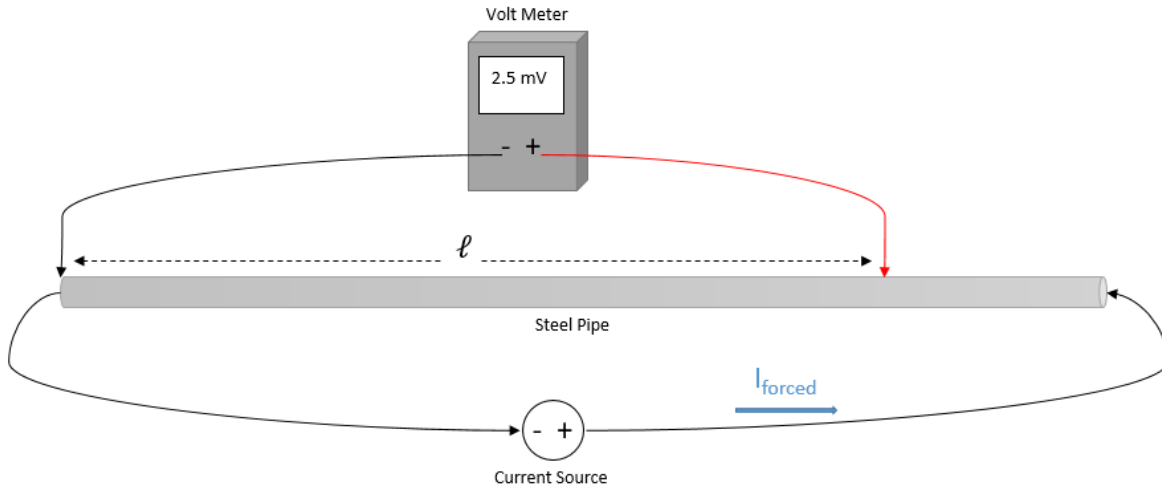


Figure 37. Conductivity measurement experiment setup

By performing the conductivity measurement experiment multiple times using a range of forced currents and varying lengths of pipe, an average bulk conductivity was calculated to be 4.15×10^6 S/m. Results and parameters of each conductivity measurement taken can be found in Appendix B: Pipe Conductivity Measurements.

Similar to conductivity, the magnetic permeability of steel is greatly affected by the composition of the metal. Values of relative permeability for steel range anywhere from 1 to 10,000, though typical steels used in “black pipe” are listed in the 10-100 range. Now, with a value for conductivity the only unknown in Equation (42) is the magnetic permeability. So from a measurement of propagation loss in the air-filled pipe of a known length, the permeability can be back calculated. Similar to the conductivity experiments, the permeability was determined through a series of S-parameter measurements taken on five different lengths of pipe. Using the S-parameter measurements the maximum available gain for each length was calculated, seen in Figure 38.

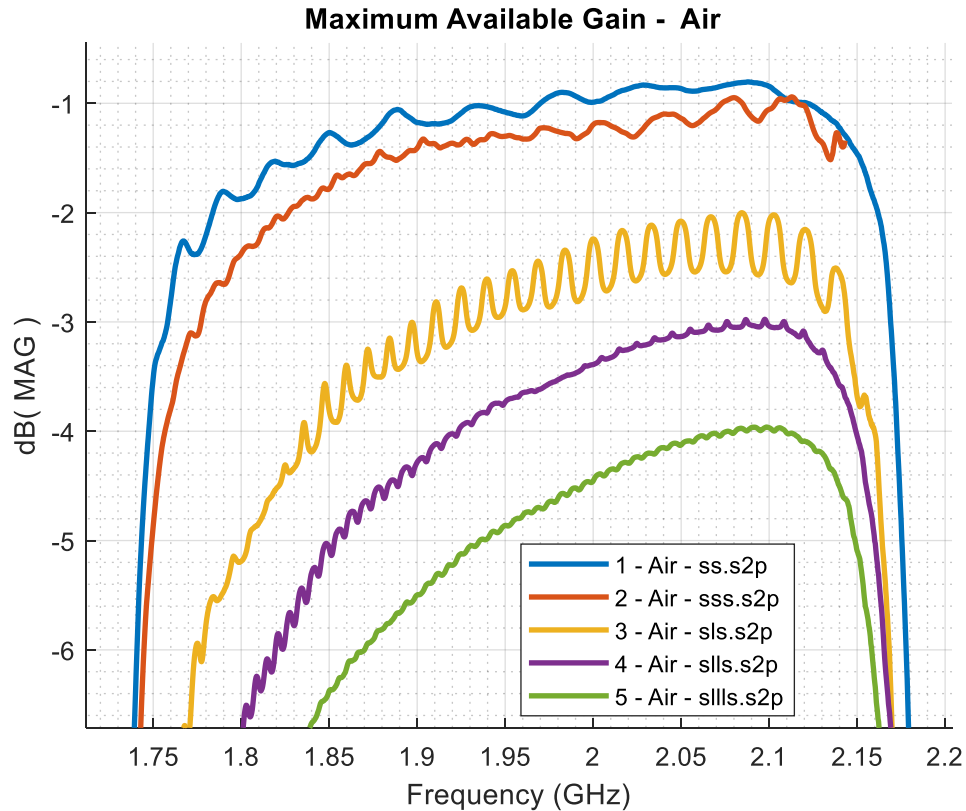


Figure 38. Maximum available gain calculate for various lengths of air filed pipe

From the MAG calculation plot, an operating frequency of 2.082 GHz was selected as the point where the gain is maximized (total loss is minimized) across all lengths of pipe measured. Converting the MAG at the selected frequency to a total loss measured and using the known lengths of a pipe a linear-least squares regression was performed in MATLAB. The data and fit curve are plotted in Figure 39. The R^2 value for the curve fit was 0.998, indicating a very good fit.

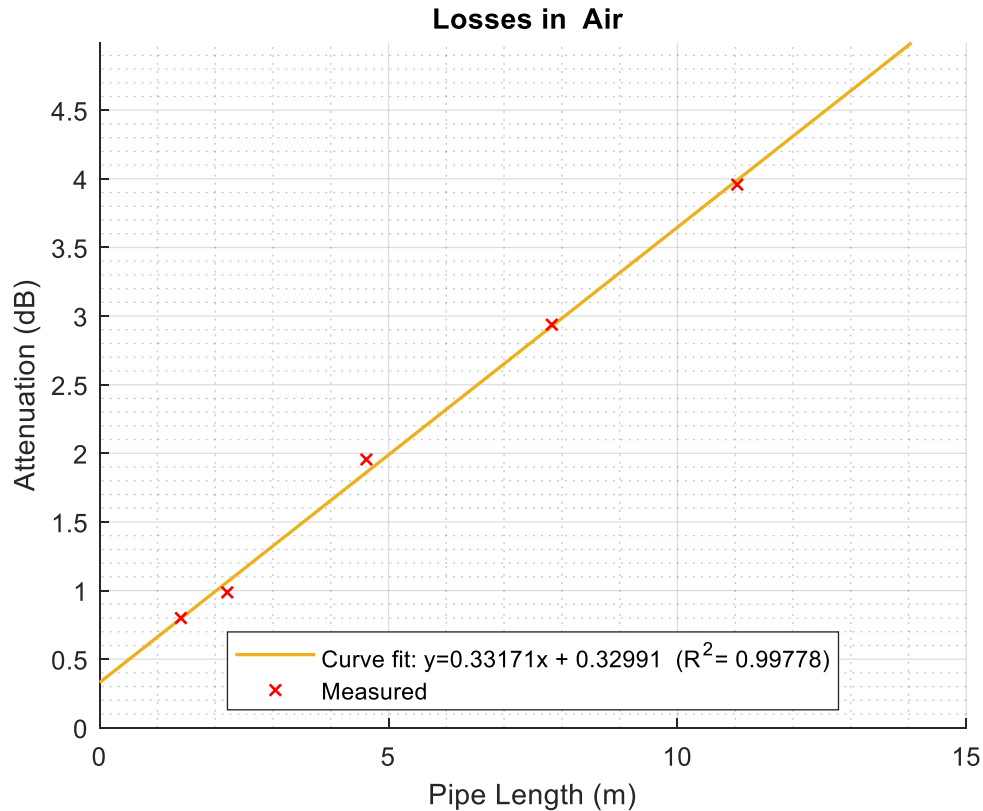


Figure 39. Measured and Curve Fit losses in air at 2.082 GHz

The key result from the regression is the slope of the line, representing the attenuation in dB per meter, which can be used to calculate the magnetic permeability. By measuring multiple lengths of pipes the losses at the probes can be seen in the vertical intercept of the fit line, meaning, in the air-filled pipe there is around 0.176 dB of signal attenuation caused by each probe. By taking the slope of 0.33171 dB/meter, converting it back to Nepers per meter, and using that value in Equation (31), the relative magnetic permeability, μ_r , was back calculated to be equal to 72.7.

If the measurement test setup were extended into a full communication system the maximum distance between signal repeaters, from Equation (51), is 270.5 meters, or 30 joints of Range 2 drill pipe.

6.1.2. Simulations

With the pipe fully characterized, more accurate simulations were possible using the detailed two-port model. The material properties of the steel were updated to model the conductivity and permeability calculated from prior experiments. The scattering parameters of a short-short section of pipe were simulated and compared to the measured results in Figure 40.

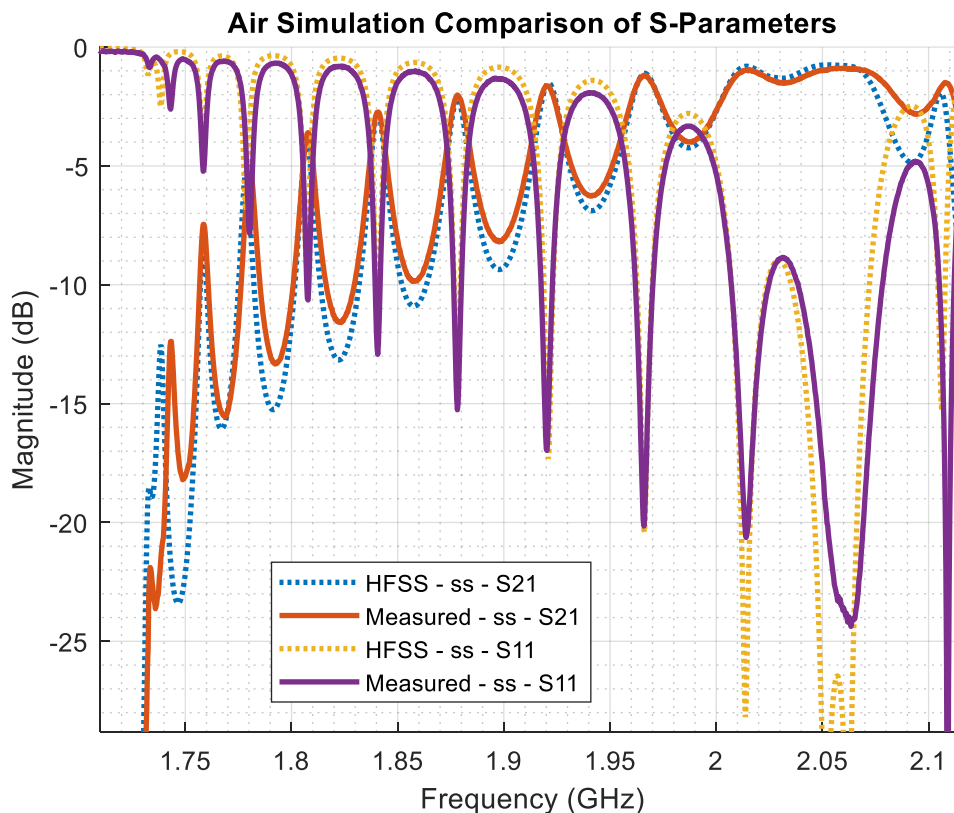


Figure 40. Comparison of simulated and measured S-Parameters of an Air Filled Pipe (short-short)

A short-short-short section of pipe was then simulated with similarly good results, seen in Figure 41. The S_{11} simulation appears to deviate from the measure results around the 2.05 GHz range but keep in mind the vertical scale is logarithmic. For S_{11} , a measurement of reflection, the difference between -20 dB and -30 dB is the difference between 1% of the signal power being reflected and 0.1% being reflected.

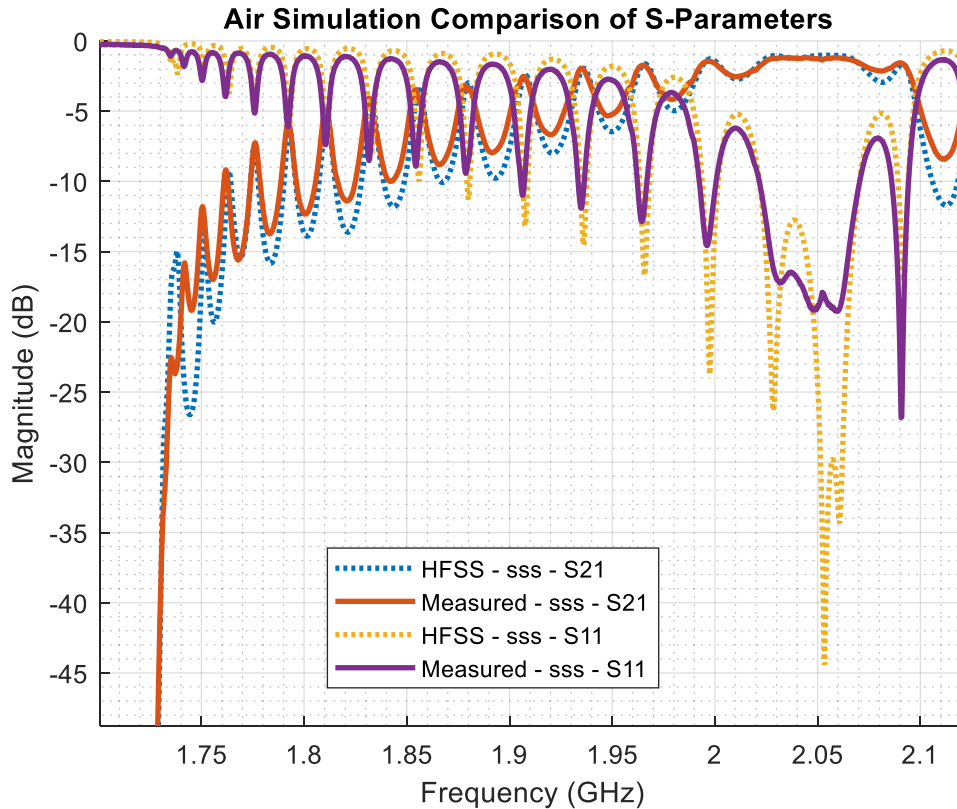


Figure 41. Comparison of simulated and measured S-Parameters of Air Filled Pipe (short-short-short)

When the simulated pipe length was extended to the short-long-short combination (4.8 meters) the simulation starts to break down. In Figure 42, the S_{21} and S_{11} measurements of the short-long-short simulation have values greater than 0 dB, but because the system is a passive these values do not make physical sense indicating the model is not working correctly. Though in the pass band of 1.8-2.1 GHz the simulation results match the measured results.

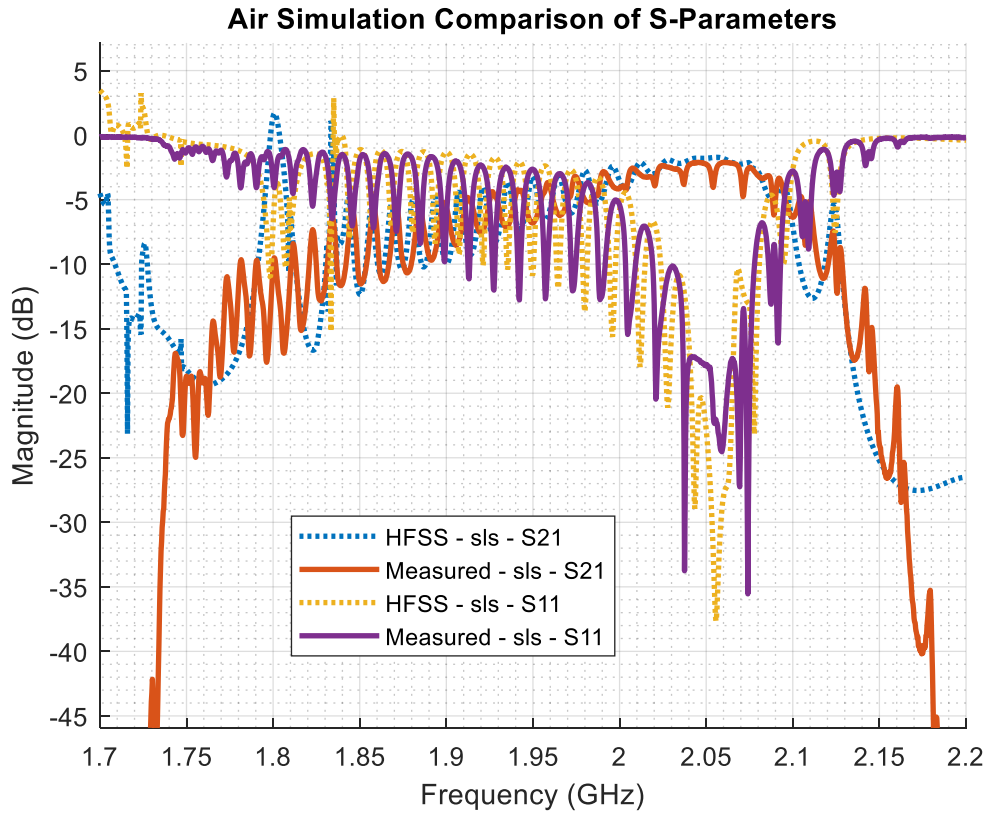


Figure 42. Comparison of simulated and measured S-Parameters of Air Filled Pipe (short-long-short)

The extend length of the short-long-short section being modeled appears to be hitting the boundaries of the single mesh solution. By adding multiple adaptive solutions, the mesh is solved at different frequencies allowing for a better mesh across the range of the frequency. When an adaptive solution was set up at 1.7, 1.9, 2.1 and 2.5 GHz the resulting frequency sweep solution was a better fit to the measured data, as seen in Figure 43.

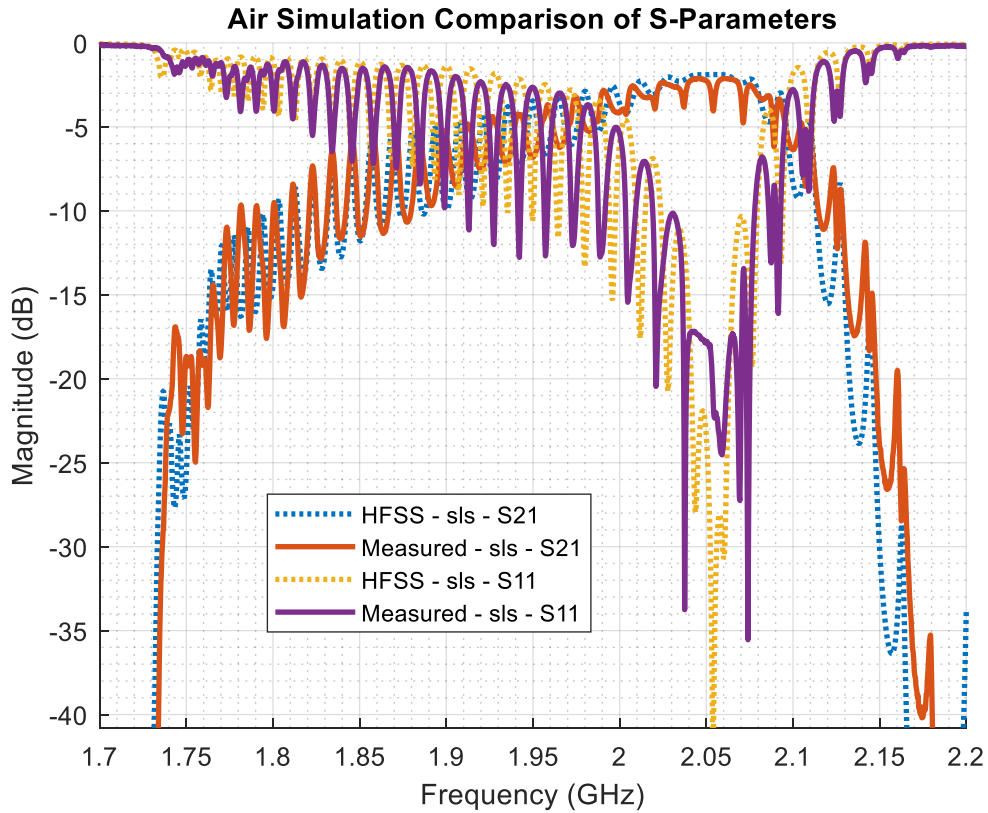


Figure 43. Updated simulation comparison of Air Filed Pipe (short-long-short)

However, when the length of the simulated pipe is increased to two shorts and two longs, the simulation again fails to track the measured results seen in Figure 44. Additional adaptive solutions do not appear to improve the longer simulations.

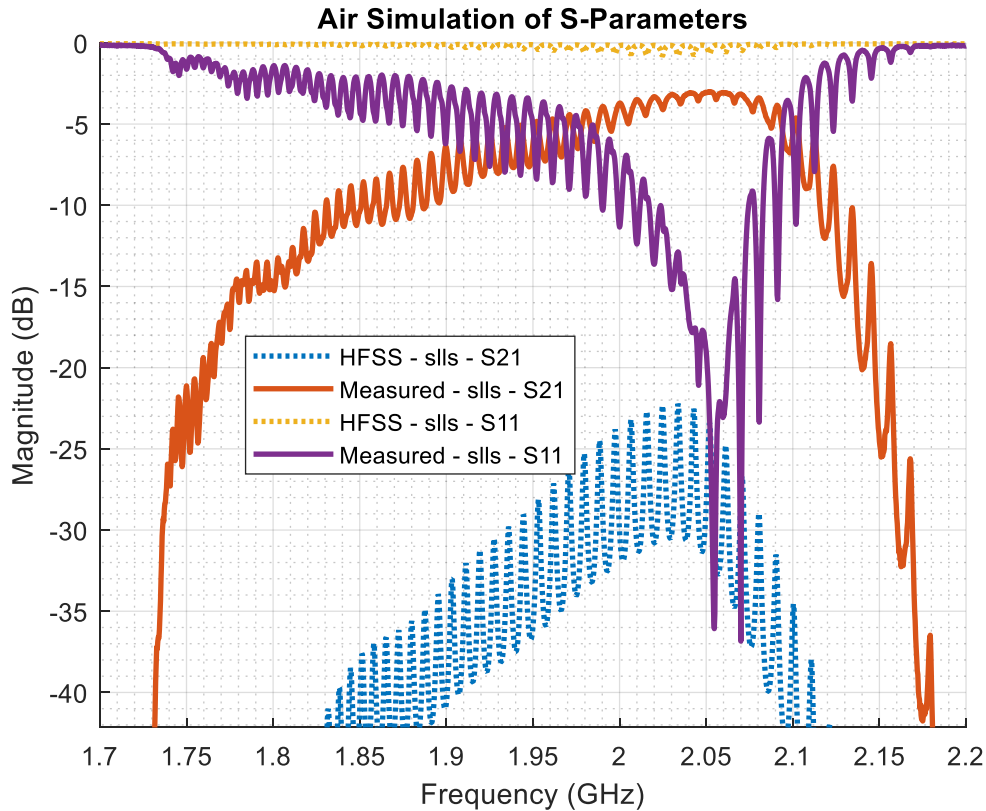


Figure 44. Comparison of simulated and measured S-Parameters of Air Filled Pipe (short-long-long-short)

6.2. Water Based Fluids

6.2.1. Distilled Water

To validate the method used for measuring fluids with unknown dielectric properties and calculating loss tangents a fluid with known properties, distilled water, was measured. Using two different lengths of pipe sections, “short-short” and “short-short-short”, the scattering parameters of distilled water at 70 degrees Fahrenheit were measured and the MAG calculated and plotted.

The point where the MAG starts to come up from negative infinity can be used to find the cutoff frequency. However if a single threshold, say -35 dB, was used to select the frequency, the longer pipe lengths will appear to have a shifted cutoff frequency because there is more total attenuation, see Figure 45. Instead, as seen in Figure 46, the MAG for each measurement was

normalized by the maximum MAG calculated and a threshold of -50 dB was used to determine cutoff frequency. For distilled water a cutoff of 193.1 MHz was found, which can be used to back calculate a dielectric constant of 78.07 from Equation (30). The same procedure was used to calculate dielectric constants for all following fluid measurements.

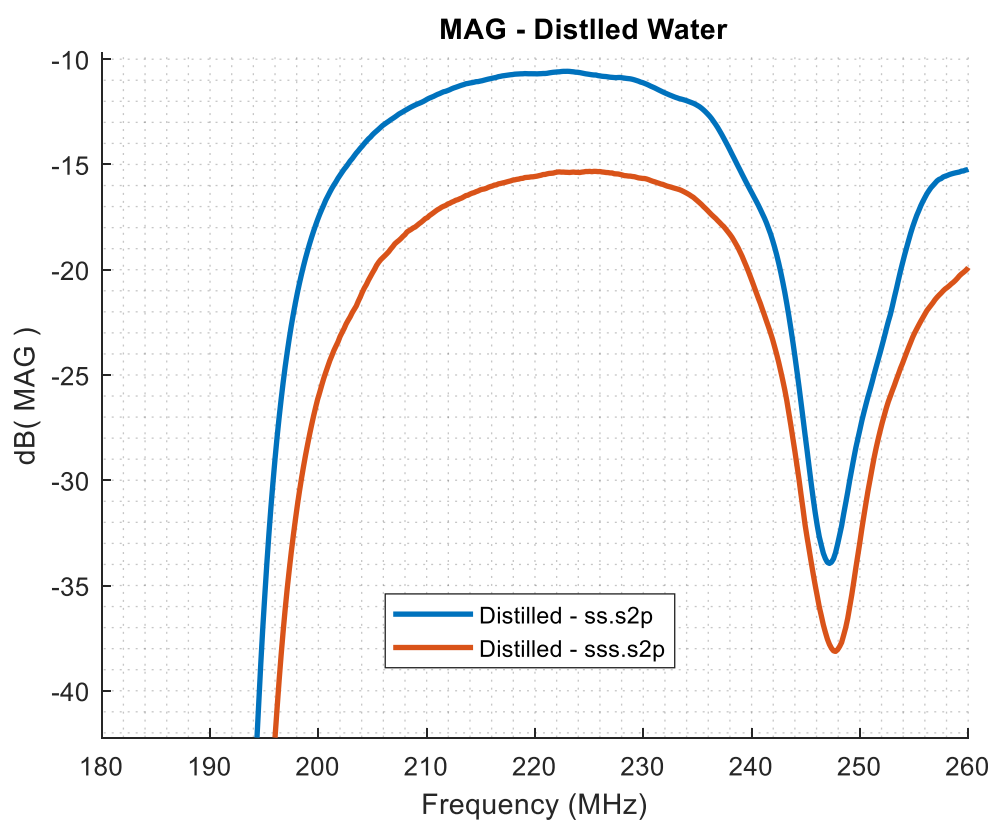


Figure 45. Calculated MAG of Distilled Water

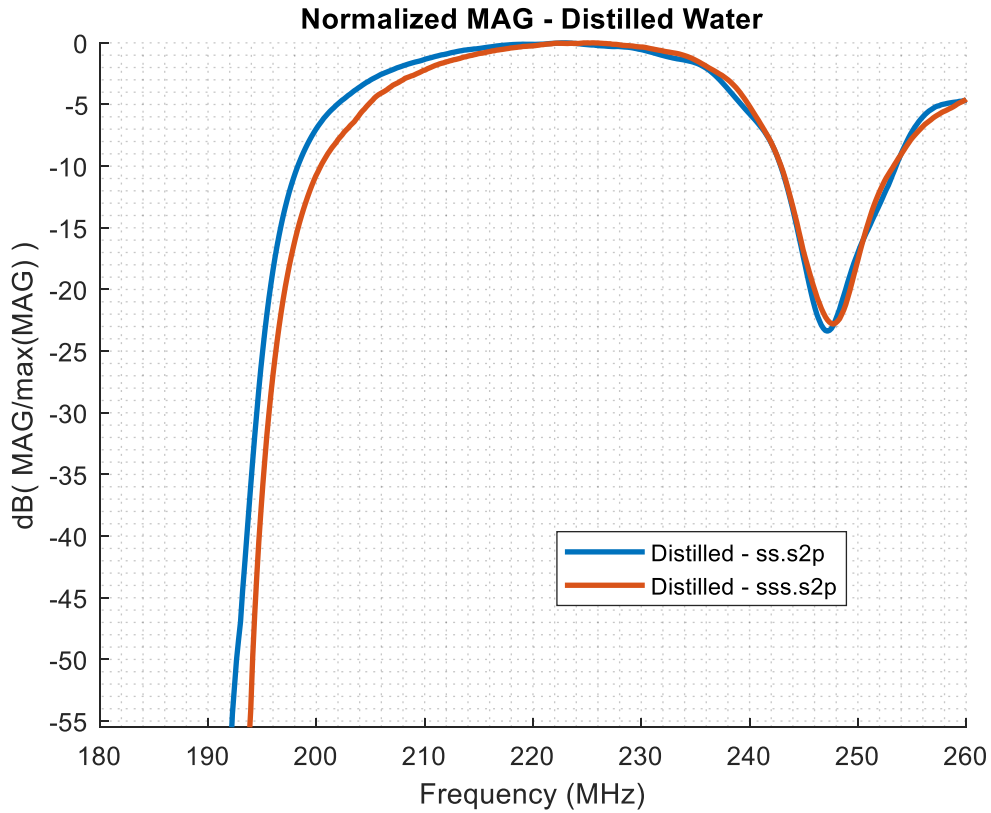


Figure 46. Normalized MAG of Distilled Water

From the MAG calculation, a frequency of 225 MHz was selected as the operating frequency in the middle of the passband that maximized the available gain. The total losses were extracted from the selected frequency and fit to a curve using the known lengths pipe sections measured, seen in Figure 47.

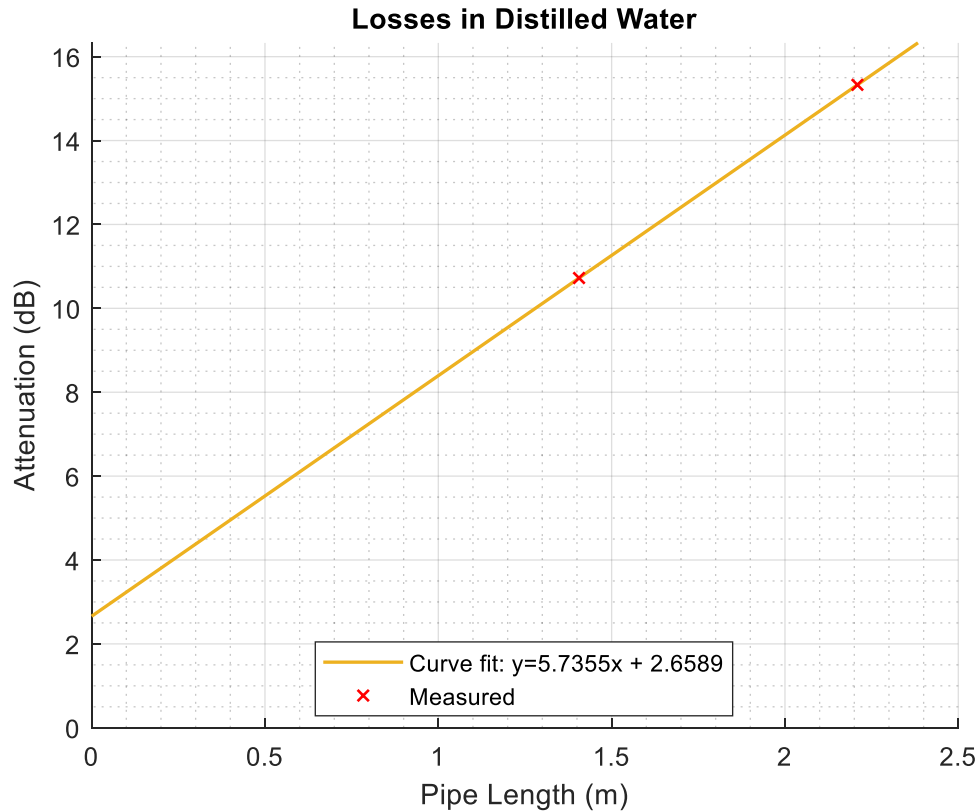


Figure 47. Measured and curve fit losses in distilled water

The selected frequency of 225 MHz and the previously measured material properties of the pipe produce a theoretical value for conductor losses calculated at 1.0626 dB/m. Subtracting the theoretical conductor loss from the total loss, given by the curve fit slope of 5.7355 dB/m, leaves 4.6728 dB/m caused by dielectric loss, which can be converted back to Np/m and substituted into Equation (45) to back calculate a loss tangent of 0.013175. Again, the same procedure was used to calculate loss tangents for all the following fluid measurements.

One study, [54], found the complex permittivity of distilled water as a function of frequency can be calculated by

$$\varepsilon^* = \varepsilon' - j\varepsilon'' = 5.62 + \frac{74.59}{1 + \frac{jf}{17.0 \times 10^9}} \quad (65)$$

where j is the imaginary unit, $j = \sqrt{-1}$, and f is the operating frequency. At 225 MHz, the equation calculates a loss tangent value of 0.01231, a 6.83 percent difference from the above measured value, and a dielectric constant of 80.19, a 1.42 percent difference.

Another paper detailing dielectric properties of water between 0-30 degrees Celsius, [53], describes the complex permittivity of water, ϵ^* , using a bi-modal distribution based on Debye relaxation:

$$\epsilon^* = \frac{\epsilon - \epsilon_2}{1 + j\omega\tau_1} + \frac{\epsilon_2 - \epsilon_\infty}{1 + j\omega\tau_2} + \epsilon_\infty \quad (66)$$

where ϵ and ϵ_2 , are the static permittivity for two modes, τ_1 and τ_2 are the relaxation time constants for the modes, ϵ_∞ is the optical permittivity, and ω is the operating frequency. The paper gives a range temperature-dependent values for each of the parameters.

Dielectric relaxation parameters of water						
T (K)	ϵ	τ_1 (ps)	ϵ_2	τ_2 (ps)	ϵ_∞	χ^2
273.35	87.57	17.67	6.69	0.9	3.92	0.131
278.15	85.89	14.92	6.76	1.0	4.10	0.094
283.15	83.93	12.70	6.57	0.9	4.08	0.118
288.15	82.24	11.00	6.64	1.0	4.34	0.071
293.15	80.31	9.60	6.53	1.2	4.42	0.067
298.15	78.32	8.38	6.32	1.1	4.57	0.106
303.15	76.39	7.39	(5.75)	0.9	4.60	0.090
308.15	74.91	6.69	6.22	1.5	4.74	0.060

Figure 48. Relaxation Parameters of Water

Using the values from the 293.15 K row, the closest temperature to 70 degrees Fahrenheit, the loss tangent was calculated to be 0.01251, a 5.18 percent difference, and dielectric constant of 80.30 calculated, a 1.53 percent difference. Two different methods for

calculating a theoretical value of the complex permittivity of distilled water result in an acceptable percent difference from the measured of less than 7%.

If pure distilled water were used as a drilling fluid, from Equation (51) and the calculated loss per meter, the maximum allowable distance between signal repeaters in a potential communication system would be 17.44 meters, so there would need to be a signal repeater every single joint of Range 2 drill pipe.

To model the propagation in water, the air-filled, detailed model was duplicated and any geometry labeled as “Air” was set to the “Distilled Water” from the default material library in HFSS and updated with the calculated loss tangent and dielectric constant. The only electrical property left as default was the conductivity value of $2e-4$ S/m.

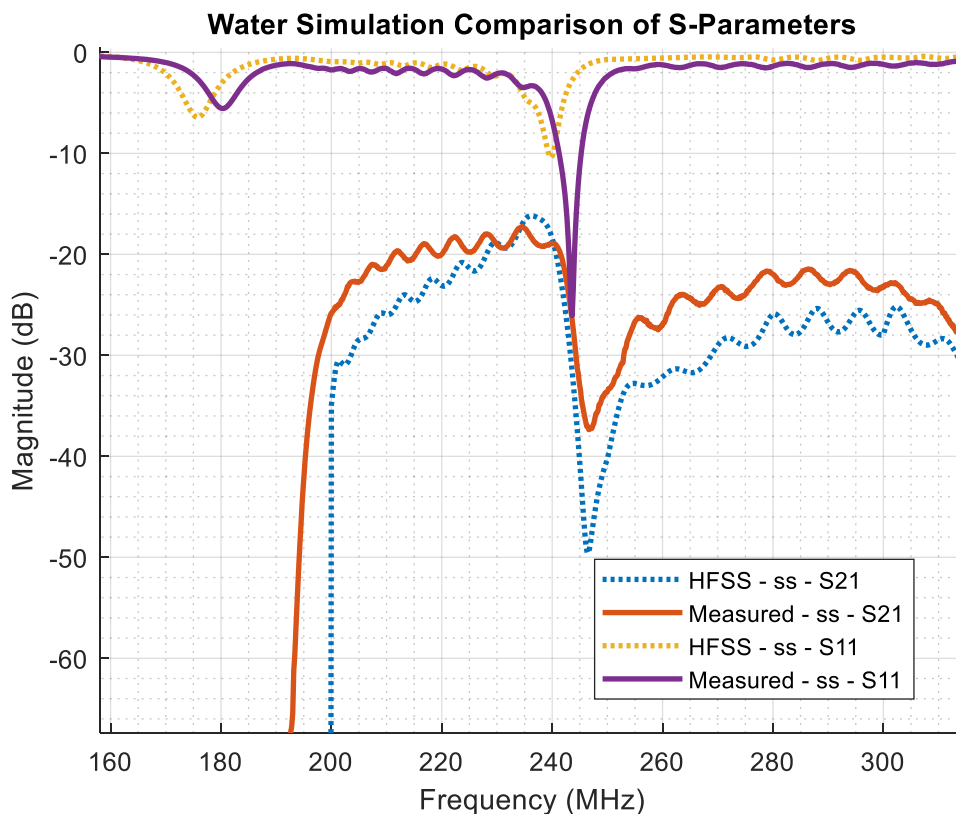


Figure 49. Comparison of simulated and measured S-Parameters of Distilled Water (short-short)

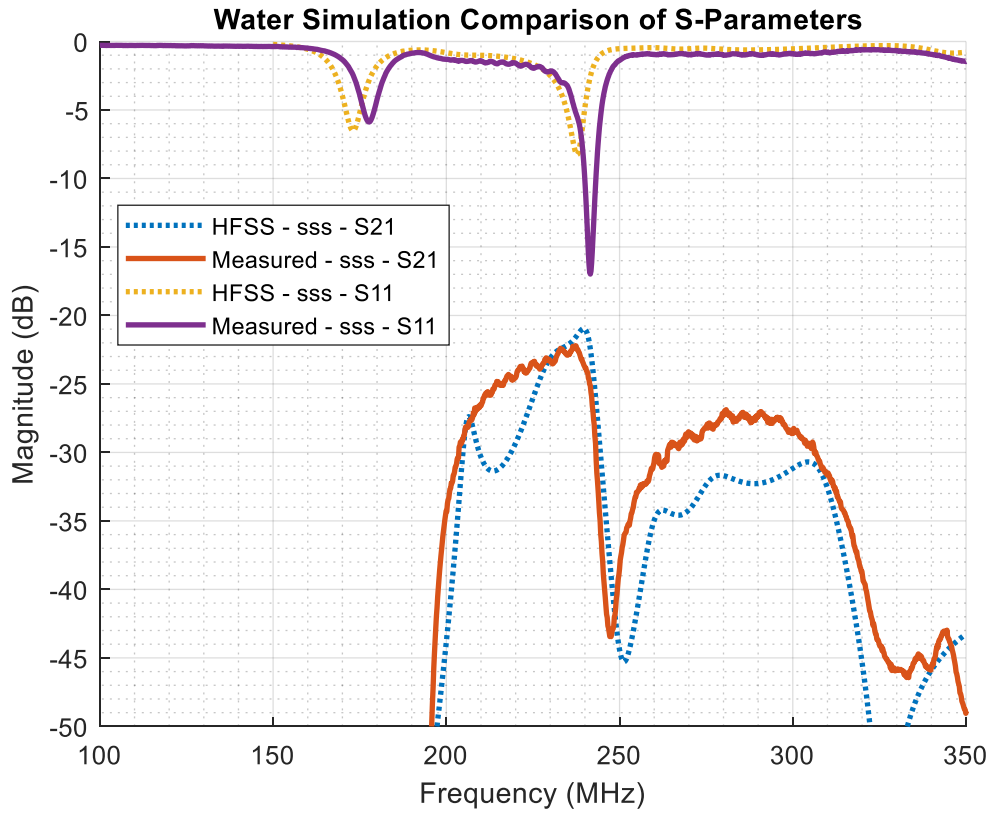


Figure 50. Comparison of simulated and measured S-Parameters of Distilled Water (short-short-short)

6.2.2. Salt Water 5% by Weight

Many water-based fluids use some sort of saltwater or brine as the base. Before any fluid was mixed, a pure brine of 5% NaCl by weight was tested. The brine solution was created by measuring 17 kg of water, adding 0.8947 kg of NaCl, and mixing with a magnetic stir bar until the added salt had fully dissolved. When sodium chloride (NaCl) is added to water the solid salt is dissolved and dissociates into positive and negative ions:



The result of the free ions in the water is an electrically conductive solution. Waveguide propagation theory is based on the assumption that the medium filling the waveguide is an

insulator, with no free charge carriers available for conduction. If the medium filling the guide is conductive then any energy applied to the probe will not be radiated as intended, but instead will be electrically shorted directly to the waveguide wall and returned to source.

A mixture of 5% NaCl to 95% H₂O, by weight, results in a conductivity of 78,000 $\mu\text{S}/\text{cm}$, or 7.8 S/m [72], a relatively low conductivity, especially when compared to the 4.15×10^6 S/m value measured for the steel pipe, but is still high enough to provide a path to ground for the current applied to the probe.

The results of the measurements indeed show there is no energy traversing the pipe with a calculated maximum available gain, seen in Figure 51, below -92 dB for only a small section of the frequency sweep and undefined (minus infinity) everywhere else.

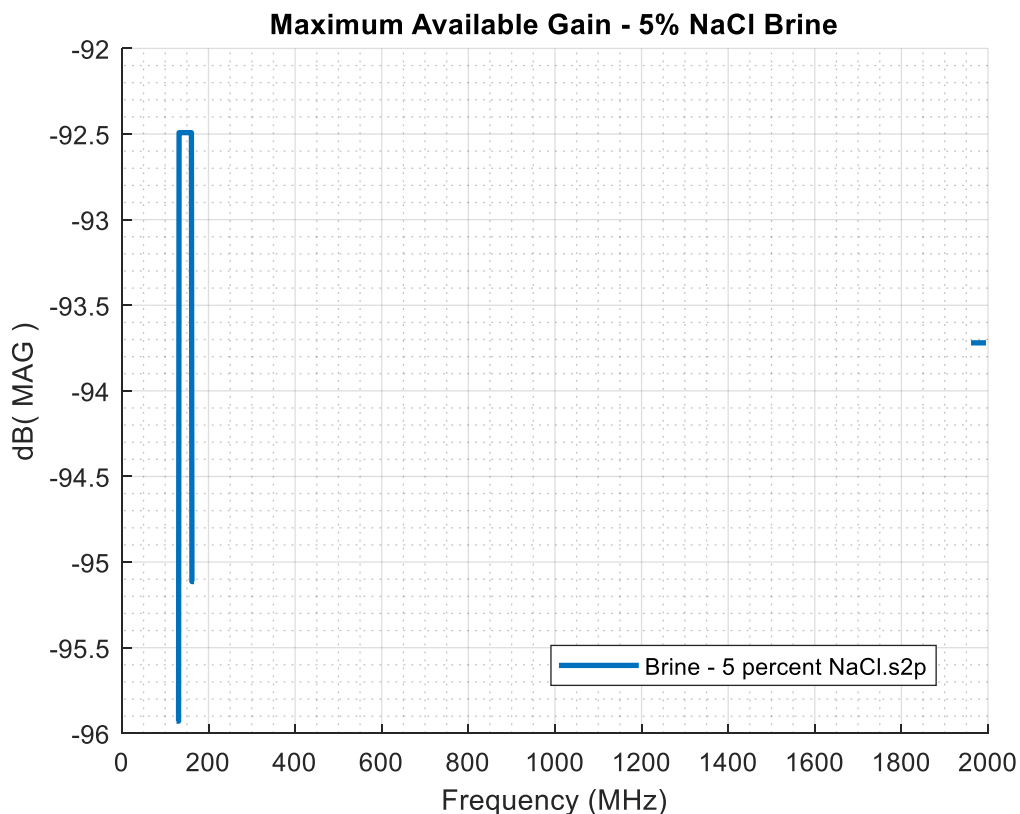


Figure 51. Maximum available gain of 5% NaCl by weight brine solution

Similarly in Figure 52, the scattering parameters show no energy transfer with the S_{21} through measurement being 100 dB down and almost 0 dB in return loss seen in the S_{11} measurement.

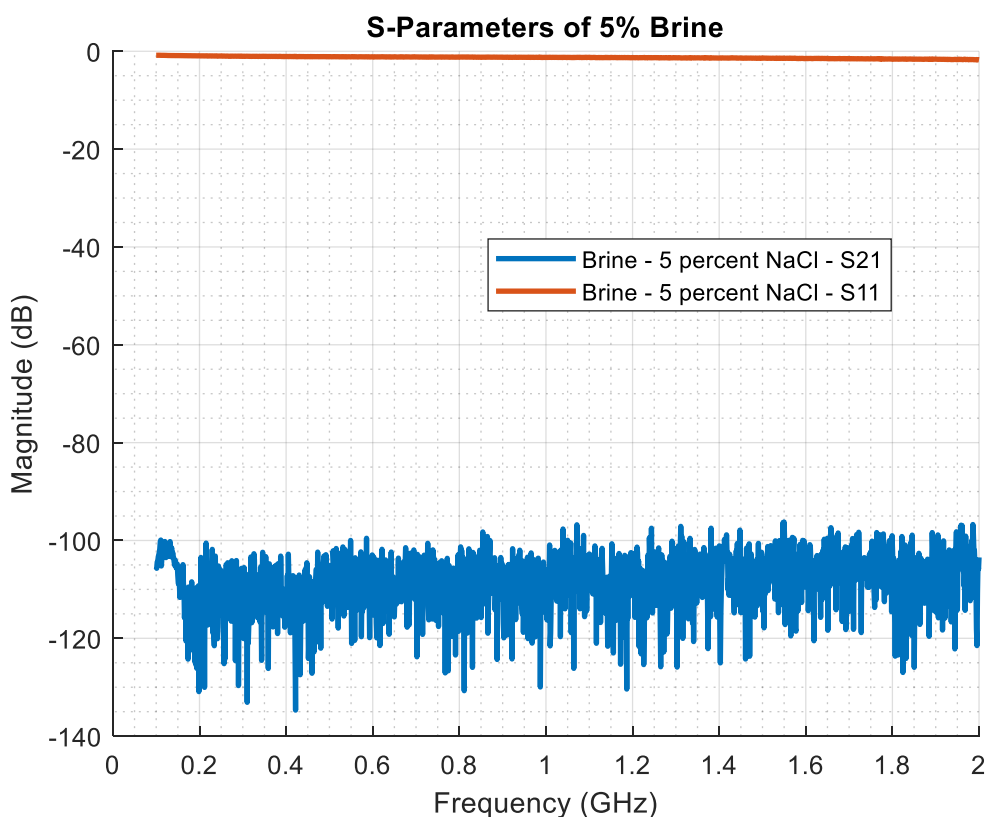


Figure 52. Scattering Parameters of 5% NaCl by weight brine solution

The magnitude plots of the scattering parameters alone are not enough to determine if the salt water was actually acting as a short to ground. One way to characterize an RF short circuit is by analyzing the reflection coefficient (S_{11} scattering parameter) measurement on a Smith Chart. A Smith Chart is a way of visualizing complex reflection coefficients scaled by a normalized impedance, usually referenced to 50Ω . The point at the center of the plot is purely resistive and equal to the reference impedance. As the point moves along the center horizontal line to the right

or left, the real impedance, or resistance, increases and decreases, respectively. Zero resistance (a short circuit) is on the left edge of the circle and infinite resistance (an open circuit) is on the right edge of the circle. Anything above the center line has an inductive reactance and anything below has a capacitive reactance.

To see the results of what an actual short circuit looks like on a Smith chart the reflection coefficient of the “short” calibration standard from the Kirkby Calibration kit was measured and plotted in Figure 53. As expected, the real part of the impedance, displayed as Z in the info bubble, is nearly zero, indicating a short circuit.

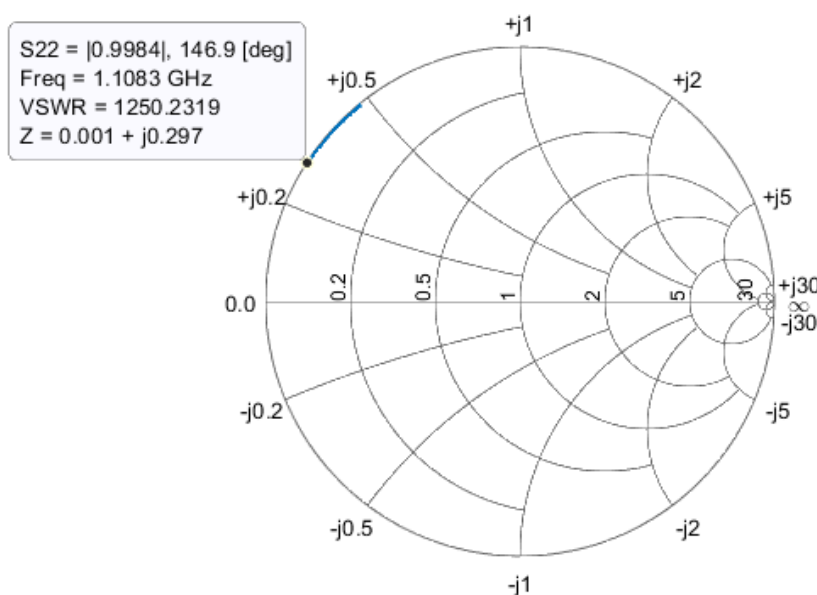


Figure 53. Smith Plot – Calibration standard “short”

Plotting the S_{11} parameter of the 5% brine solution measurement on a Smith chart, seen in Figure 54, gives a similar result with a real value of nearly zero, indicating the conductive salt-water is providing a short circuit to ground.

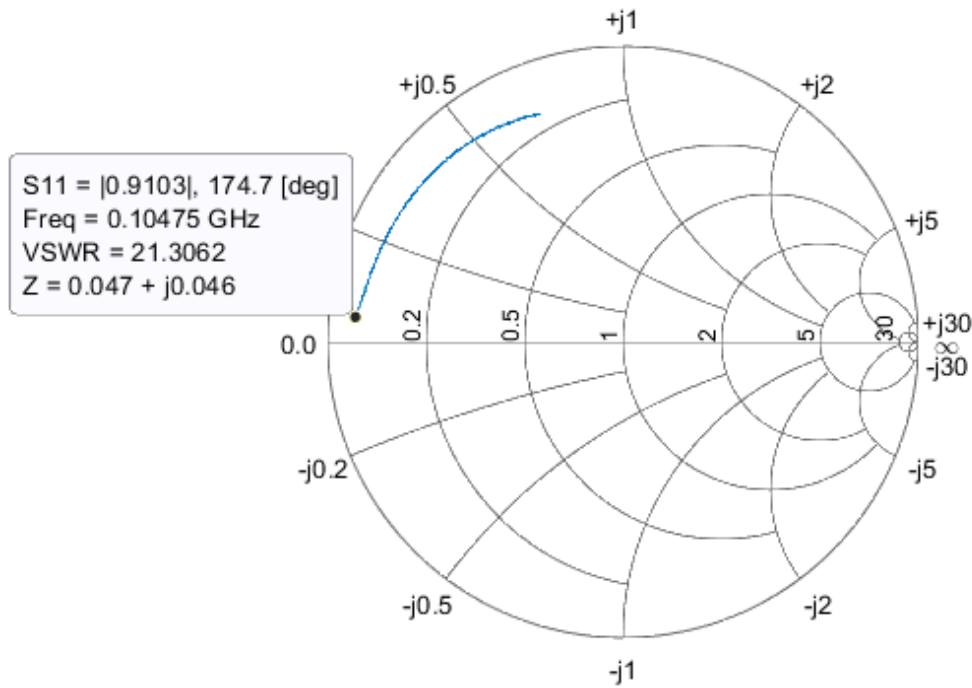


Figure 54. Smith Plot of S_{11} Parameter of 5% NaCl by weight brine solution

The continuous phase of water-based fluids is the water, or brine, meaning there is always a direct, continuous path through the water so it is reasonable to assume any brine based WBF will result in a direct short between the probe and the wall of the pipe. As a result, a brine based WBF will not be a viable option for a waveguide transmission medium.

6.3. Oil-Based Fluids

Oil-based fluids are created using an oil product, such as diesel fuel or mineral oil, as the continuous phase and mixing in a brine or water at different ratios. The selected percentage of oil and water depends on the desired characteristics for the particular formation being drilled.

6.3.1. Pure Diesel

Before creating more realistic drilling fluids, pure diesel fluid was measured for a baseline to determine the effects of the different ratios of oil-water mixtures. Red-dyed diesel is standard diesel fuel but has been dyed red to designate it for non-taxable use only. It is not subject the same taxes as on-road diesel making it the more cost effective solution for a base when mixing oil-based fluids.

The scattering parameters for three lengths of pipe were measured and the calculated MAG was plotted in Figure 55. From the cutoff frequency of 1.166 GHz a dielectric constant of 2.167 was calculated.

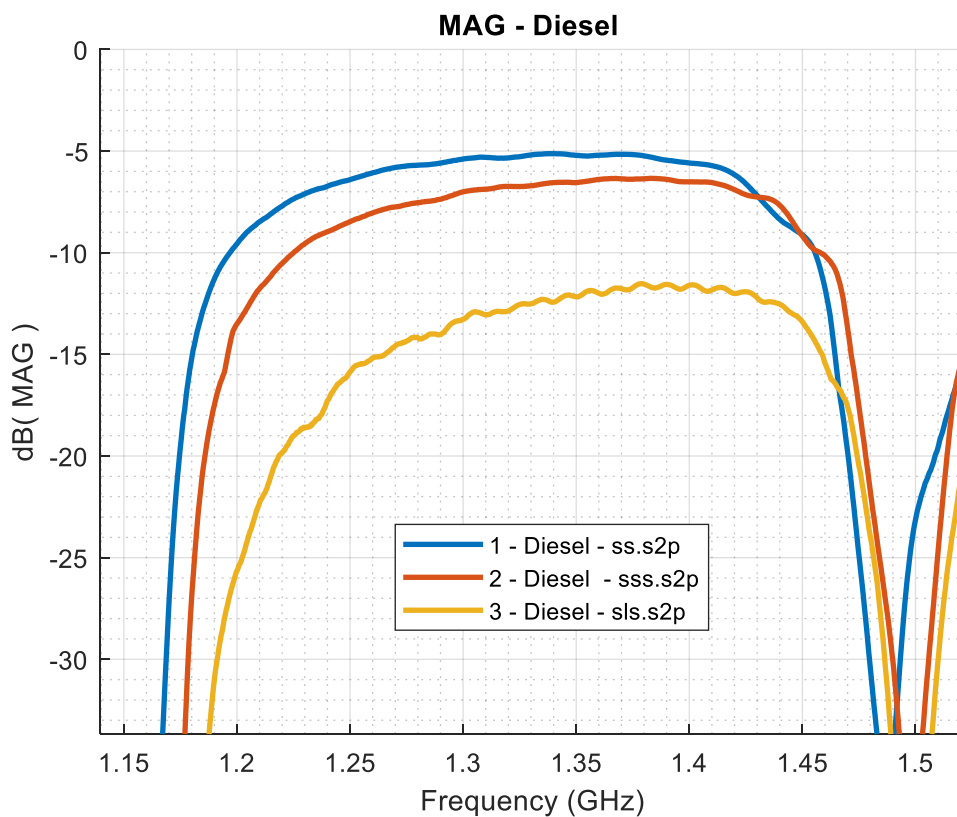


Figure 55. Maximum available gain of red-dyed diesel.

A frequency of 1.3588 GHz was selected as the operating frequency in the middle of the passband to maximize the available gain. The total losses were extracted from the selected frequency and fit to a curve using the known lengths pipe sections measured, seen in Figure 56.

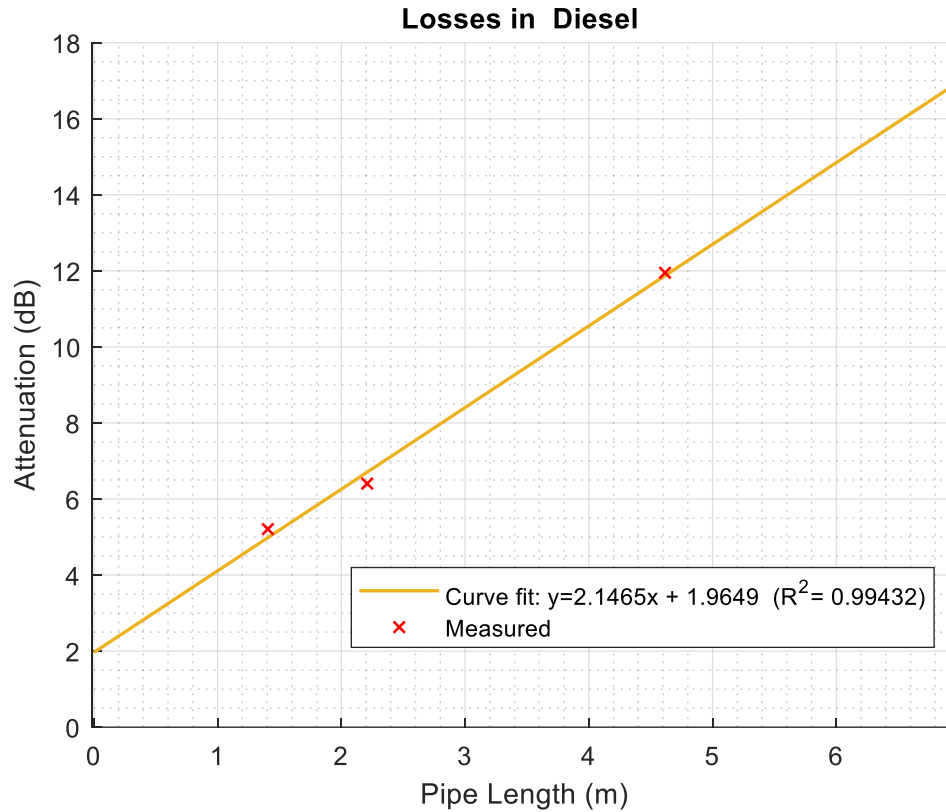


Figure 56. Measured and curve fit losses of red-dyed diesel.

The linear regression gave a total attenuation constant of 2.1465 dB/m, with a very good fit of 0.99432. At 1.3588 GHz there is a theoretical 0.43237 dB/m conductor loss, so 1.7142 dB/m was due to dielectric loss which corresponds to a loss tangent of 0.004833.

Pure diesel would allow for up to 46.59 meters, or 5 joints, between signal repeaters in a drilling string communication system using pipe of similar characteristics to the measurement setup.

Using the calculated parameters, simulations were run for all three lengths with good results in all three comparisons shown in Figure 57, Figure 58, and Figure 59.

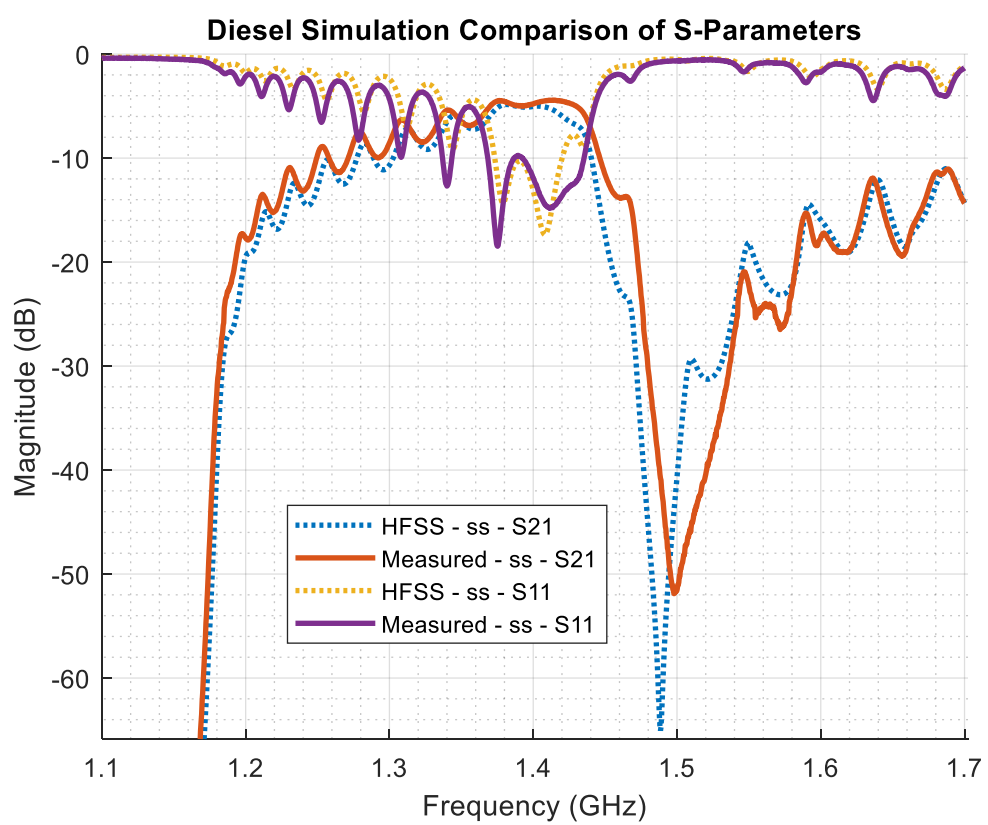


Figure 57. Comparison of simulated and measured S-Parameters of Diesel Fuel (short-short)

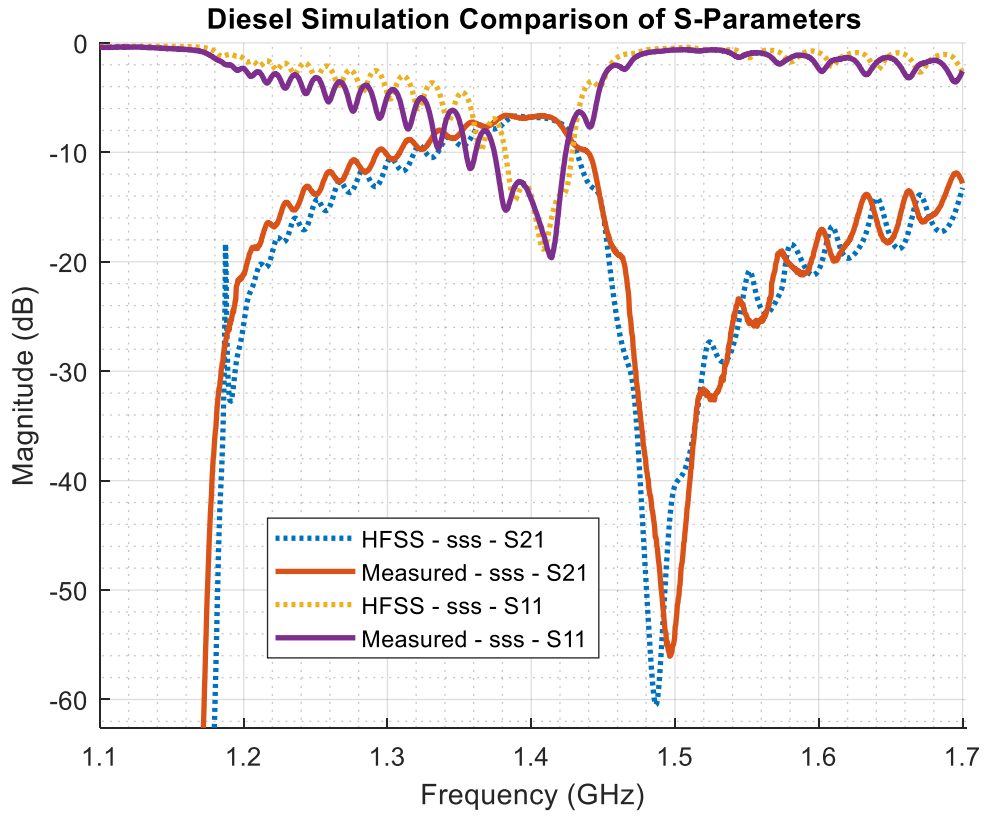


Figure 58. Comparison of simulated and measured S-Parameters of Diesel Fuel (short-short-short)

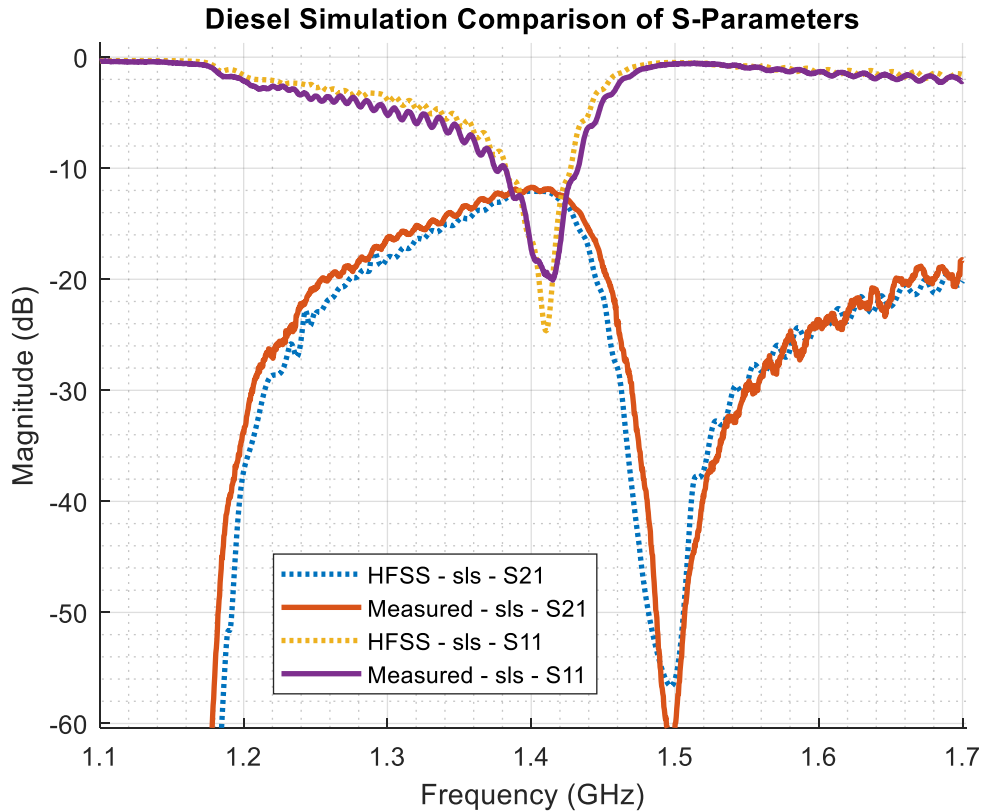


Figure 59. Comparison of simulated and measured S-Parameters of Diesel Fuel (short-long-short)

6.3.2. OBF Mixing Procedure

Due to the polar nature of water and the non-polar nature of oils, a stable mixture of the two fluids cannot occur without an emulsifier. The emulsifier and oil wetting agent used to mix the oil-based fluids in the follow experiments was Haliburton EZ-MUL[®] NT. In oil based fluids, the continuous phase of the emulsion is the oil and the water or brine is the dispersed phased. Figure 60 depicts four stages of emulsion. In Stage A, Phase I, the oil, and Phase II, the water, are not emulsified. Stage B, Phase II is dispersed in Phase I. Stage C, shows an unstable emulsion that eventually separates. Stage D, shows a stabilized emulsion.

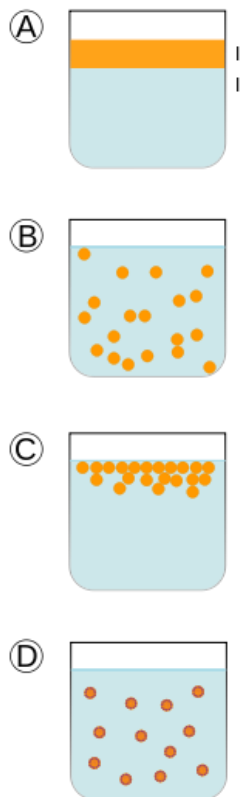


Figure 60. Four stages of emulsions [73]

The procedure to achieve a stable emulsion in an oil-based fluid will now be discussed. When creating an OBF a proper oil to water ratio is required to achieve the necessary fluid characteristics for the particular well being drilled. The ratio, usually in the range of 90:10 to 70:30, is given in percent volumes where 90:10 would correspond to 90% oil and 10% water by volume. If a brine solution is to be used as the dispersed phase of the emulsion it is also necessary to mix up a desired concentration of salt and water. Brine concentrations are determined using salt tables to get the proper ratios of salt and water by weight, rather than volume. For the following experiments a 10% brine solution with sodium chloride (NaCl) as the salt was used in the oil-brine mixtures.

With a final total volume of fluid in mind, the percent volume of oil was placed into a 5-gallon bucket and stirred with a vertical mixer. The Haliburton EZ-MUL[®] NT emulsifier was then slowly added using a total of 28.6 grams of emulsifier per liter of the total volume. Then, to activate the emulsifier, 14.3 grams of lime, $\text{Ca}(\text{OH})_2$, per liter of total volume was added. The combination of oil, emulsifier, and lime was mixed for 20-30 minutes before continuing. Next, the first 25% of the brine solution was slowly added over the course of 10-15 minutes and allowed to mix for another 20-40 minutes. The final 75% of the brine was then added, again over the course of 10-15 minutes. The full mixture was mixed until the emulsion was deemed stable, usually two to three hours.

The stability of a water-in-oil emulsion is tested using an Emulsion Stability (ES) Tester to determine the breakdown voltage of the mixture. The ES meter uses a probe with two electrodes separated by 1.55 mm that is submerged into the fluid under test. A sinusoidal voltage applied to the probes is slowly ramped in amplitude to a maximum voltage of 2,000 V_{peak} . When the measured conducted current across the probe hits a threshold of 61 microamps the breakdown of the emulsion has been reached and the voltage is displayed. Minimum values of a stable ES reading can vary with the base oil and emulsifiers used but the emulsion is typically considered stable if the breakdown voltage is above 600 V [74], [75]. During the final mix the ES of the fluid was measured periodically until it reached a value over 600 V.

6.3.3. 90:10 OBF

The first OBF mixed was a 90% oil, 10% brine mix. By starting with a low concentration of brine, batches with higher concentrations of brine could be easily built using the 90:10 mix as a base after all measurements were made.

The parameters for the 90:10 mixture of oil-based fluid are shown in Table V. The first batch made was initially for testing the mixing procedure to determine the mixing times required for a reliable ES reading. With a good ES value in a reasonable amount of time a full batch with enough volume to fill a short-short section of pipe was built. Batches 1 and 2 were then combined and remixed until they had similar ES values. A third batch was later made to create enough volume to measure the short-short-short section.

Table V: OBF 90:10 Parameters

	Batch 1	Batch 2	Batch 3
Diesel (liters)	3.6	12.6	5.4
Brine (liters)	0.4	1.4	0.6
Emulsifier (grams)	114.4	400	171.6
Lime (grams)	56.9	200	85.8
Total Mix Times (hh:ss)	2:13	2:35	2:07
ES 1 (V)	660	650	560
ES 2 (V)	620	676	510
ES 3 (V)	658	660	600
Remix Times (hh:ss)	0:30	0:30	1:25
ES 1 (V)	670	684	710
ES 2 (V)	655	655	735
ES 3 (V)	675	667	722

The scattering parameters for both lengths were measured and the MAG plotted in Figure 61. From the cutoff frequency of 969.94 MHz a dielectric constant of 3.134 was calculated.

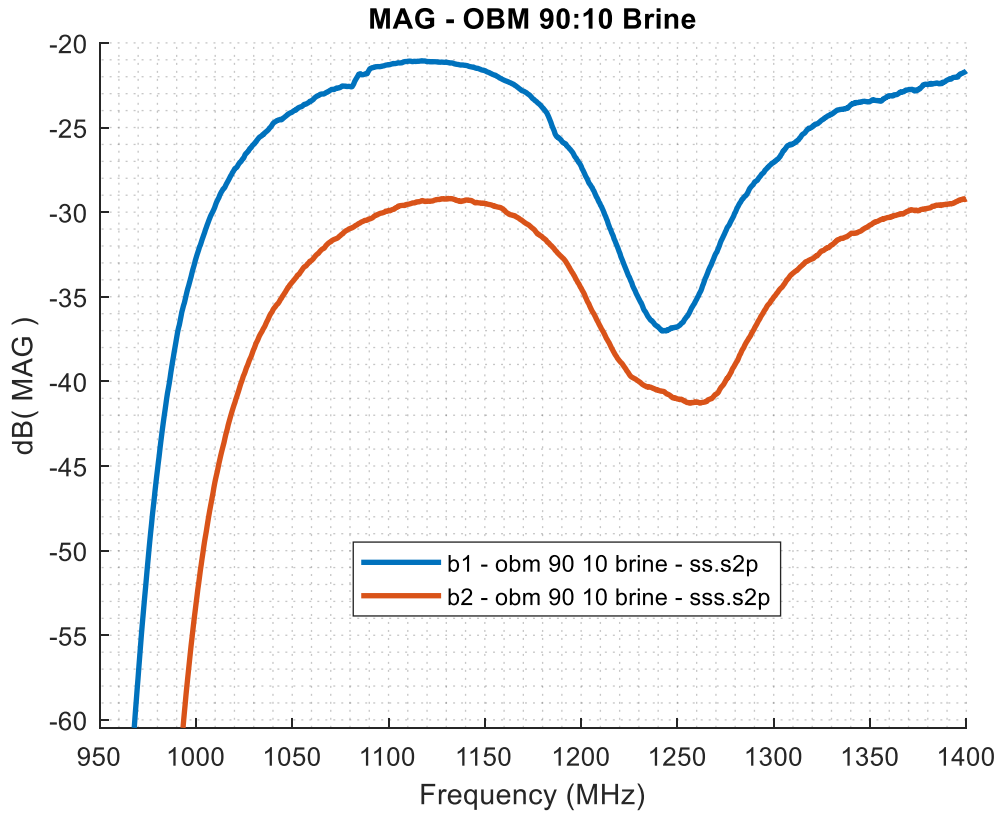


Figure 61. Maximum available gain of an Oil-based fluid ratio of 90:10.

To maximize the MAG, an operating frequency of 1.130 GHz was selected and a curve fit to the loss data and known lengths of pipe to get a total loss per meter of 10.075 dB. At 1.130 GHz the theoretical conductor losses are 0.4741 dB/m leaving 9.5996 dB/m as a result from dielectric attributed to a loss tangent of 0.027067.

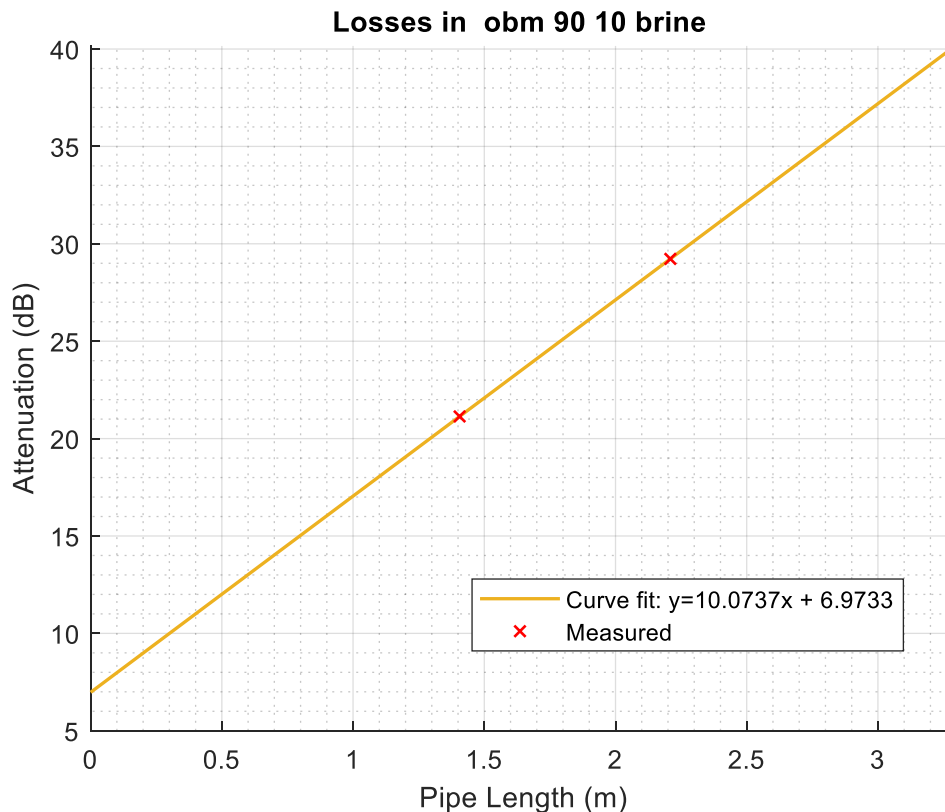


Figure 62. Measured and curve fit losses of an Oil-based fluid ratio of 90:10.

The maximum allowable distance between signal repeaters in a potential communication system using a 90:10 oil-based fluid would be 9.93 meters, so there would need to be a signal repeater every single joint.

A handful of oil and water simulations were attempted but the computer used to run the HFSS software was at the lower end of the specifications recommended by Ansys. Consequently, when the more detailed models were built the simulations ran out of memory and failed.

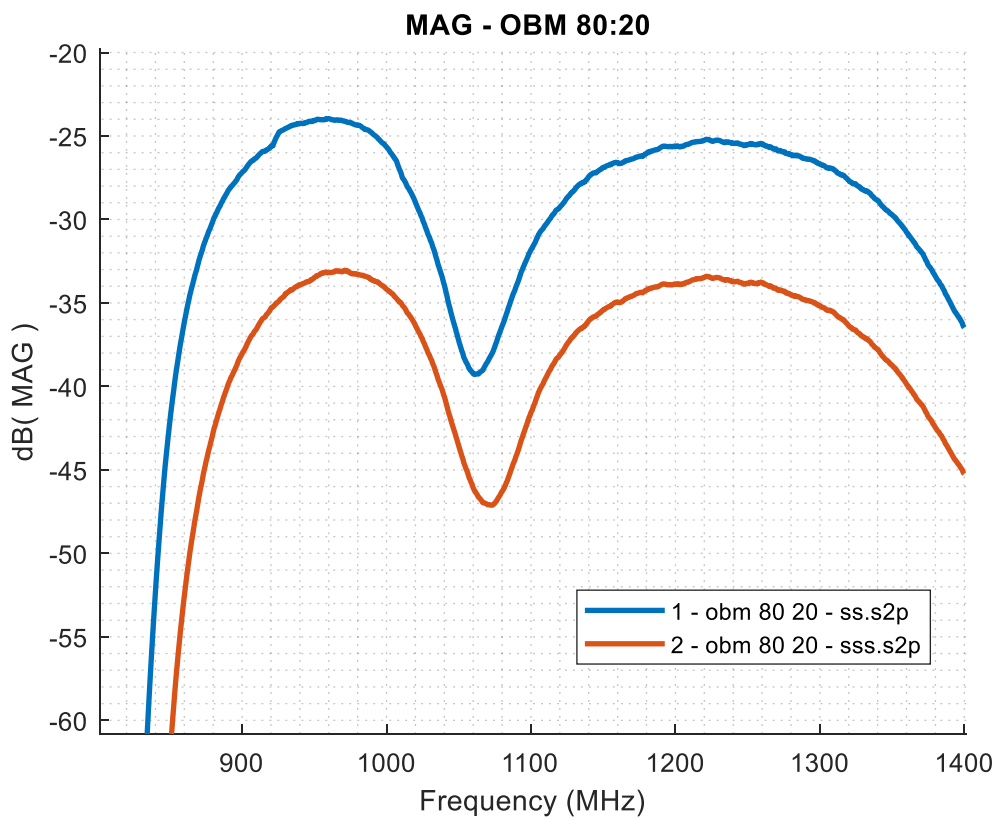
6.3.4. 80:20 OBF

Using the 90:10 mixture as a base, the proper ratios of brine, emulsifier, and lime were added to create an 80:20 oil-based fluid, the parameters for the mixture are in Table VI.

Table VI: OBF 80:20 Parameters

	Batch 1	Batch 2
90:10 Mix (liters)	11.4	10.8
Brine (liters)	1.425	1.35
Emulsifier (grams)	40.8	38.6
Lime (grams)	20.4	19.3
Total Mix Times (hh:ss)	1:40	2:15
ES 1 (V)	664	678
ES 2 (V)	651	660
ES 3 (V)	640	668

Scattering parameters were again measured for two lengths and MAG calculated and plotted in Figure 63. From the cutoff frequency of 831.25 MHz a dielectric constant of 4.2666 was calculated.

**Figure 63. Maximum available gain of an Oil-based fluid ratio of 80:20.**

An operating frequency of 968.4 MHz was used to select the loss data for the curve fit and a total loss was calculated as 11.298 dB/m. A theoretical conduction loss of 0.5126 dB/m was calculated, leaving 10.7861 dB/m of dielectric loss. The loss tangent calculated was 0.03041.

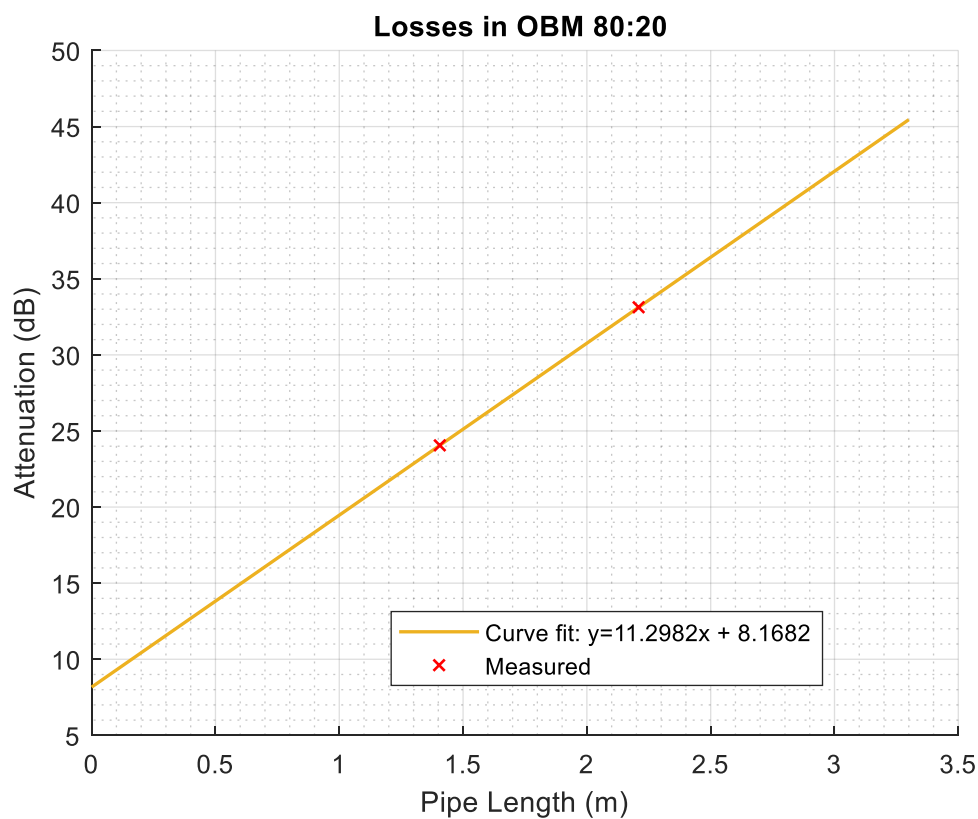


Figure 64. Measured and curve fit losses of an Oil-based fluid ratio of 80:20.

The maximum allowable distance between signal repeaters for 80:20 OBF would be 8.85 meters, which is less than a single joint so no repeater system would be viable using drill pipe of similar composition to the test setup.

6.3.5. 70:30 OBF

Using the 80:20 mixture as a base, more brine, emulsifiers, and lime were added to create a 70:30 oil-based fluid. The parameters for the mixture are in Table VII.

Table VII: OBF 70:30 Parameters

	Batch 1	Batch 2
80:20 Mix (liters)	12.6	12
Brine (liters)	1.8	1.71
Emulsifier (grams)	51.48	49
Lime (grams)	25.74	24.5
Total Mix Times (hh:ss)	3:37	3:22
ES 1 (V)	598	611
ES 2 (V)	604	627
ES 3 (V)	601	617

Using the same procedure as previous measurements, 722.927 MHz was used to calculate a dielectric constant of 5.6408.

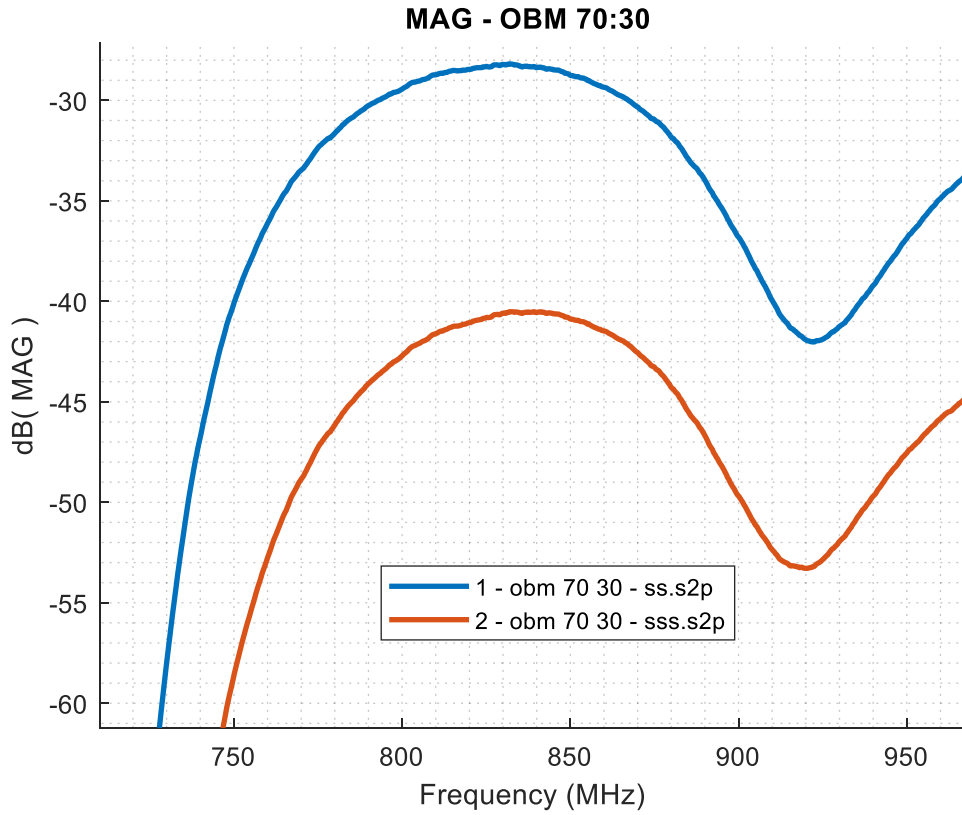


Figure 65. Maximum available gain of an Oil-based fluid ratio of 70:30.

An operating frequency of 842.22 MHz gives 15.1388 dB/m total loss, 0.54919 dB/m conductor loss, 14.5896 dB/m dielectric loss, and a calculated loss tangent of 0.04114.

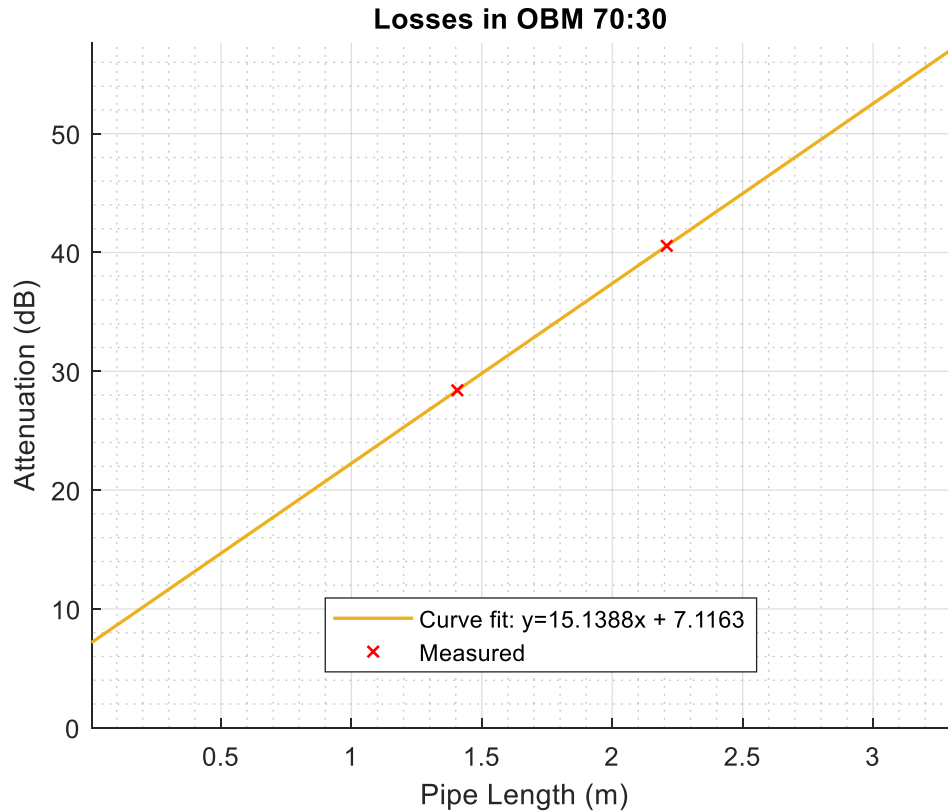


Figure 66. Measured and curve fit losses of an Oil-based fluid ratio of 70:30.

From Equation (51) and the calculated loss per meter, the maximum allowable distance between signal repeaters in a potential communication system would be 6.61 meters, which, again, is less than a single joint so no repeater system would be viable.

6.3.6. 90:10 OBF – Distilled Water

To determine the effect the salt in the brine phase has on dielectric properties, a fresh batch of 90:10 OBF was mixed up. However distilled water was used instead of the brine solution. Parameters for the mixture are shown in Table VIII.

Table VIII: OBF 90:10 Distilled Parameters

	Batch 1	Batch 2
Diesel (liters)	9	9
Distilled Water (liters)	1	1
Emulsifier (grams)	286	286
Lime (grams)	240	240
Total Mix Times (hh:ss)	1:30	2:06
ES 1 (V)	833	751
ES 2 (V)	794	786
ES 3 (V)	809	769

A cutoff frequency of 997.3 MHz results in a dielectric constant of 2.9642.

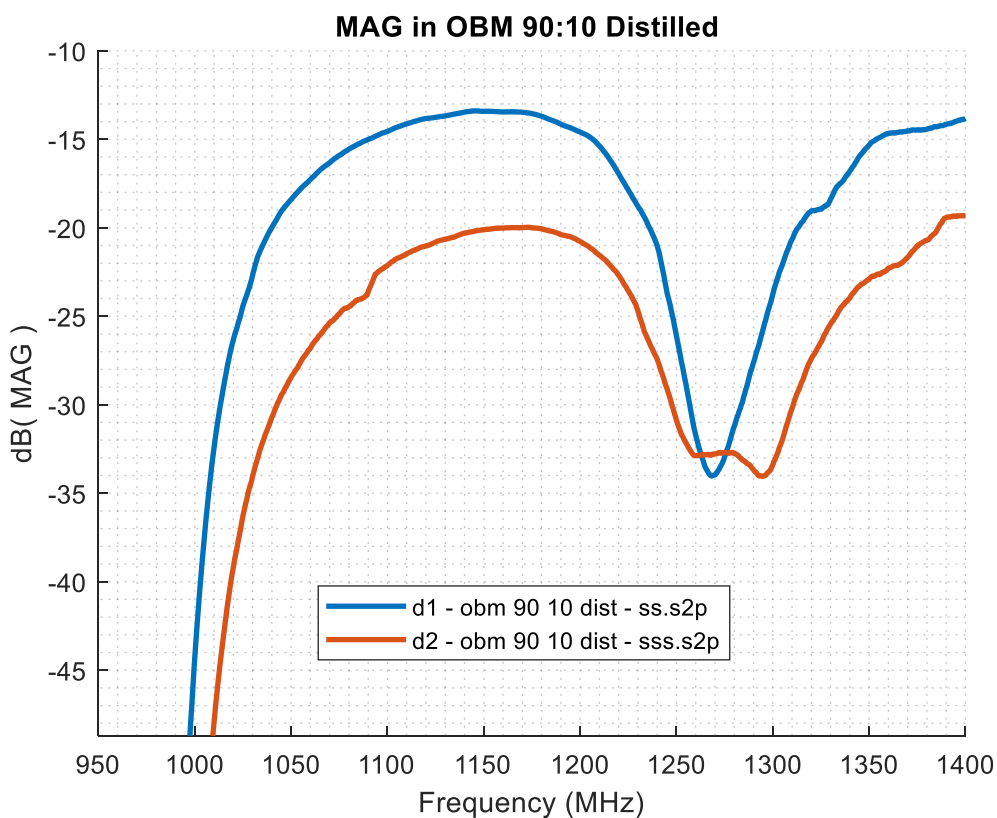


Figure 67. MAG of 90:10 OBF using distilled water.

An operating frequency of 1.1618 GHz gives 8.1578 dB/m total loss, 0.46759 dB/m conductor loss, 7.69020 dB/m dielectric loss, and a calculated loss tangent of 0.021683.

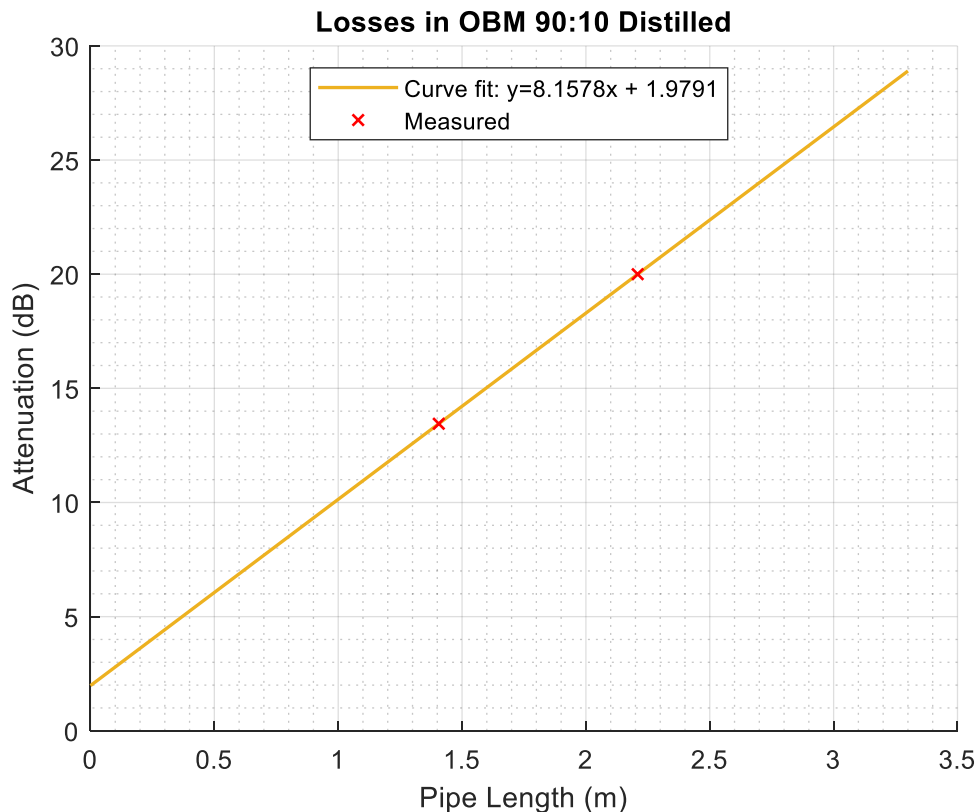


Figure 68. Measured and curve fit losses of an Oil-based fluid ratio of 90:10 using distilled water.

At first glance it may seem strange the attenuation constant of a mixture of diesel fuel ($\alpha = 2.417$) and distilled water ($\alpha = 5.736$) has a higher attenuation constant ($\alpha = 8.158$) than the constituent fluids. While there was emulsifier and lime added to the mix, the amounts were small relative to the total volume. It is crucial to keep in mind the frequency dependence of the loss tangent to understand the results. The dielectric constant of the oil-distilled mixture remains relatively low compared to pure distilled water, so the cutoff frequency is higher. Going back to Equation (66) to calculate a loss tangent for distilled water at the higher operating frequency the expected loss tangent is 0.06353. In other words, at 1.16 GHz distilled water is almost five times more lossy than at 225 MHz.

Compared to the results of the brine based 90:10 OBF, the distilled mixture has a slightly lower attenuation constant and loss tangent. However, the improvement is not enough to suggest a fresh water based OBF is a good fluid for a waveguide communication system. The calculated maximum distance between repeaters was 12.26 meters, or one joint.

6.3.1. Mineral Oil

Mineral oil is another fluid used for the continuous phase in oil-based fluids. Thirteen gallons of Durvet mineral oil were purchased and three different lengths of mineral-oil filled pipe were measured: short-short, short-short-short, and short-long-short. The calculated MAG from all three measurements are shown in Figure 69. The cutoff frequency of 1.177 GHz corresponds to a dielectric constant of 2.128.

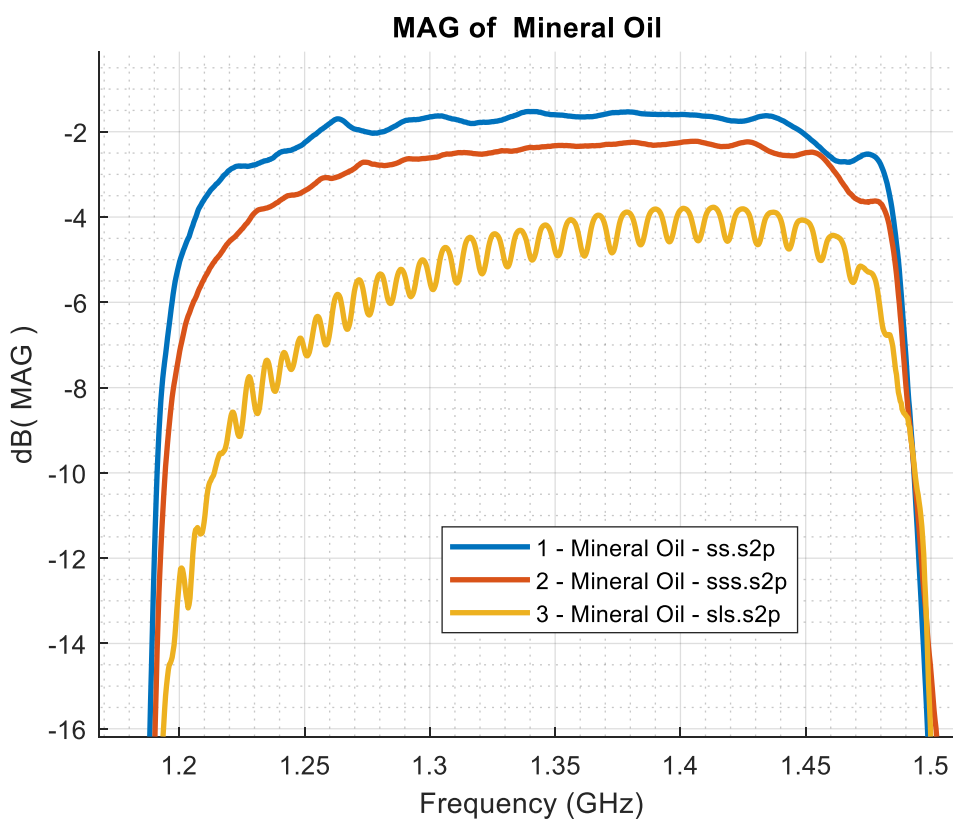


Figure 69. Maximum available gain of Mineral Oil

With an operating frequency of 1.37 GHz the total loss was calculated by the linear regression, with an R^2 value of 0.9997, was 0.9676 dB/m. The conductor loss was calculated at 0.4304 dB/m leaving dielectric losses of 0.5372 dB/m, giving a loss tangent of 0.001515.

A study looking at dielectric properties of insulating oils [55], found the dielectric constant of mineral oil is 2.21 and the loss tangent is 0.0015. Compared to the above measurements there is a 1 percent difference from the loss tangent and 3.9 percent difference for dielectric constant.

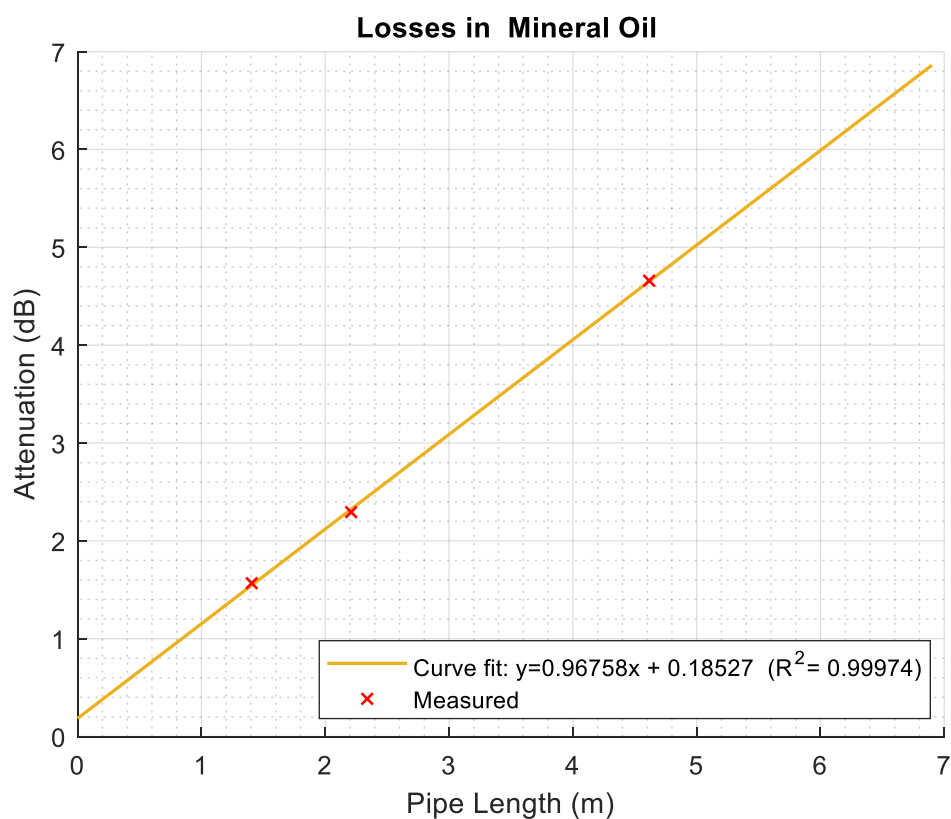


Figure 70. Measured losses in Mineral Oil

From Equation (51) and the calculated loss per meter, the maximum allowable distance between signal repeaters in a potential communication system would be 103.35 meters, or 11 joints.

HFSS simulations with parameters updated to those calculated for mineral oil continue to track the measured results.

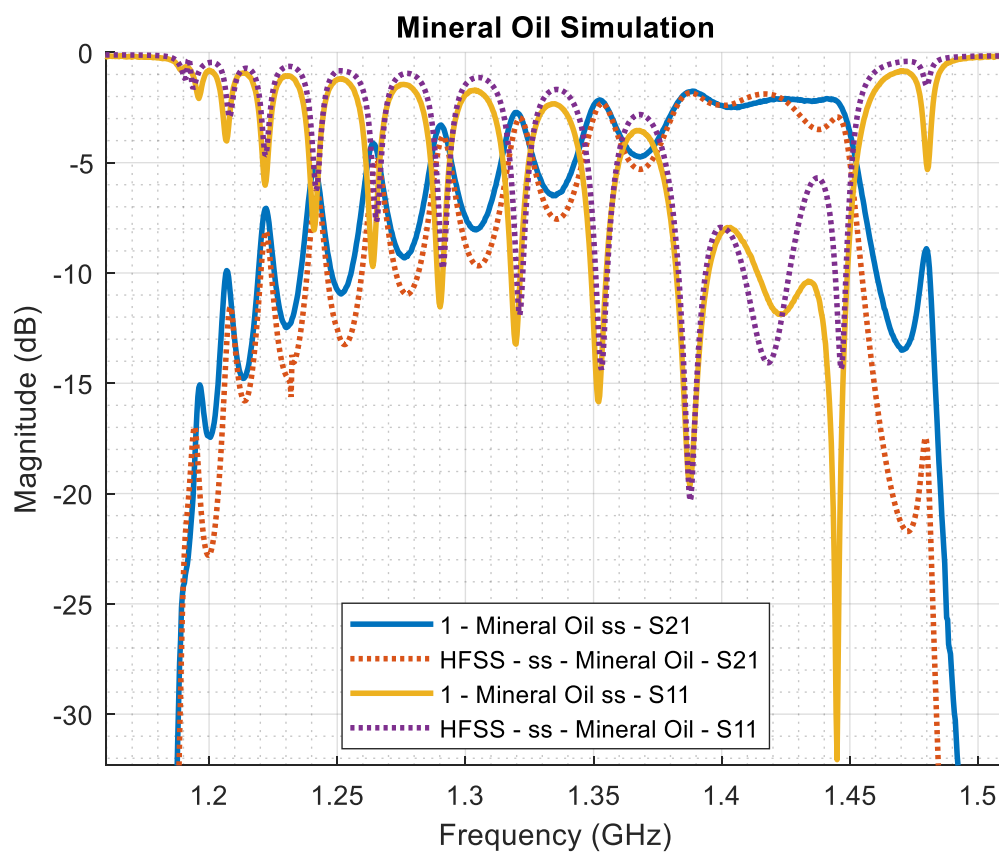


Figure 71. Comparison of simulated and measured S-Parameters of Mineral Oil (short-short)

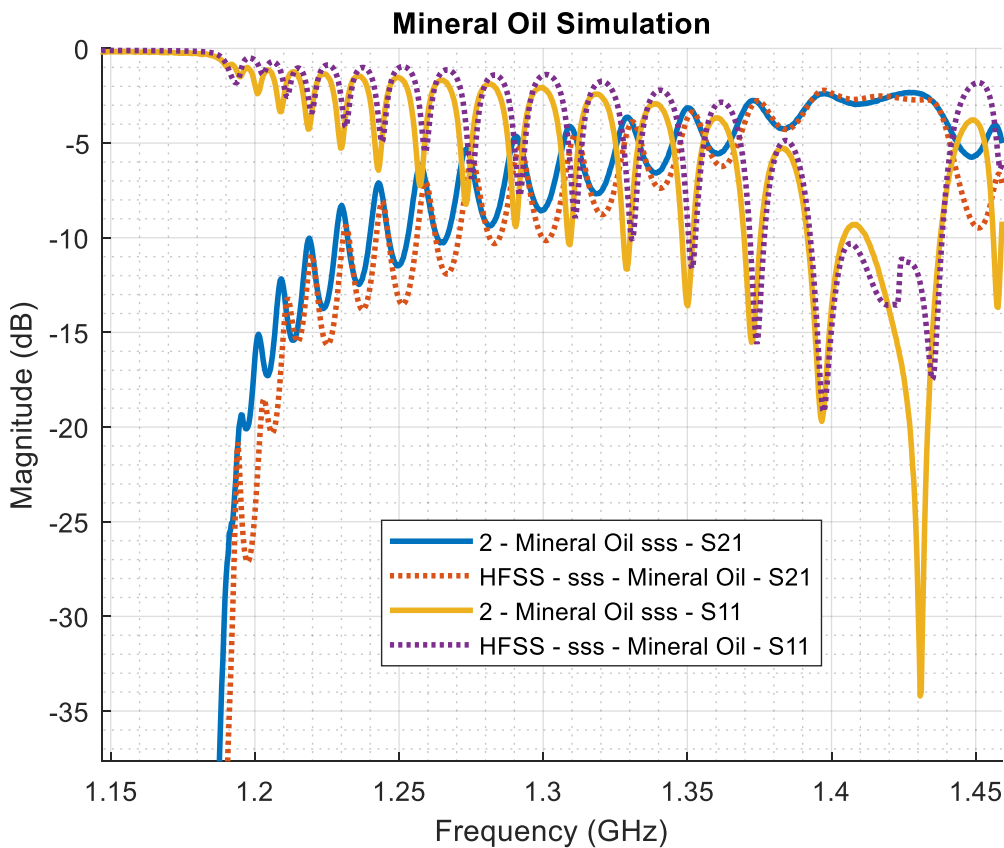


Figure 72. Comparison of simulated and measured S-Parameters of Mineral Oil (short-short-short)

6.3.2. Escaid™ 110

Escaid™ 110 is a proprietary synthetic-based fluid designed by ExxonMobil for use in long reach wells and offshore use. Five gallons of Escaid™ 110 were donated to the project. Unfortunately it was not possible to obtain a larger volume of Escaid™ 110. With just five gallons it was only possible to measure one length of pipe so no linear regression could be performed. Using the one measurement the cutoff frequency of 1.19 GHz a dielectric constant of 2.081 was calculated. When compared to mineral oil, Escaid™ 110 appears to have very similar dielectric properties, though Escaid™ 110 has a slightly lower dielectric constant, as seen by the higher cutoff frequency in Figure 73. The MAG of mineral oil and Escaid™ 110 are nearly identical, but with only one measurement the effect of the probe loss cannot be determined.

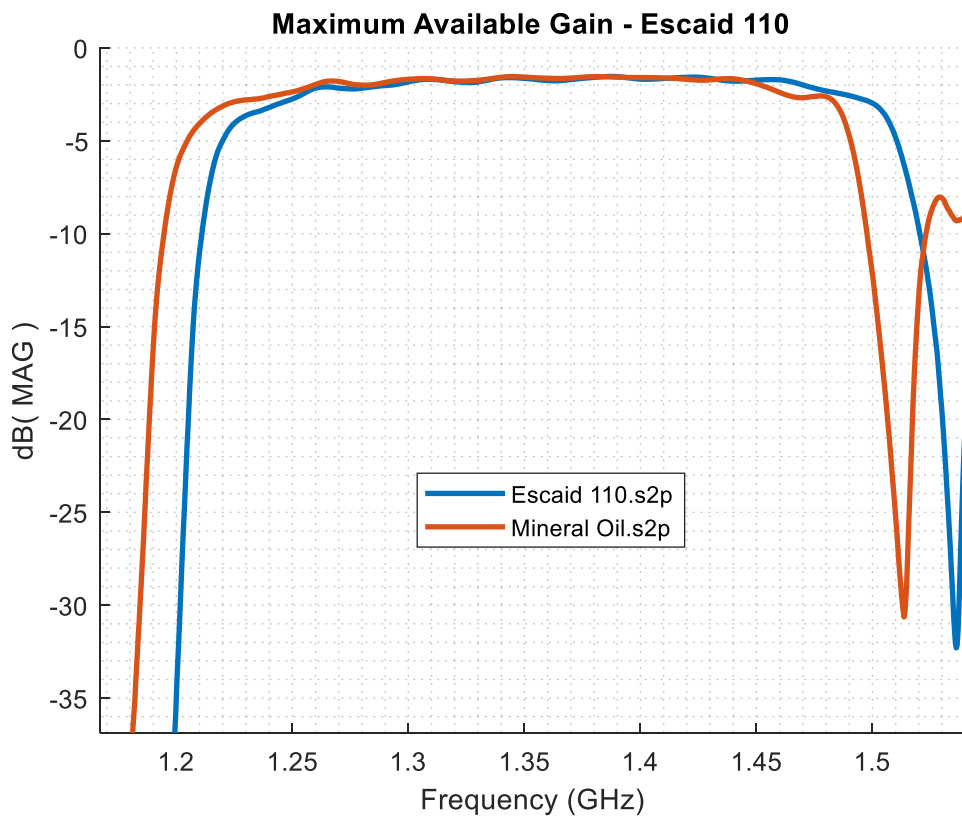


Figure 73. Maximum available gain of Escaid™ 110

7. Conclusions

A measurement system and methodology to effectively determine dielectric properties of unknown fluids was developed and validated. A summary of the fluids measured and dielectric properties calculated is given in Table IX.

Table IX: Summary of Results

Material	ϵ_r	$\tan \delta$ $\times 10^{-3}$	α (dB/m)	@ f (MHz)	d_{max} (m)	d_{max} (joints)
Air	1.00	0.00	0.332	2082.28	270.5	30
Distilled Water	78.07	13.18	5.736	224.95	17.4	1
Pure Diesel	2.17	4.83	2.147	1358.82	46.6	5
90:10 OBF	3.13	27.08	10.073	1129.98	9.93	1
80:10 OBF	4.27	30.41	11.298	831.25	8.85	0
70:30 OBF	5.64	41.14	15.139	722.93	6.61	0
90:10 OBF (distilled)	2.96	21.68	8.158	1161.83	12.26	1
Mineral Oil	2.13	1.52	0.967	1371.21	103.35	11
Escaid™ 110	2.08	X	X	X	X	X

To further evaluate electromagnetic wave propagation in a fluid filled pipe a finite element analysis model was built and validated for pipe lengths of at least 4.8 meters. While the results of most of the HFSS simulations were adequate to validate the general dielectric properties calculated, there is still room for improvement.

As for the feasibility of a downhole RF communication system utilizing the drill string as a waveguide, the results are not promising when using liquids. While pure diesel fuel, mineral oil, and Escaid™ 110 have the best potential of the liquids, it should be noted that all measurements were made in an ideal lab environment with no contaminants added to the fluids. Meaning, calculations for maximum distances between signal repeaters are best case scenario. In a real-world system there will be impurities in the fluids that could significantly increase signal attenuation.

There is still potential for more research into oil- or synthetic-based fluids using mineral oil or Escaid™ 110 for the base, but the results of the diesel-based fluids suggest any addition of water or brine will immediately introduce unacceptable amounts of attenuation.

Water based fluids have the worst potential for a waveguide based communication system. The results of the 5% NaCl solution suggest any brine-based WBF would just short the signal directly to the pipe of the wall. Fresh water based fluids would not necessarily have the conductivity problems of brine, but the distilled water results show enough signal attenuation to make even an uncontaminated system impractical.

Air-filled pipe is the most promising of the fluids studied. While it is not prominently used, certain formations lend themselves to what is called “underbalanced drilling” where the formation pressure is low enough the drilling fluid does not need to provide the usual hydrostatic pressure. Air or foam can be used as a drilling fluid for these type of formations.

An ideal setup for a drill string communication system would be an air-filled pipe made of highly conductive, non-magnetic metal operating in the TE₀₁ propagation mode, due to the decrease in conductor losses as operating frequency increases. While TE₀₁ is susceptible to coupling with other modes it is possible to make minor modifications to the waveguide that discourage coupling [35].

Following a similar methodology used to obtain an operating frequency for the TE₁₁ mode, a TE₀₁ mode operating frequency can be found in the pass band between the cutoff frequency of TE₀₁, with a Bessel Solution of 3.8318, to the cutoff frequency of the next circular electric mode TE₀₂, with a Bessel Solution of 7.0156, resulting in a TE₀₁ operating range of:

$$f_{cTE01} < f < 1.83 f_{cTE01} \quad (68)$$

An operating frequency, f , around 1.415 times the cutoff frequency of TE_{01} would land in middle of the propagating range. If a metal such as aluminum, with a conductivity value of 3.816×10^7 S/m [36] and magnetic permeability of 1.00002 [39], were used with the same 4” inner diameter pipe, the resulting attenuation coefficient of 0.00726 dB/m. Still assuming the radios being used can tolerate 100 dB of path loss, the maximum distance between repeaters would be just over 13,760 meters, which is longer than the current deepest drilled oil well, the Z-44 Chayvo, at 12,376 meters [76]. Meaning, a system could potentially be built to communicate through an entire drill string without the need for any signal repeaters, though a well of that length may not be practical to drill using air drilling techniques.

There are currently wells in the Val Verde Basin of West Texas that have been air drilled to depths around 4,500 meters [77]. If the wells were air drilled using pipe with similar material properties to the measurement setup, a communication system could be built to enable megabits per second of data transfer with only microseconds of latency using only 17 signal repeaters.

8. Future Work

One limitation of the research performed is all measurements were made in a room temperature laboratory at atmospheric pressure. Dielectric properties are dependent on temperature so more research is needed to get a better picture of propagation losses in a more realistic system representing the high temperatures of downhole. A system could be designed to study the temperature and pressure effects on the dielectric properties of the various drilling fluids.

Another avenue of further research is studying potential materials that could be used in the dispersed phase of oil-based fluids. An additive that would yield the same fluid rheology as water without increasing the dielectric loss of the overall fluid could enable a waveguide communication system using oil-based fluids.

The results of the air-filled pipe suggest an RF communication system could be possible for use in air drilling. More experiments on the various gases, foams, and aerated fluids used in air drilling would need to be performed. The current measurement system could be used as a base for a gas-based setup, but a gas injection system would need to be designed to adequately study anything other than air.

As for the HFSS simulation, a refinement of physical geometries to include any ridges or surface roughness may improve simulation results. The addition of frequency dependent values for parameters such as loss tangent and dielectric constant are also possible. Better models for the multi-phase emulsions could be built to simulate the oil-water mixtures, but a more powerful computer will be required to run the simulations.

References

- [1] R. L. Rudoff and P. V. R. Suryanarayana, “Kicks Caused by Tripping-in the Hole on Deep, High Temperature Wells,” *SPE Asia Pacific Oil Gas Conf.*, 1997.
- [2] L. Deshu and F. Ding, “Application of Downhole Pulse Signal Transmission Technology in Rotary Steering Drilling Tool,” *J. Residuals Sci. Technol.*, vol. 13, no. 8, 2016.
- [3] I. Wasserman, D. Hahn, D. H. Nguyen, H. Reckmann, and J. Macpherson, “Mud-pulse telemetry sees step-change improvement with oscillating shear valves,” *Oil Gas J.*, vol. 106, no. 24, pp. 39–47, 2008.
- [4] L. Hongtao *et al.*, “Propagation of Measurement-While-Drilling Mud Pulse during High Temperature Deep Well Drilling Operations,” vol. 2013, pp. 1–32, 2013.
- [5] D. S. Drumheller and S. S. Kuszmaul, “Acoustic telemetry system,” *Hart’s E P*, no. OCT., 2003.
- [6] J. Chen, S. Li, C. MacMillan, G. Cortes, and D. Wood, “Long Range Electromagnetic Telemetry Using An Innovative Casing Antenna System,” 2015.
- [7] J. Schnitger and J. D. Macpherson, “Signal Attenuation for Electromagnetic Telemetry Systems,” no. March, pp. 17–19, 2009.
- [8] J. Zhou, H. Xie, and X. Li, “The Study of the Transducer Used in the Acoustic Telemetry Technology While Drilling,” *Sensors & Transducers*, vol. 168, no. 4, pp. 155–161, 2014.
- [9] M. Fosse, “Wired Drill Pipe Technology: Technical and Economic Overview,” University of Stavanger, 2017.
- [10] X. Liu and X. Xue, “Continuous-wave mud telemetry digital communication system design and the simulation test,” *Procedia Eng.*, vol. 15, pp. 2364–2368, 2011.
- [11] X. Haiming, Z. Jing, and Z. Feng, “The Design of the Acoustic Isolator Used in Acoustic

- Telemetry While Drilling,” *Open Pet. Eng. J.*, vol. 8, 2018.
- [12] I. Navarro De Almeida, P. Duarte Antunes, F. O. Centeno Gonzalez, R. Akira Yamachita, A. Nascimento, and J. L. Goncalves, “A Review of Telemetry Data Transmission in Unconventional Petroleum Environments Focused on Information Density and Reliability,” *J. Softw. Eng. Appl.*, vol. 8, pp. 455–462, 2015.
- [13] R. Hutin, R. W. Tennent, and S. V Kashikar, “New Mud Pulse Telemetry Techniques for Deepwater Applications and Improved Real-Time Data Capabilities,” 1977.
- [14] M. E. Reeves, P. L. Camwell, and J. McRory, “High Speed Acoustic Telemetry Network Enables Real-Time Along String Measurements, Greatly Reducing Drilling Risk,” 2011.
- [15] M. J. Jellison *et al.*, “Telemetry Drill Pipe: Enabling Technology for the Downhole Internet,” *SPE/IADC Drill. Conf.*, pp. 1–10, 2003.
- [16] J. Neff and P. Camwell, “Field-Test Results of an Acoustic MWD System,” 2007.
- [17] A. Jarrot, A. Gelman, and J. Kusuma, “Wireless Digital Communication Technologies for Drilling: Communication in the Bits/s Regime,” *IEEE Signal Process. Mag.*, vol. 35, no. 2, pp. 112–120, 2018.
- [18] P. L. Camwell, J. G. McRory, and J. M. Neff, “Acoustic telemetry, with multiple nodes in drillstring, used to achieve distributed MWD,” *Innov. While Drill.*, no. March/April, pp. 30–35, 2009.
- [19] S. M. Mwachaka, A. Wu, and Q. Fu, “A review of mud pulse telemetry signal impairments modeling and suppression methods,” *J. Pet. Explor. Prod. Technol.*, vol. 0, no. 0, pp. 1–14, 2018.
- [20] J. B. White and S. GeoMark Re, “GIS-based New Well Second Inter Well Outco d White S,” 2017.

- [21] A. K. Farraj, "Acoustical communications for wireless downhole telemetry systems," no. December, p. 143, 2012.
- [22] G. Jannin, J. Chen, L. E. DePavia, L. Sun, and M. Schwartz, "Deep electrode: A game-changing technology for electromagnetic telemetry," pp. 1059–1063, 2017.
- [23] G. G. Technology, "Megadrill/IXO Bench test," *Green Gecko Technology*, 2015.
[Online]. Available: <https://www.youtube.com/watch?v=jzj1Xuurg6I>.
- [24] S. S. Bae and J. Myoung, "Adaptive Method for High Data Rate Communication in Wells," 2009.
- [25] R. Hay, "Methods and Apparatus for Transmission of Telemetry Data," US8833472B2, 2014.
- [26] S. F. Roca and R. Cited, "Communication Arrangement For Transmission Of Communication Signals Along A Pipeline," 2006.
- [27] U. S. Shashkov P., Khomutov G., Yerokhin A., "Electromagnetic Wellbore Telemetry System for Tubular Strings," US7605715B2, 2012.
- [28] C. T. Spracklen and T. Aslam, "Advanced data communications for downhole data logging and control applications in the oil industry," *IOP Conf. Ser. Mater. Sci. Eng.*, vol. 51, no. 1, 2013.
- [29] J. D. Fitzpatrick, "Well Bottom Hole Status System," 3905010, 1975.
- [30] M. Gearhart, "Telemetry System Involving Gigahertz Transmission In A Gas Filled Tubular Waveguide," 53831549, 1998.
- [31] V. Varveropolous and R. Tajeroam, "Wireless Telemetry Through Drill Pipe," 9500768B2, 2016.
- [32] S. J. Orfanidis, *Electromagnetic Waves and Antennas Chp 9 Waveguides. .*

- [33] S. E. Miller, "Waveguide as a Communication Medium," *BELL Syst. Tech. J.*, vol. XXXIII, no. 6, pp. 1209–1265, 1954.
- [34] P. Wade, "Understanding Circular Waveguide-Experimentally," *QEX*, no. Jan/Feb, pp. 37–48, 2001.
- [35] C. A. Balanis, "Circular waveguides," *Int. J. Electron.*, no. 5, pp. 551–564, 1996.
- [36] D. Pozar, *Microwave Engineering*. 2012.
- [37] D. K. Cheng, *Field and Wave Electromagnetics*. 1989.
- [38] Microwaves101.com, "Waveguide to coax transitions," 2019. [Online]. Available: <https://www.microwaves101.com/encyclopedias/waveguide-to-coax-transitions>.
- [39] C. A. Balanis, *Advanced Engineering Electromagnetics*. John Wiley & Sons, 1989.
- [40] S. J. Orfanidis, *Electromagnetic Waves and Antennas*. Rutgers University, 2016.
- [41] N. Marcuvitz, *MIT Waveguide Handbook*, vol. 10. 2017.
- [42] W. C. Chew, "Lectures on Theory of Microwave and Optical Waveguides," *Lect. Theory Microw. Opt. Waveguides*, p. 362, 2012.
- [43] K. W. Whites, "Electromagnetic Wave Propagation Through Circular Waveguides Containing Radially Inhomogeneous Lossy Media," *USACERL Tech. Manuscr.*, vol. 11, no. September, 1989.
- [44] M. J. Black and M. N. Noui-Mehidi, "High salinity permittivity models to aid water cut meter design," *9th North Am. Conf. Multiph. Technol.*, no. 9, pp. 87–98, 2014.
- [45] S. Beer *et al.*, "In line monitoring of the preparation of water-in-oil-in-water (W/O/W) type multiple emulsions via dielectric spectroscopy," *Int. J. Pharm.*, vol. 441, no. 1–2, pp. 643–647, 2013.
- [46] G. R. Paranjpe and P. Y. Deshpande, "Dielectric properties of some vegetable oils," *Proc.*

- Indian Acad. Sci. - Sect. A*, vol. 1, no. 12, pp. 880–886, 1935.
- [47] K. E. Acoustics, “Dielectric Constants of Common Materials,” vol. الحا العدد, p. 43, 2001.
- [48] S. (Ehsan) Shahidi, C. R. Koch, S. Bhattacharjee, and M. Sadrzadeh, “Dielectric behavior of oil–water emulsions during phase separation probed by electrical impedance spectroscopy,” *Sensors Actuators, B Chem.*, vol. 243, pp. 460–464, 2017.
- [49] R. Lang, Y. Zhou, C. Utku, and D. Le Vine, *Accurate measurements of the dielectric constant of seawater at L band*, vol. 51, no. 1. 2016.
- [50] “Dielectric Constant, Strength, & Loss Tangent,” *RF Cafe*, 2019. [Online]. Available: <http://www.rfcafe.com/references/electrical/dielectric-constants-strengths.htm>.
- [51] D. H. Gadani, V. A. Rana, S. P. Bhatnagar, A. N. Prajapati, and A. D. Vyas, “Effect of salinity on the dielectric properties of water,” *Indian J. Pure Appl. Phys.*, vol. 50, no. June, pp. 405–410, 2012.
- [52] H. J. Liebe, G. A. Hufford, and T. Manabe, “A model for the complex permittivity of water at frequencies below 1 THz,” *Int. J. Infrared Millimeter Waves*, vol. 12, no. 7, pp. 659–675, 1991.
- [53] R. Buchner, J. Barthel, and J. Stauber, “The dielectric relaxation of water between 0 ° C and 35 ° C,” *Chem. Phys. Lett.*, vol. 306, no. 1–2, pp. 57–63, 1999.
- [54] V. Komarov, S. Wang, and J. Tang, “Permittivity and Measurements,” *Encycl. RF Microw. Eng.*, 2005.
- [55] A. Rajab, A. Sulaeman, S. Sudirham, and S. Suwarno, “A Comparison of Dielectric Properties of Palm Oil with Mineral and Synthetic Types Insulating Liquid under Temperature Variation,” *ITB J. Eng. Sci.*, vol. 43, no. 3, pp. 191–208, 2011.
- [56] Shell Chemicals, “Cargo Handling Sheet,” no. April, pp. 1–4, 2018.

- [57] R. Lee, "File:Annulus diagram for oil wells.jpg." [Online]. Available:
https://commons.wikimedia.org/wiki/File:Annulus_diagram_for_oil_wells.jpg.
- [58] E. R. Drilling, "Drilling Fluids Reference Manual," *Ref. Man.*, pp. 1–775, 2006.
- [59] G. E. Wilson, "A General Overview of Air Drilling and Deviation Control," *J. Pet. Technol.*, vol. 33, no. 12, pp. 2307–2315, 2007.
- [60] Petrowiki, "Drilling fluid types," 2015. [Online]. Available:
https://petrowiki.org/Drilling_fluid_types.
- [61] Wikipedia, "Logging While Drilling." [Online]. Available:
https://en.wikipedia.org/wiki/Logging_while_drilling.
- [62] S. Bargach *et al.*, "Real-Time LWD: Logging for Drilling," *Oilfield Rev.*, no. Autumn, pp. 58–78, 2000.
- [63] Schlumberger, "measurements-while-drilling - Oilfield Glossary," 2019. [Online].
Available: <https://www.glossary.oilfield.slb.com/Terms/m/measurements-while-drilling.aspx>.
- [64] Petrowiki, "Measurement while drilling (MWD)," *Society of Petroleum Engineers*, 2018.
[Online]. Available: [https://petrowiki.org/Measurement_while_drilling_\(MWD\)](https://petrowiki.org/Measurement_while_drilling_(MWD)).
- [65] R. Hydro, "Sound Speeds in Water, Liquid and Materials," 2019. [Online]. Available:
<https://www.rshydro.co.uk/sound-speeds/>.
- [66] Tkgd2007, "File:Coaxial cable cutaway.svg," 2008. [Online]. Available:
https://commons.wikimedia.org/wiki/File:Coaxial_cable_cutaway.svg.
- [67] SuperManu, "File:Onde electromagnetique.svg," 2007. [Online]. Available:
https://en.wikipedia.org/wiki/File:Onde_electromagnetique.svg.
- [68] Wikipedia, "Minimum detectable signal,"

- https://en.wikipedia.org/wiki/Minimum_detectable_signal, 2019. .
- [69] Hyperphysics, “File:Diel.png,” 2011. [Online]. Available:
<https://en.wikipedia.org/wiki/Permittivity#/media/File:Diel.png>.
- [70] Archimerged, “File:Dielectric responses.svg,” 2008. [Online]. Available:
https://commons.wikimedia.org/wiki/File:Dielectric_responses.svg.
- [71] ANSYS Inc., “Ansys 18.2 HFSS Online Help,” no. July. 2017.
- [72] Invensys Foxboro, “Conductivity Ordering Guide,” *Invensys Price Sheet*, no. 6–3PREF. p. 1, 1999.
- [73] Fvasconcellos, “File:Emulsions.svg,” 2007. [Online]. Available:
<https://en.wikipedia.org/wiki/File:Emulsions.svg>.
- [74] F. B. Growcock, C. F. Ellis, D. D. Schmidt, and J. J. Azar, “Electrical Stability, Emulsion Stability, and Wettability of Invert Oil-Based Muds,” *SPE Drill. Complet.*, vol. 9, no. 01, pp. 39–46, 2007.
- [75] A. Ali, D. D. Schmidt, and J. Harvey III, “Investigation of the Electrical Stability Test for Oil Muds,” in *SPE/IADC Drilling Conference*, 1987.
- [76] “Z-44 Chayvo Well: The Deepest Oil Extraction (Infographic),” *Oil & Gas IQ News*, 2017. [Online]. Available: <https://www.oilandgasiq.com/drilling-and-development/articles/z-44-chayvo-well-the-deepest-oil-extraction>.
- [77] M. Patin, G. D’Ablaing, A. Orr, and J. Meyers, “Optimizing Operational Parameters Can ‘Save You Money’ as Well as Improving Bit Life and ROP,” *AADE Natl. Tech. Conf. Exhib.*, no. 07-NTCE-26, pp. 0–3, 2007.

Appendix A: Kirkby 3.5mm Cal Kit Standards Coefficients

Male Open

C0 50.389

C1 761.36

C2 -968.22

C3 68.376

Delay: 55.1 ps

Loss 3.0 G ohm/s

Female Open

C0 53.004

C1 135.167

C2 95.6305

C3 30.937

Delay: 39.8 ps

Loss 3.0 G ohm/s

Male Short:

Delay 57.834 ps

L0=L1=L2=L3=0

Loss 3.0 G ohm/s

Female Short:

Delay 41.398 ps

L0=L1=L2=L3=0

Loss 3.0 G ohm/s

Male-Male thru

Delay 75.722 ps

Loss 3.0 G ohm/s

Female-Female thru

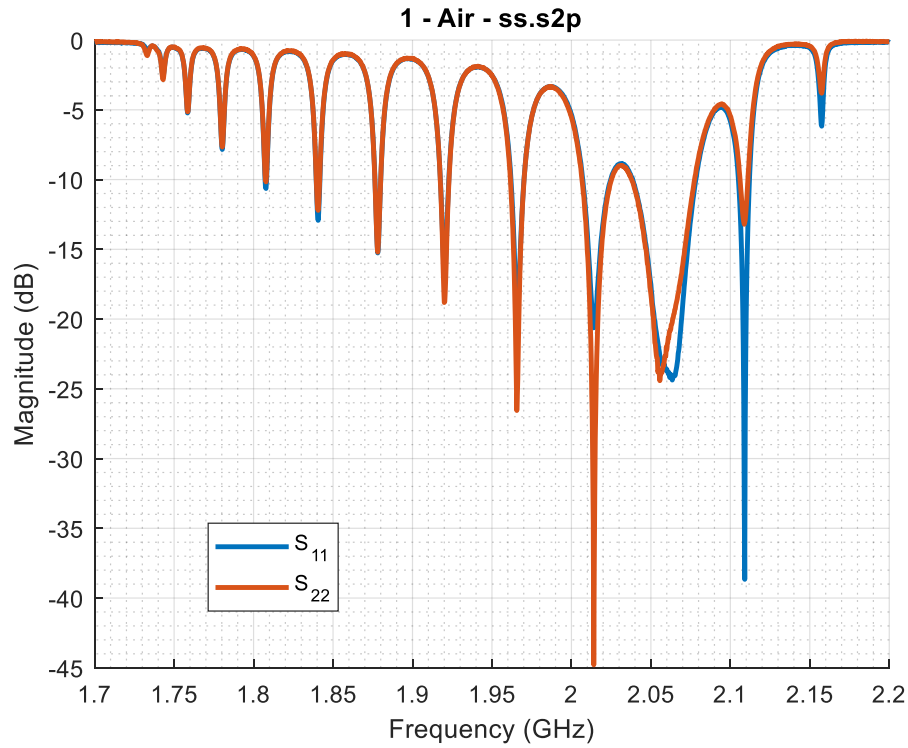
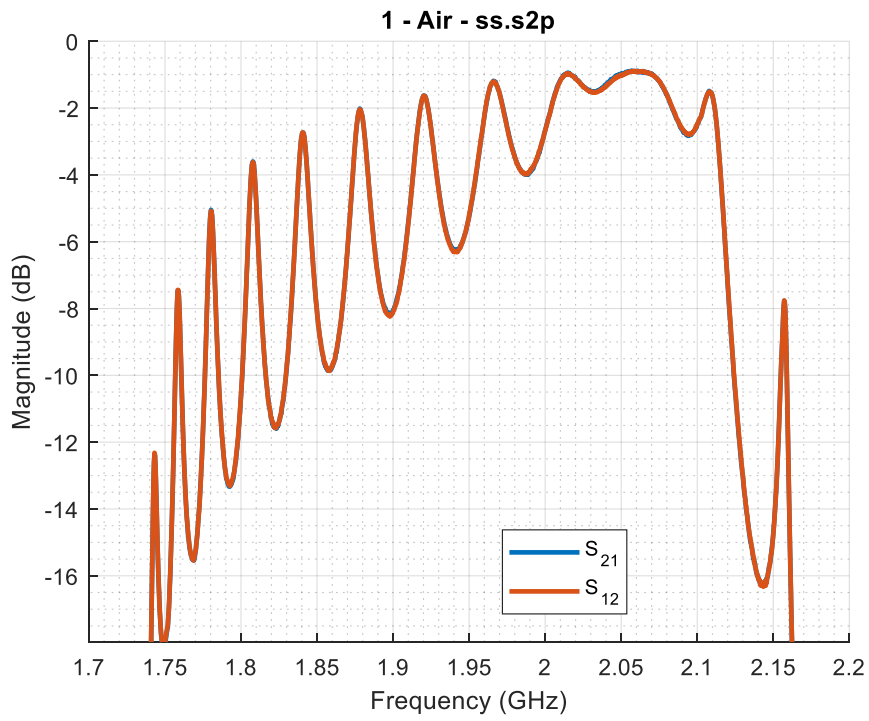
Delay 41.398

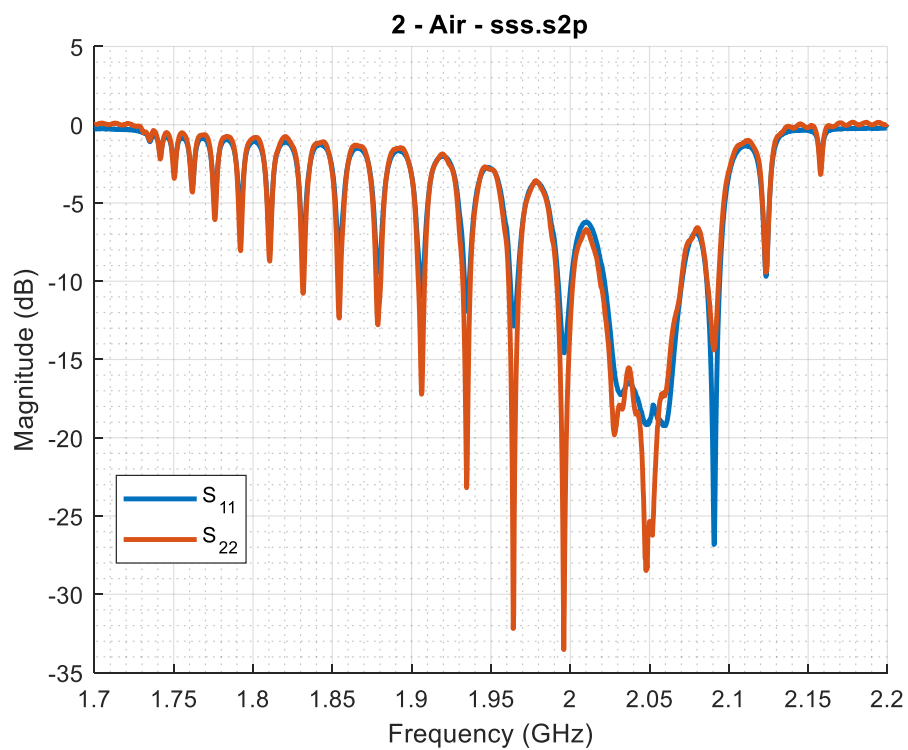
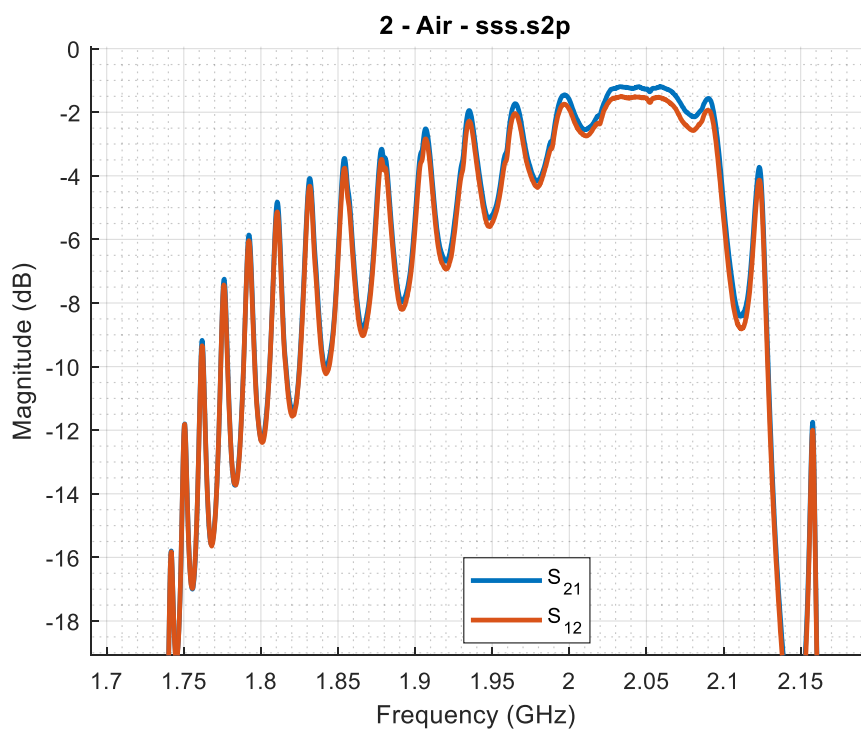
Loss 3.0 G ohm/s

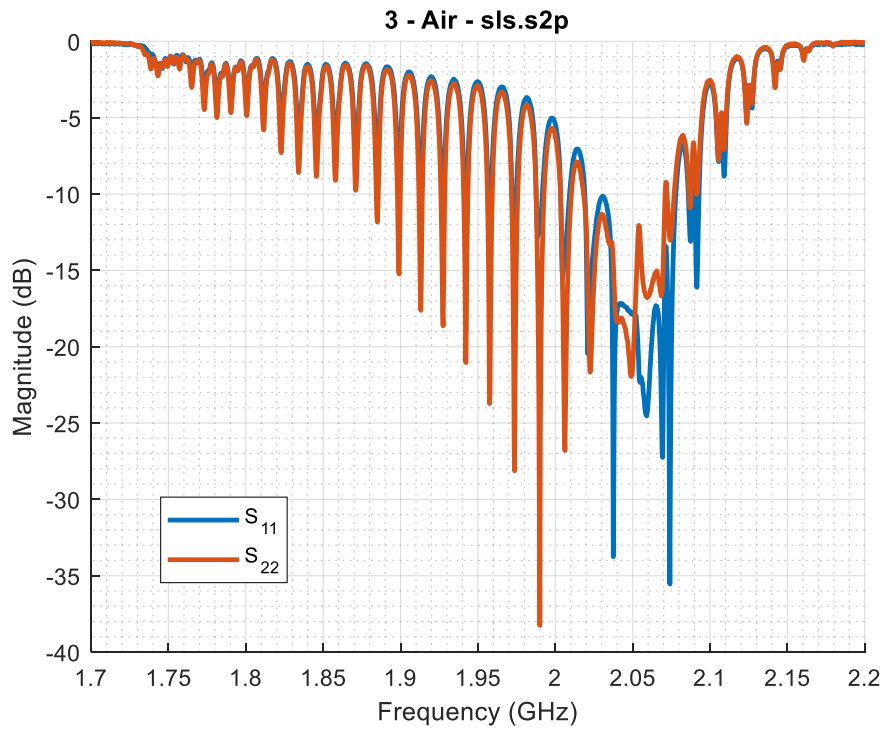
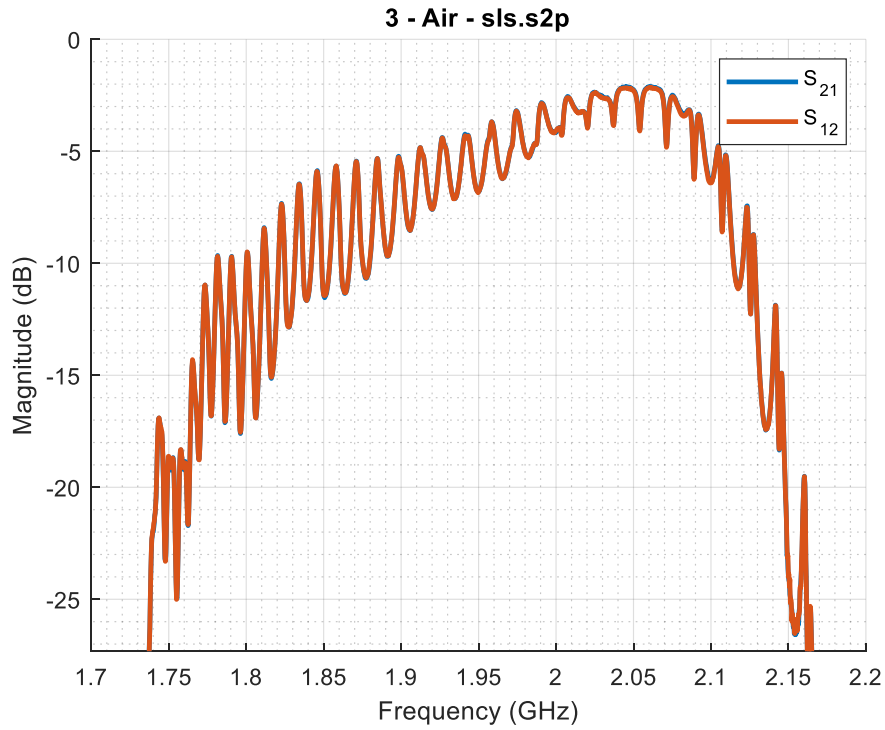
Appendix B: Pipe Conductivity Measurements

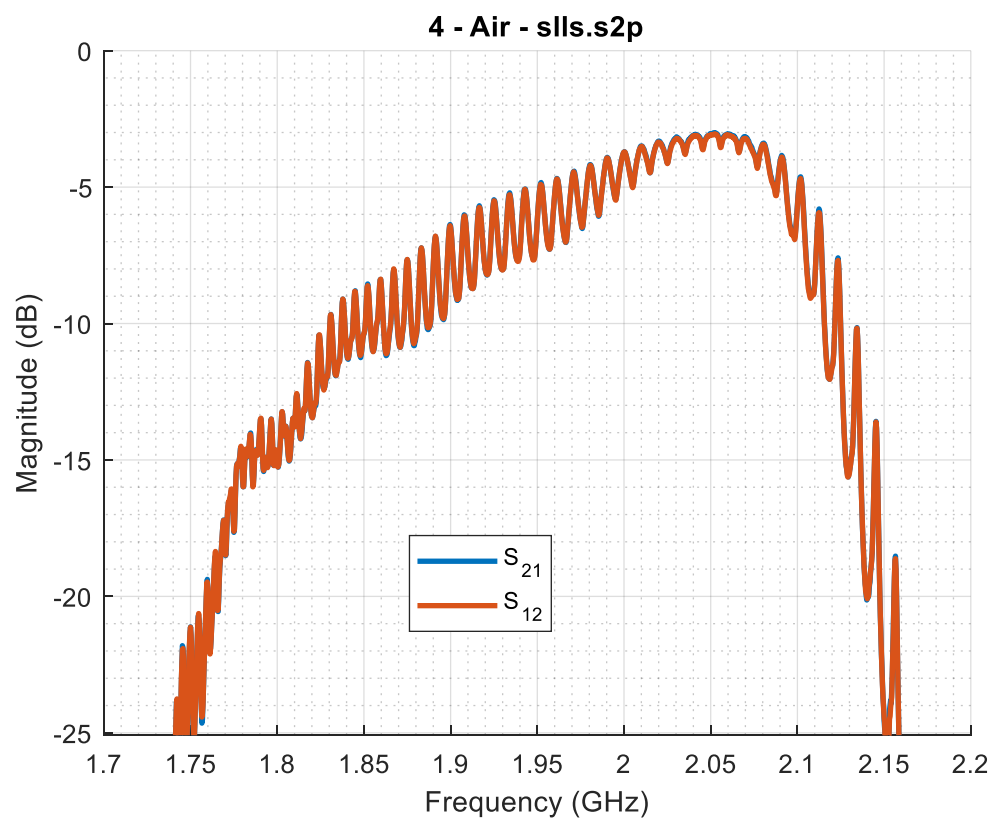
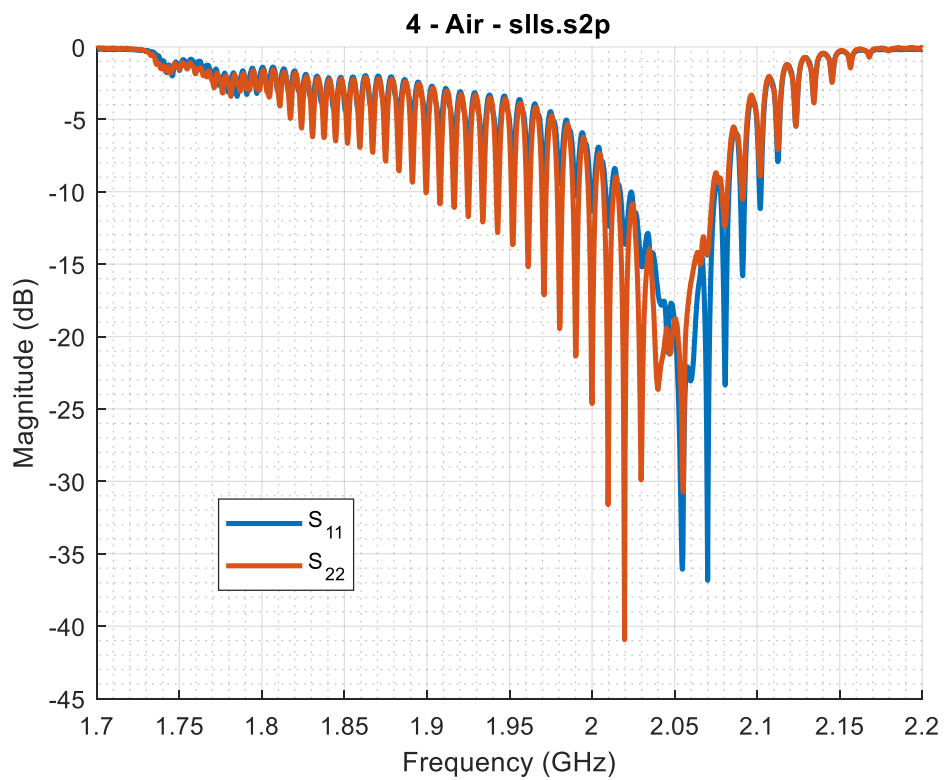
Pipe Length (m)	Current Forced (A)	Voltage Measured (mV)	Resistance (mΩ)	Conductivity (S/m)
10.33	0.998	0.865	0.867	4.12E+06
10.33	2.015	1.756	0.871	4.10E+06
10.33	3.045	2.660	0.874	4.09E+06
10.33	3.987	3.480	0.873	4.09E+06
10.33	5.040	4.389	0.871	4.10E+06
10.33	5.980	5.218	0.873	4.09E+06
9.60	1.000	0.793	0.793	4.18E+06
9.60	1.945	1.547	0.795	4.17E+06
9.60	3.012	2.398	0.796	4.16E+06
9.60	4.020	3.194	0.795	4.17E+06
9.60	4.970	3.954	0.796	4.17E+06
9.60	6.040	4.804	0.795	4.17E+06
9.51	1.018	0.797	0.783	4.20E+06
9.51	2.010	1.574	0.783	4.19E+06
9.51	3.013	2.366	0.785	4.18E+06
9.51	4.000	3.145	0.786	4.18E+06
9.51	5.050	3.959	0.784	4.19E+06
9.51	6.000	4.705	0.784	4.19E+06
6.37	0.998	0.528	0.529	4.16E+06
6.37	1.995	1.059	0.531	4.15E+06
6.37	3.001	1.599	0.533	4.13E+06
6.37	3.980	2.118	0.532	4.14E+06
6.37	5.040	2.683	0.532	4.14E+06
6.37	6.010	3.189	0.531	4.15E+06
6.32	0.983	0.509	0.518	4.22E+06
6.32	2.016	1.047	0.519	4.21E+06
6.32	3.005	1.561	0.519	4.20E+06
6.32	4.010	2.086	0.520	4.20E+06
6.32	5.020	2.606	0.519	4.21E+06
6.32	6.010	3.122	0.519	4.20E+06
3.16	0.998	0.275	0.276	3.96E+06
3.16	2.013	0.555	0.276	3.96E+06
3.16	3.036	0.845	0.278	3.92E+06
3.16	4.020	1.120	0.279	3.92E+06
3.16	5.010	1.395	0.278	3.92E+06
3.16	6.080	1.688	0.278	3.93E+06
3.09	1.005	0.250	0.249	4.30E+06
3.09	1.998	0.500	0.250	4.28E+06
3.09	2.966	0.743	0.251	4.27E+06
3.09	4.020	1.007	0.250	4.27E+06
3.09	4.970	1.245	0.251	4.27E+06
3.09	5.990	1.501	0.251	4.27E+06
			Average:	4.15E+06

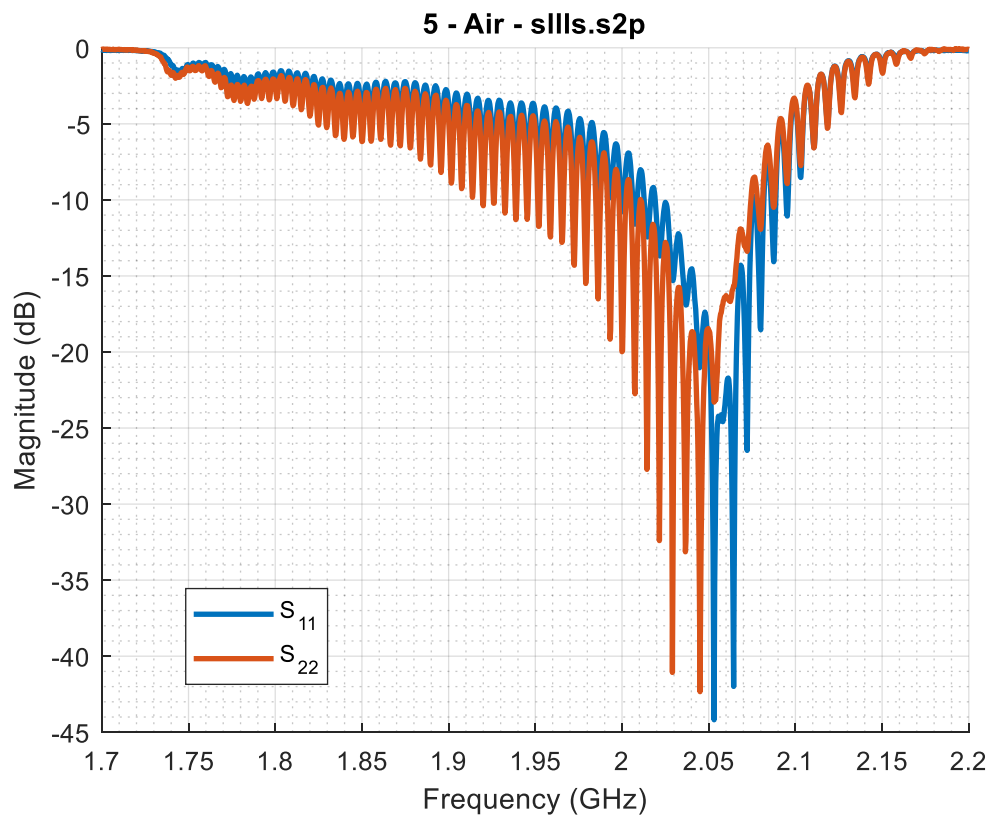
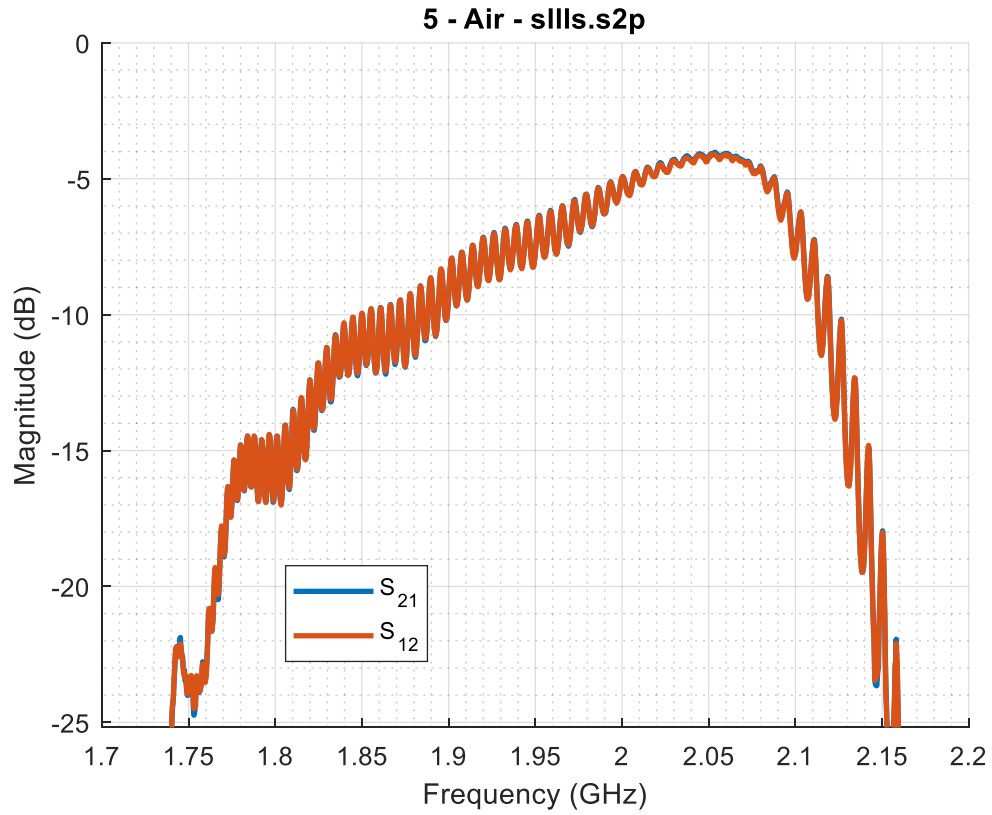
Appendix C: Air S-Parameter Plots



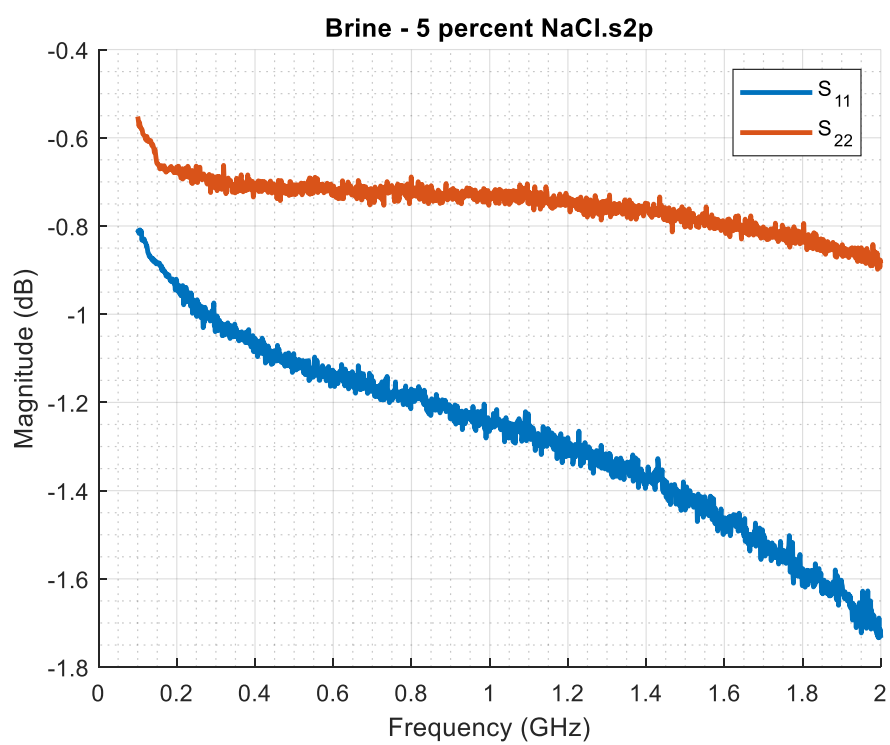
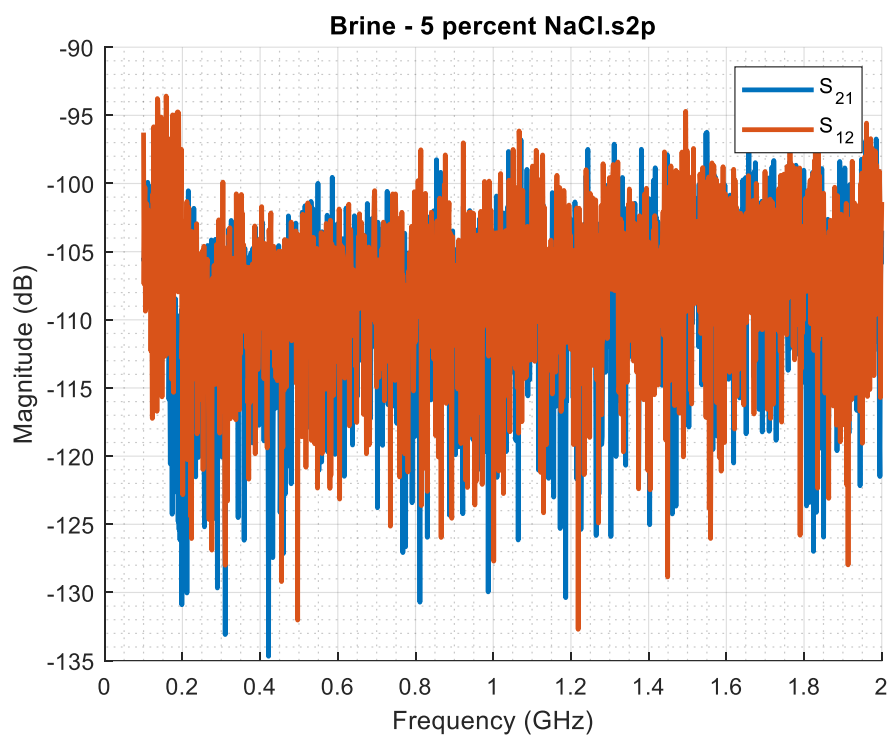


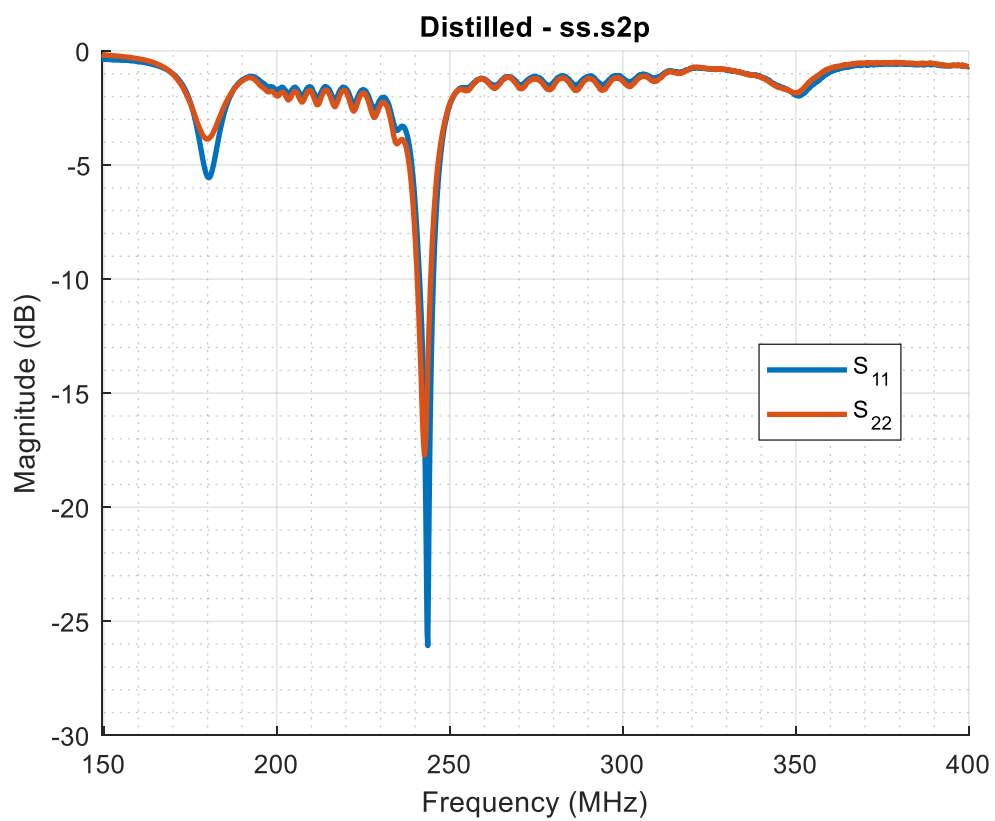
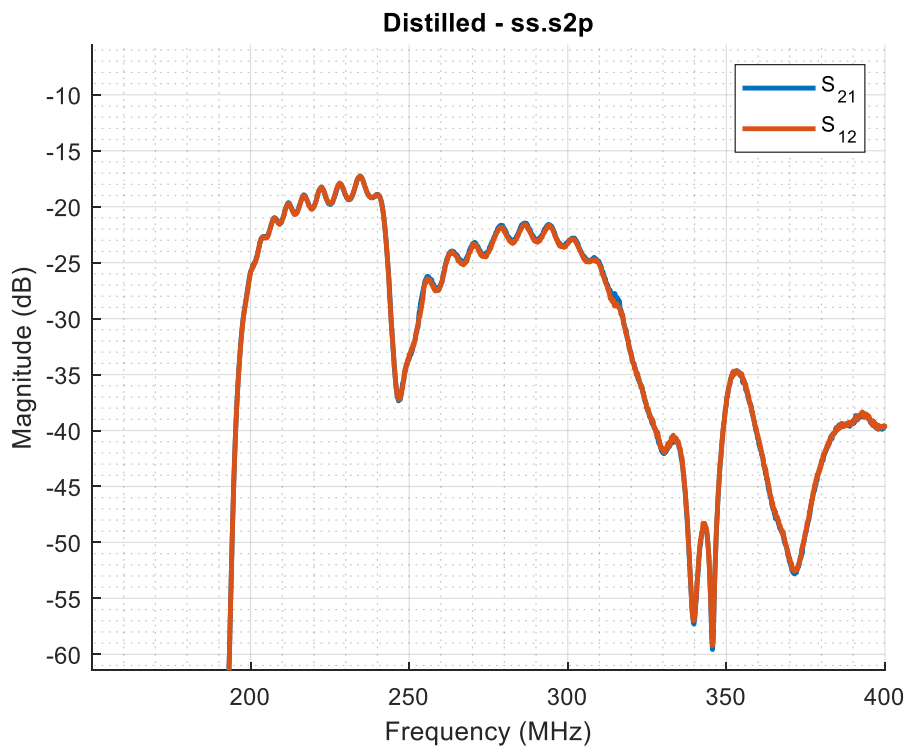


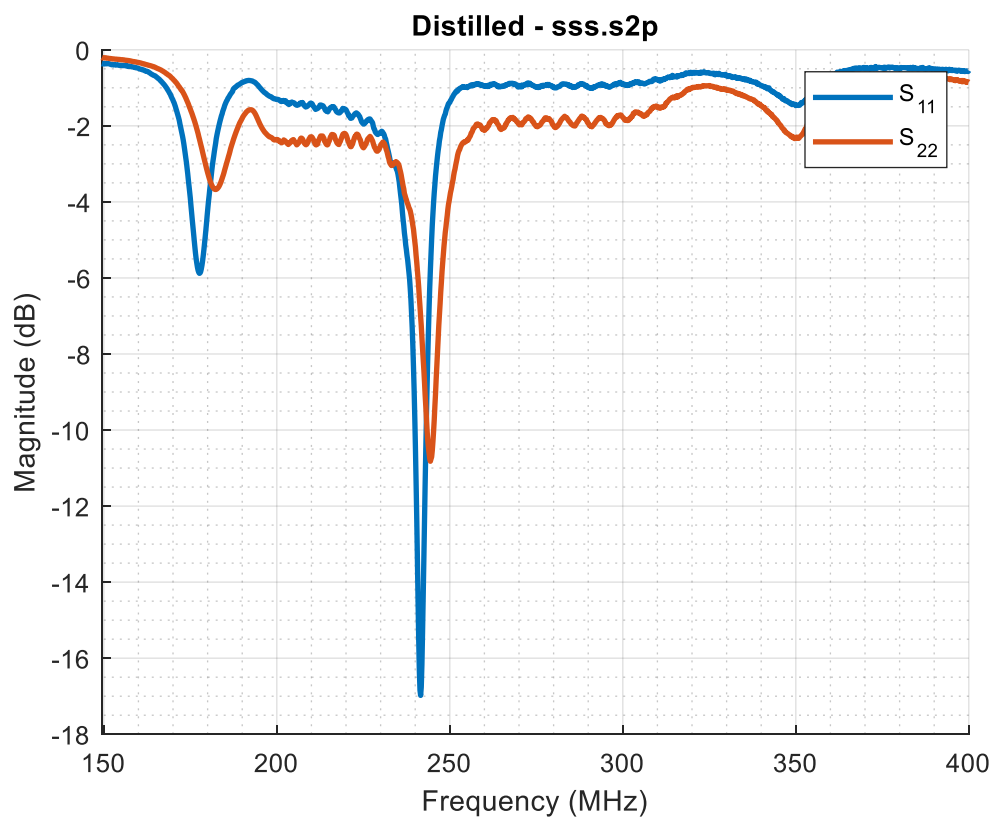
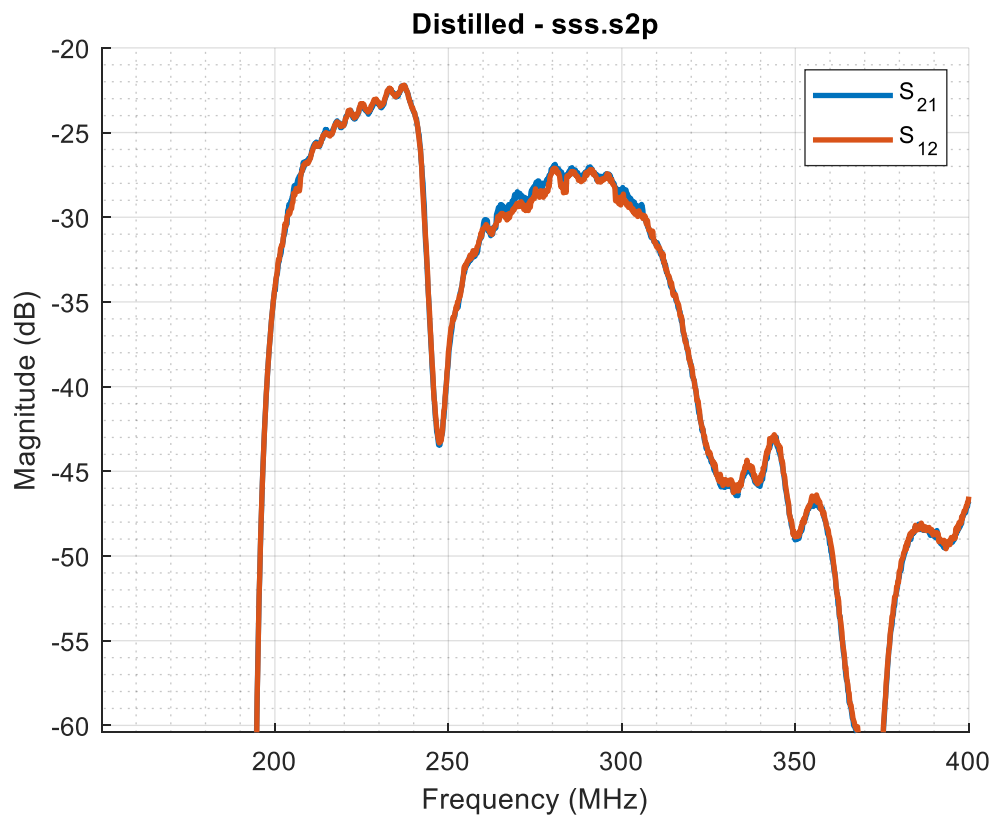




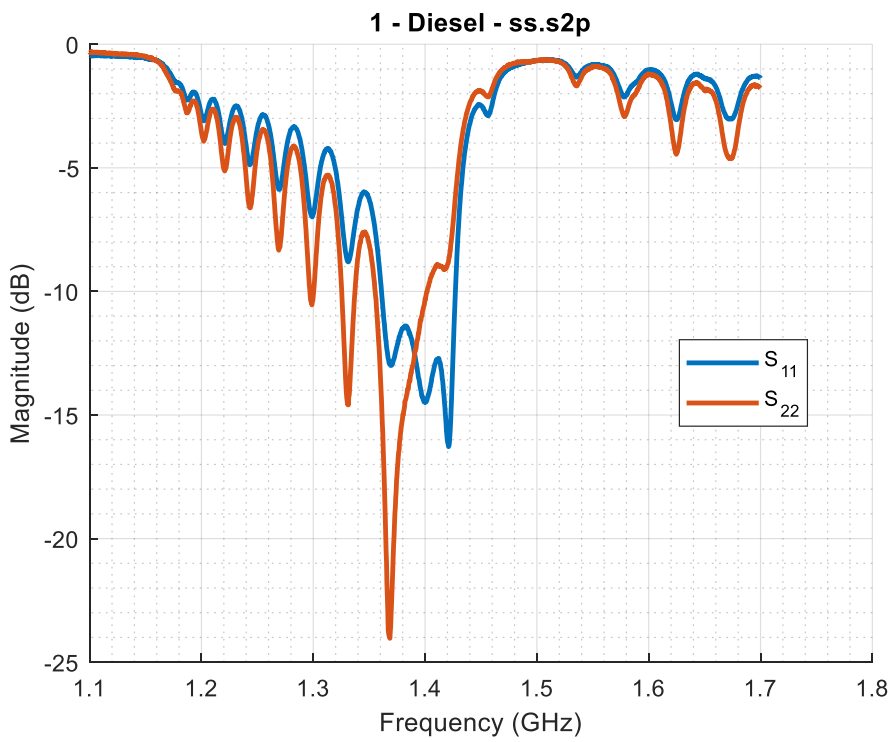
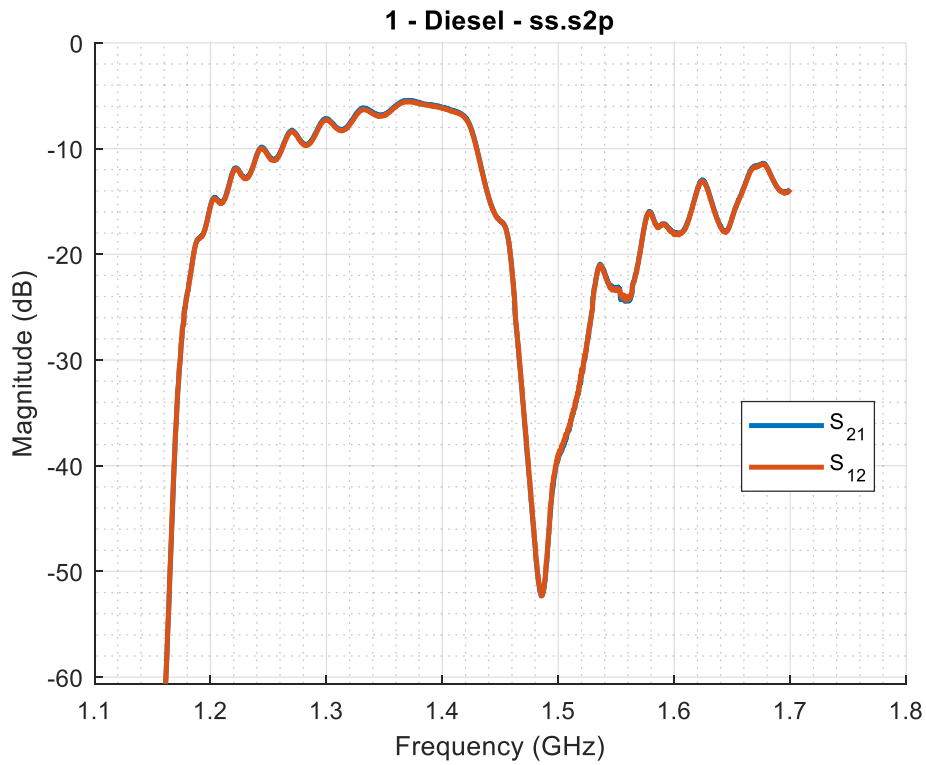
Appendix D: Water S-Parameter Plots

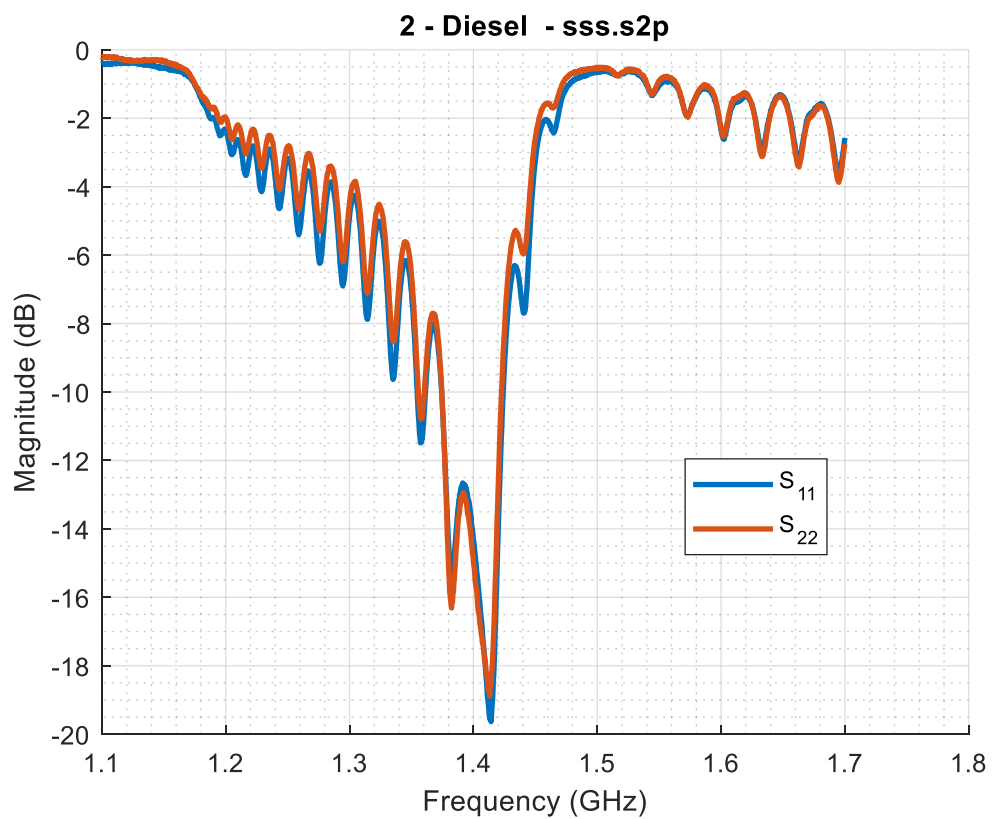
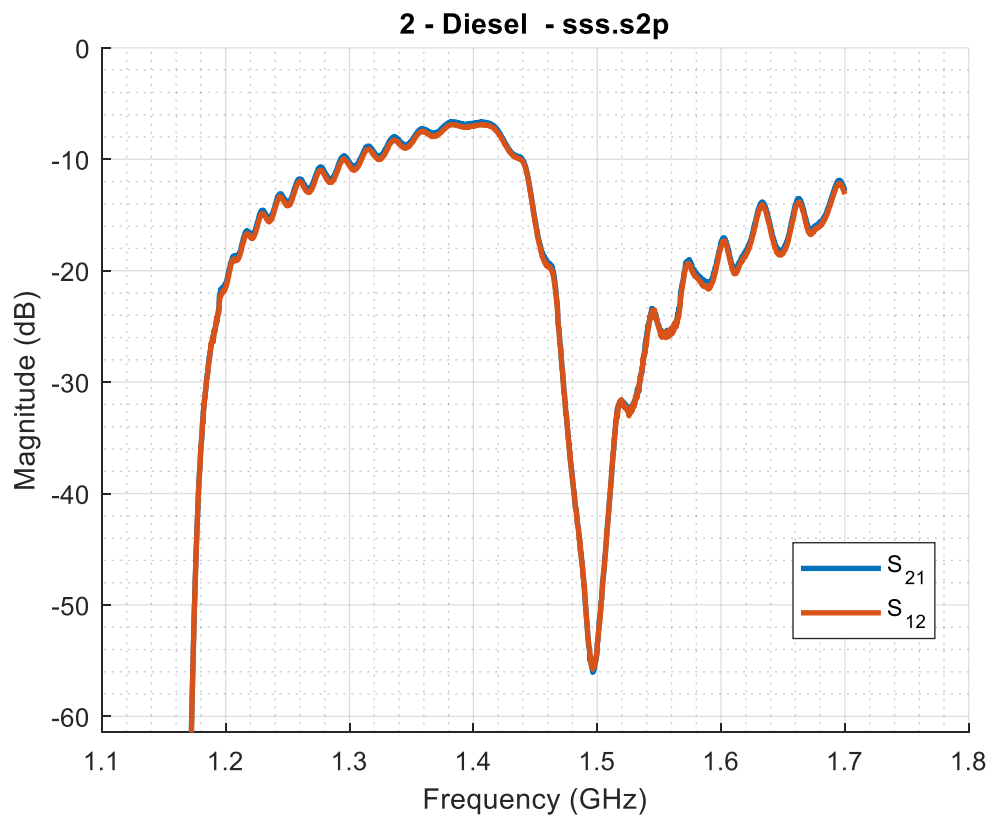


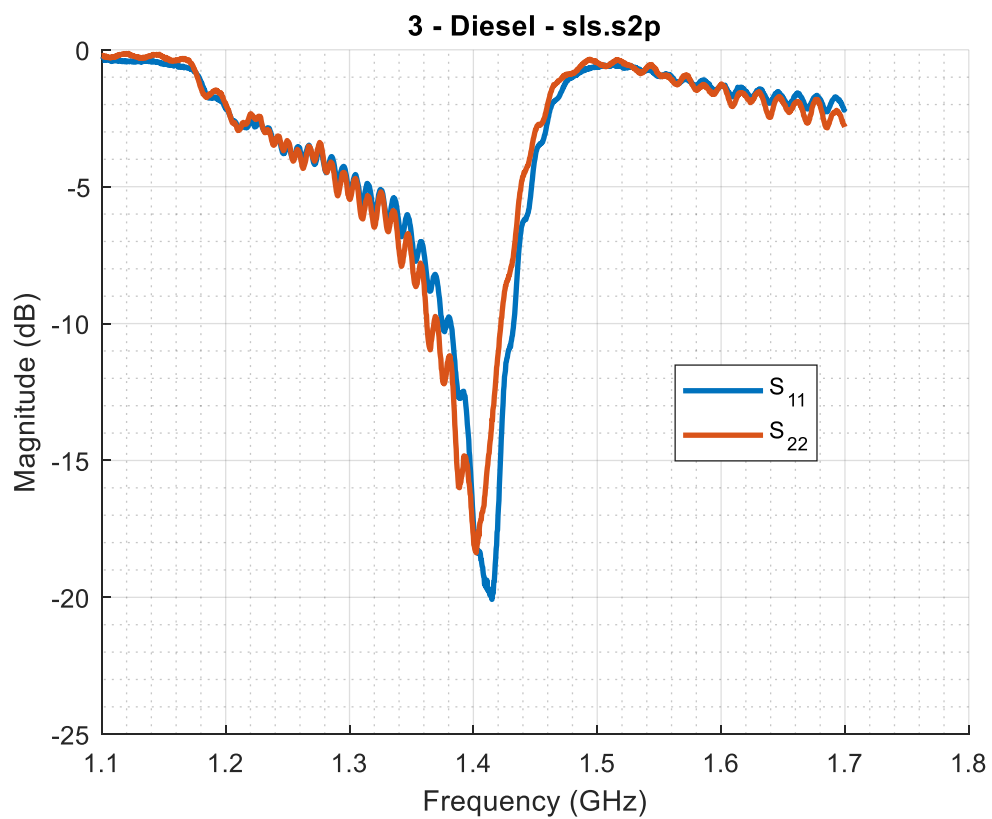
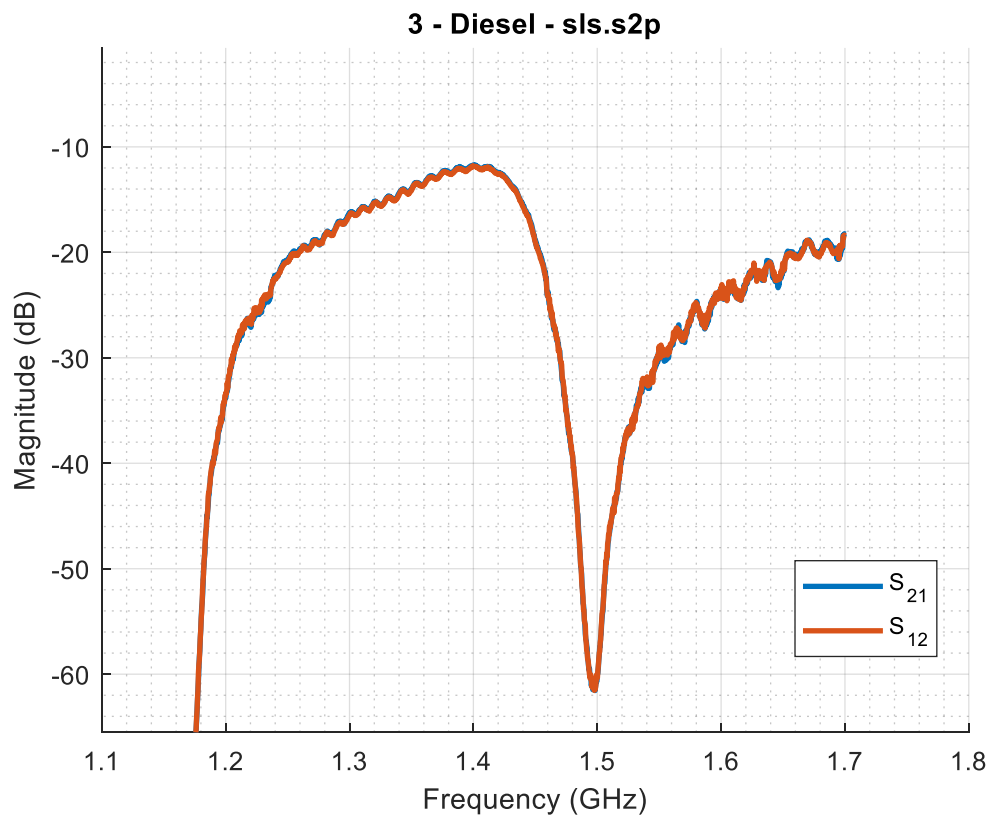




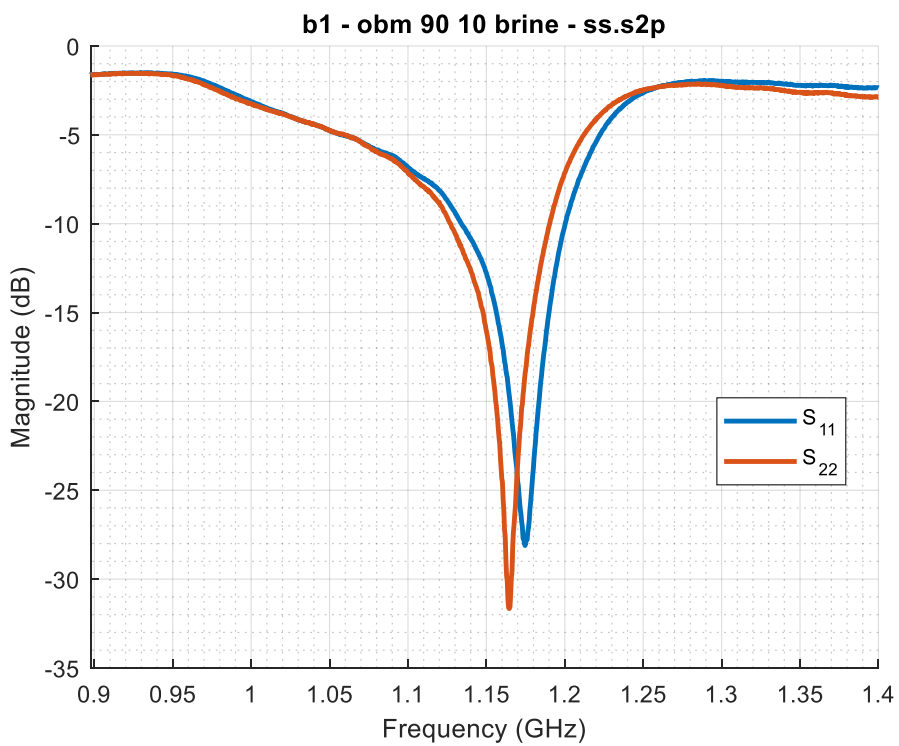
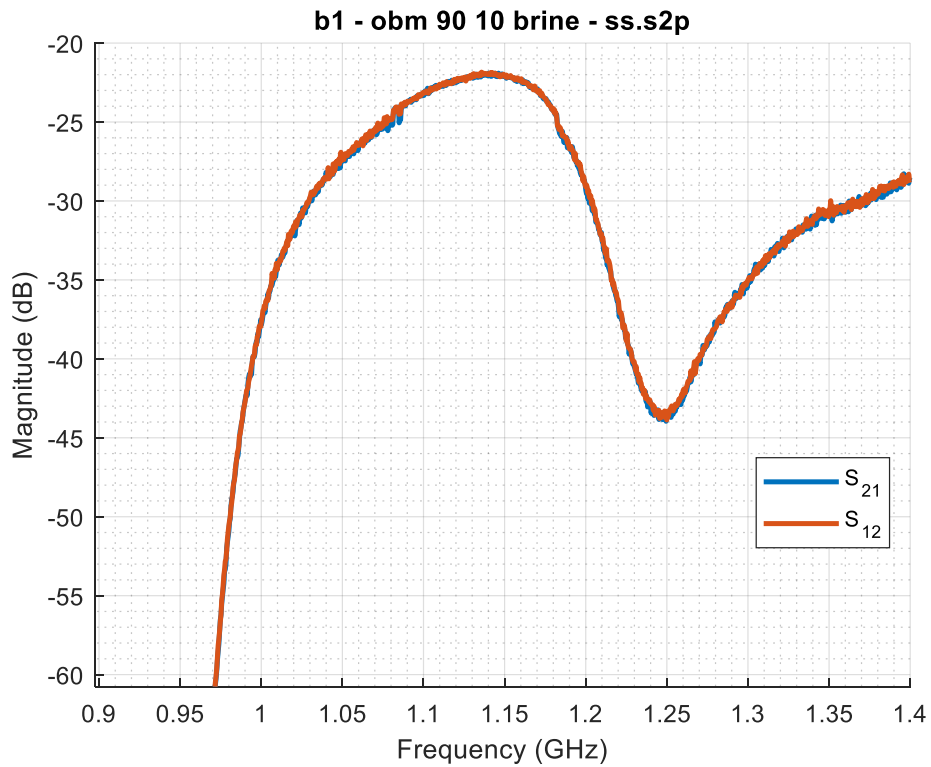
Appendix E: Diesel S-Parameter Plots

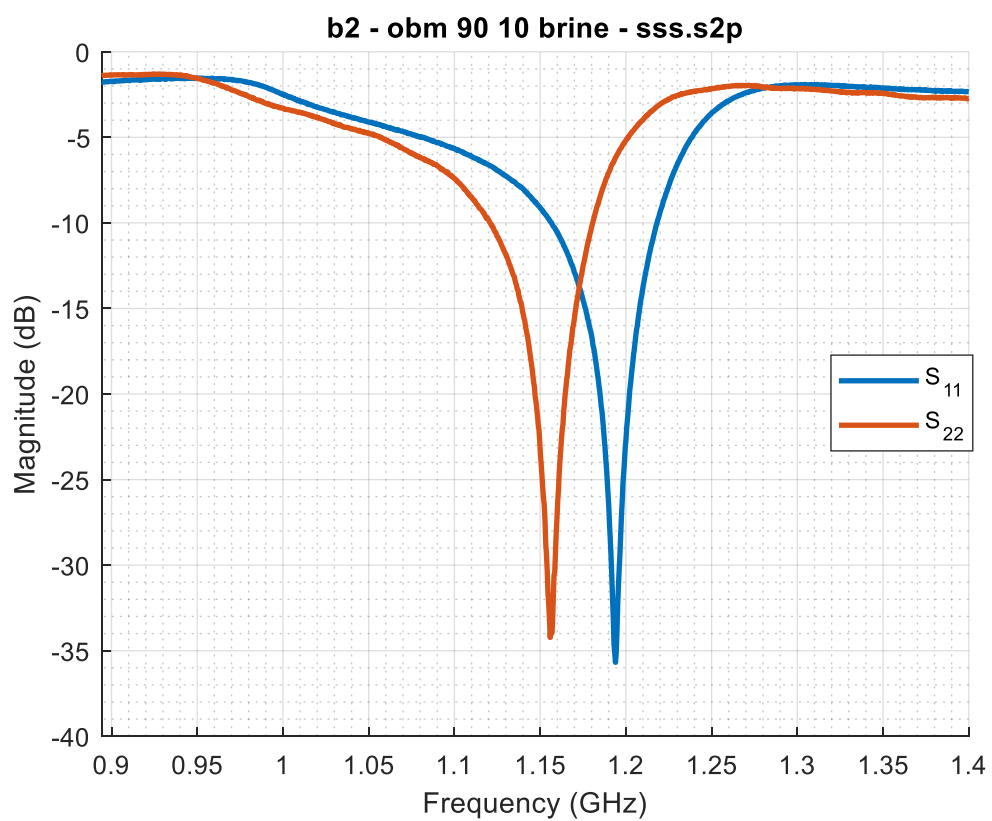
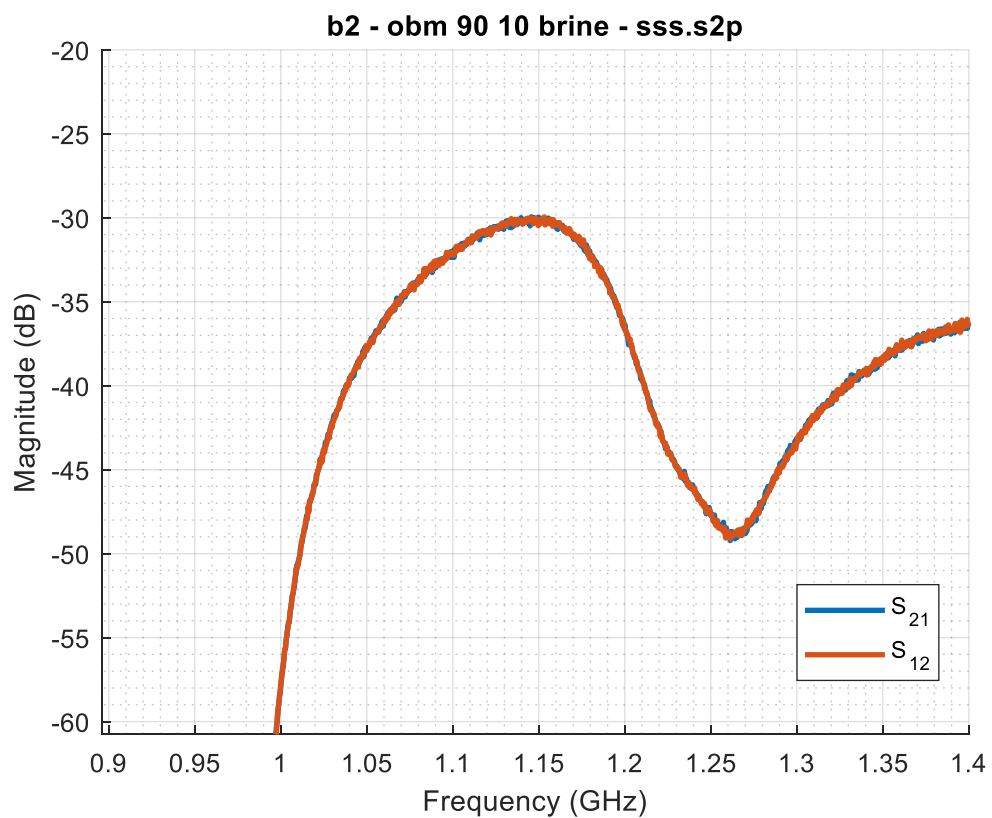


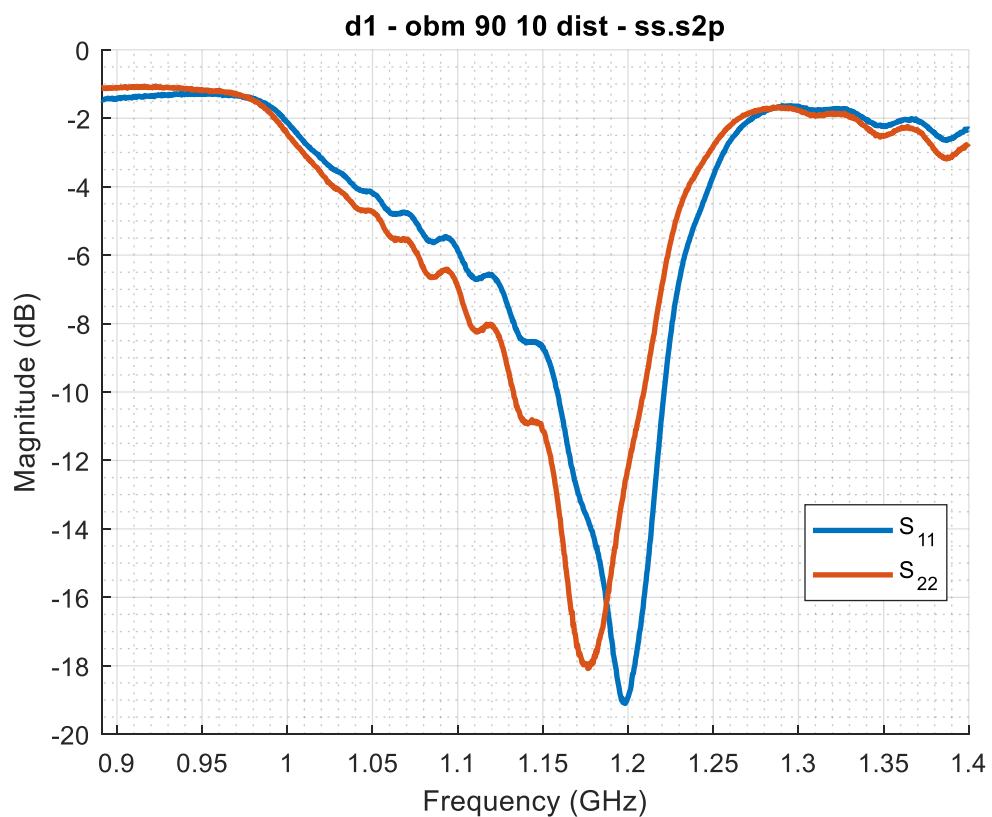
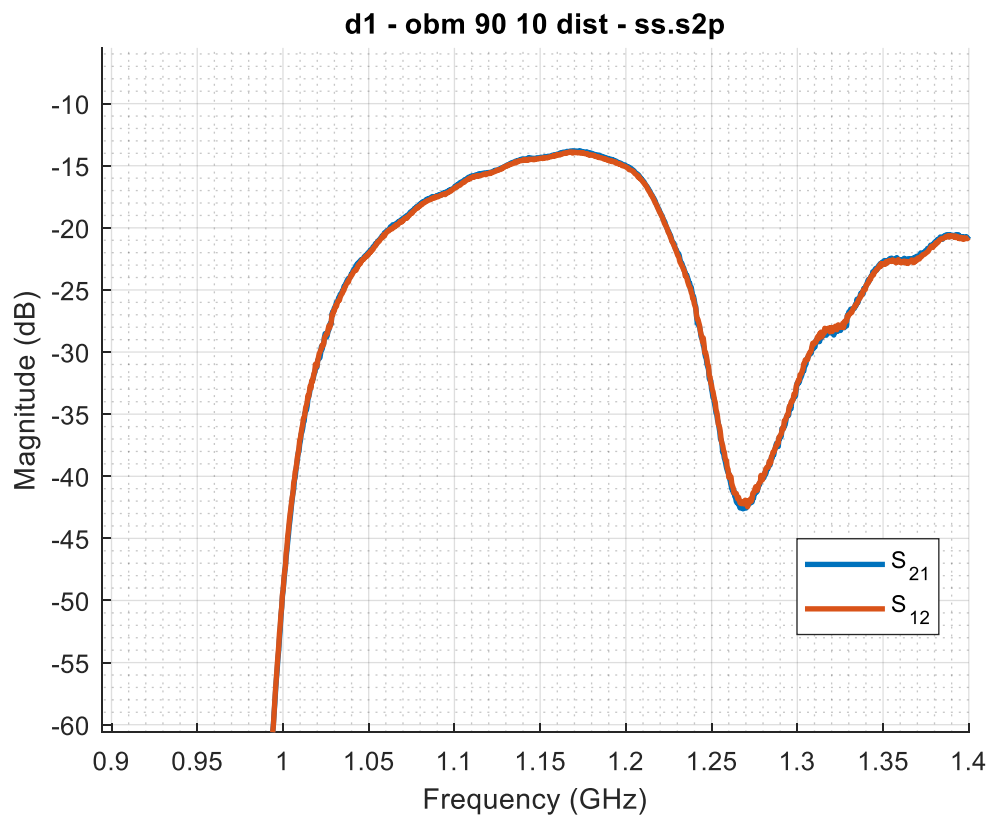


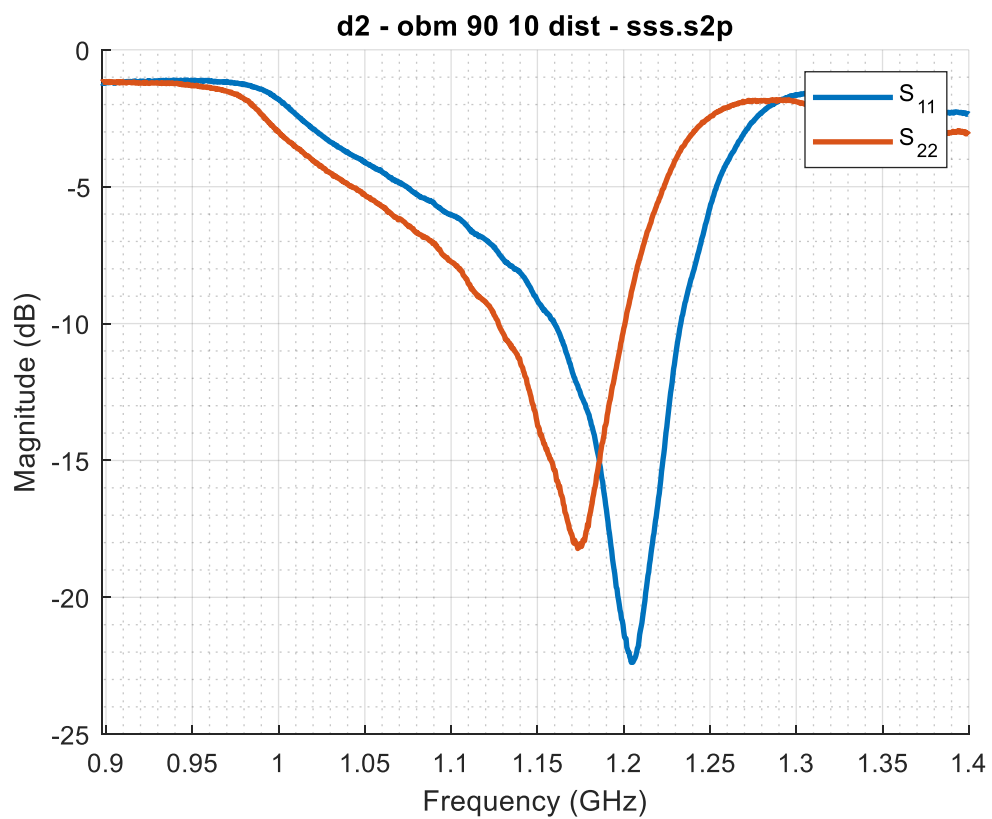
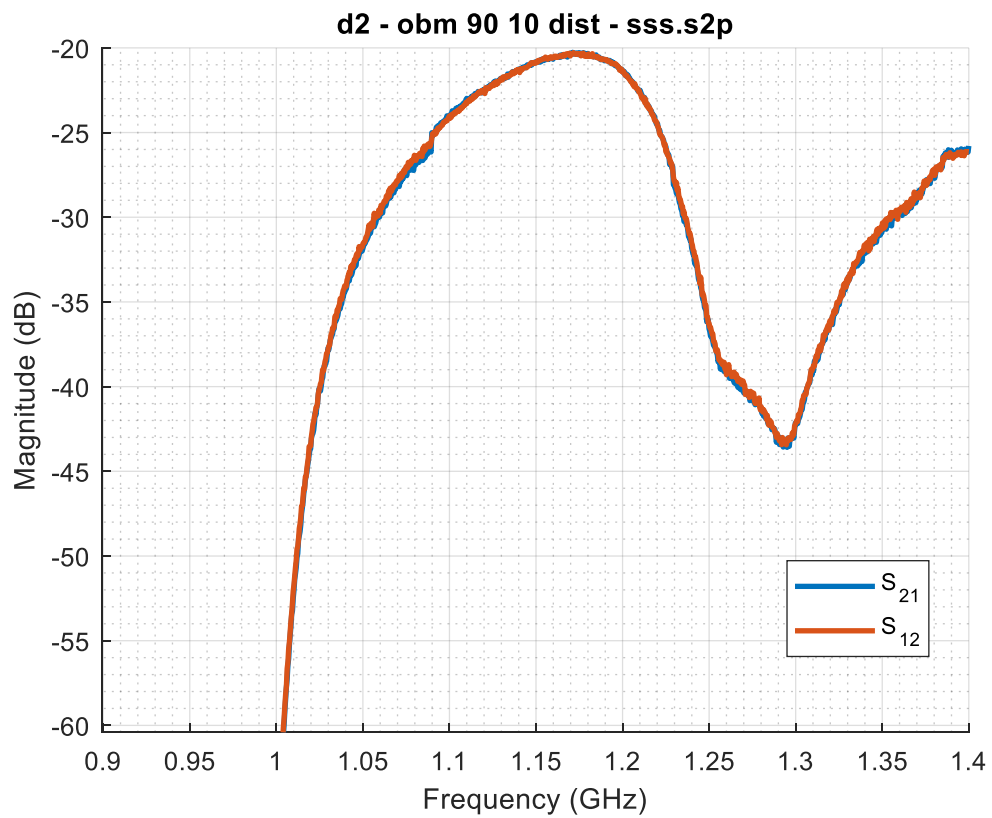


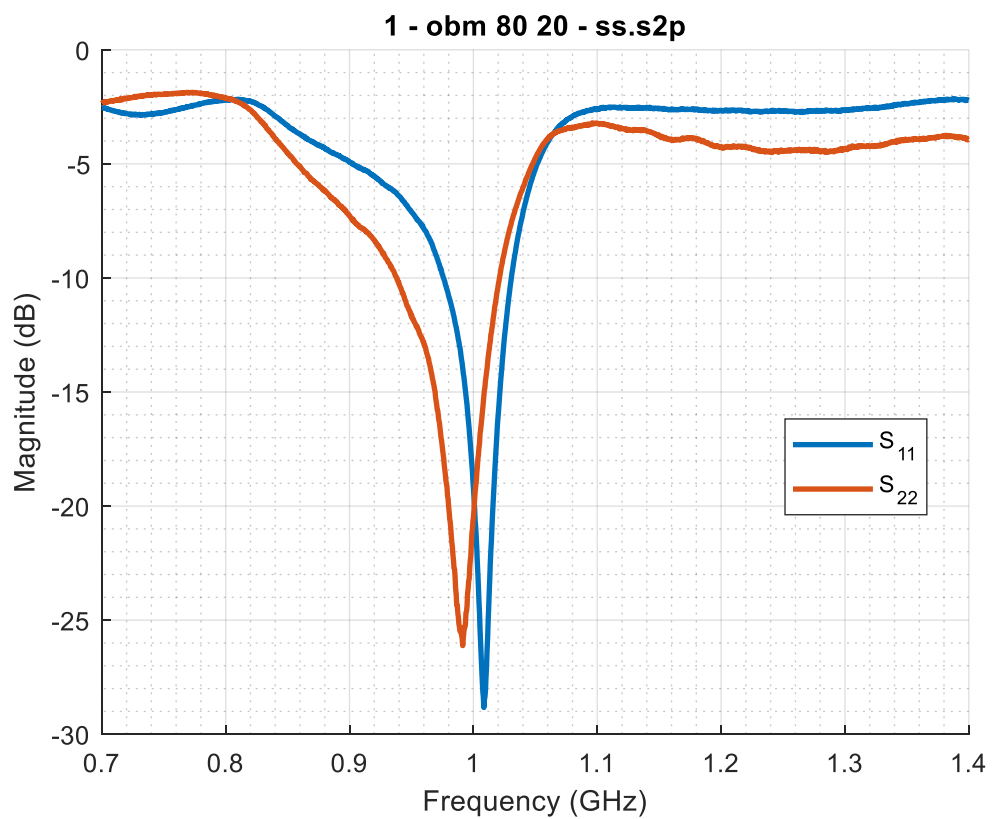
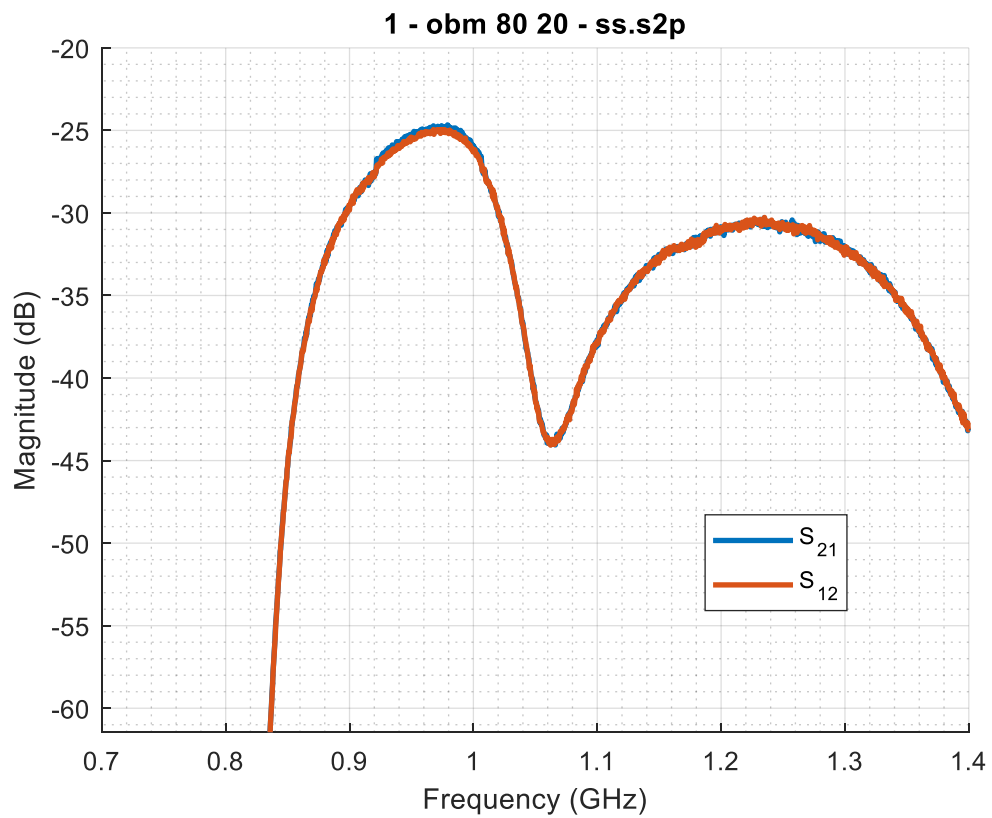
Appendix F: OBF S-Parameter Plots

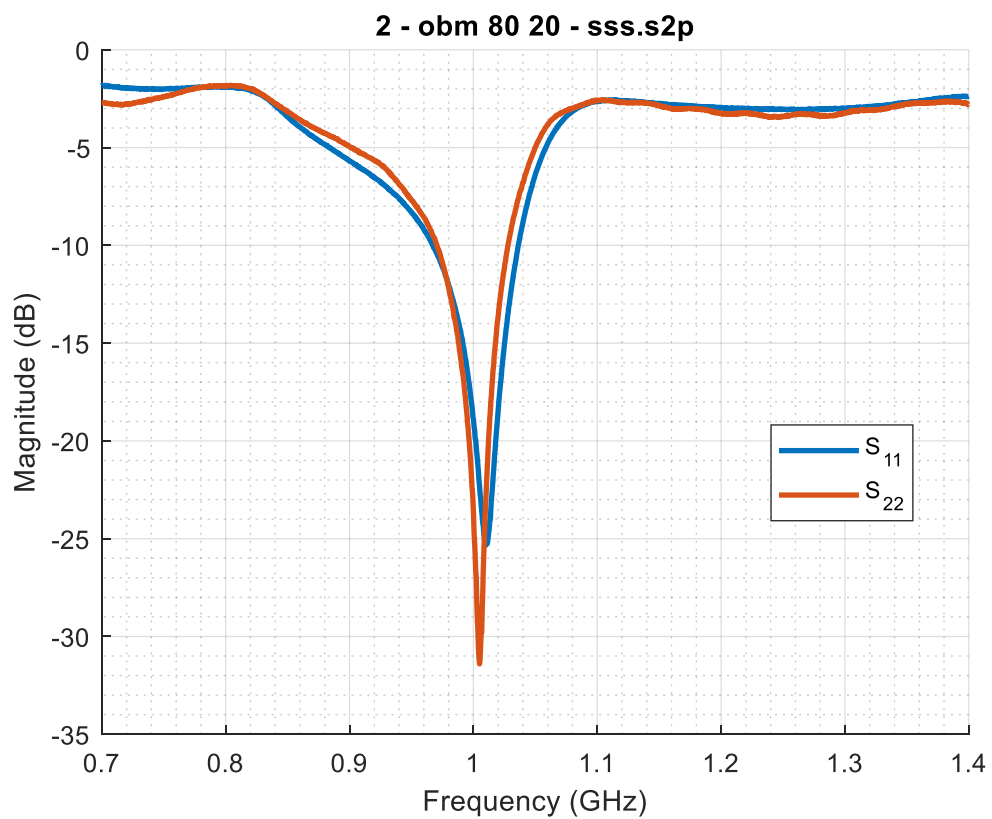
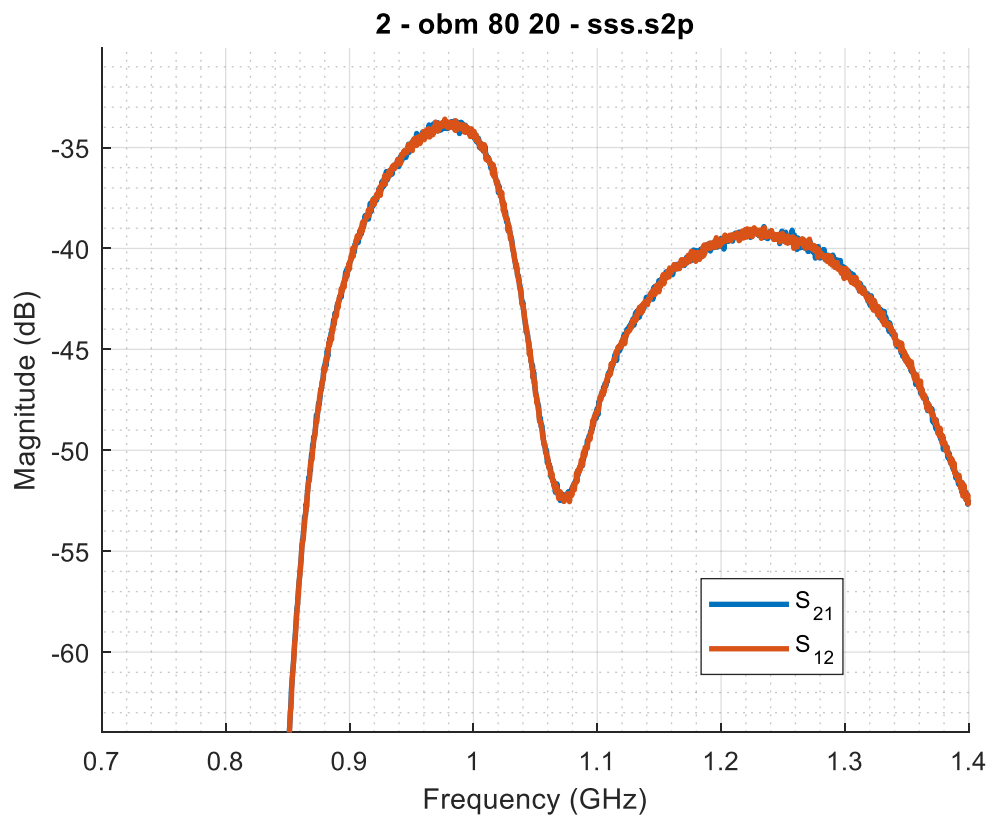


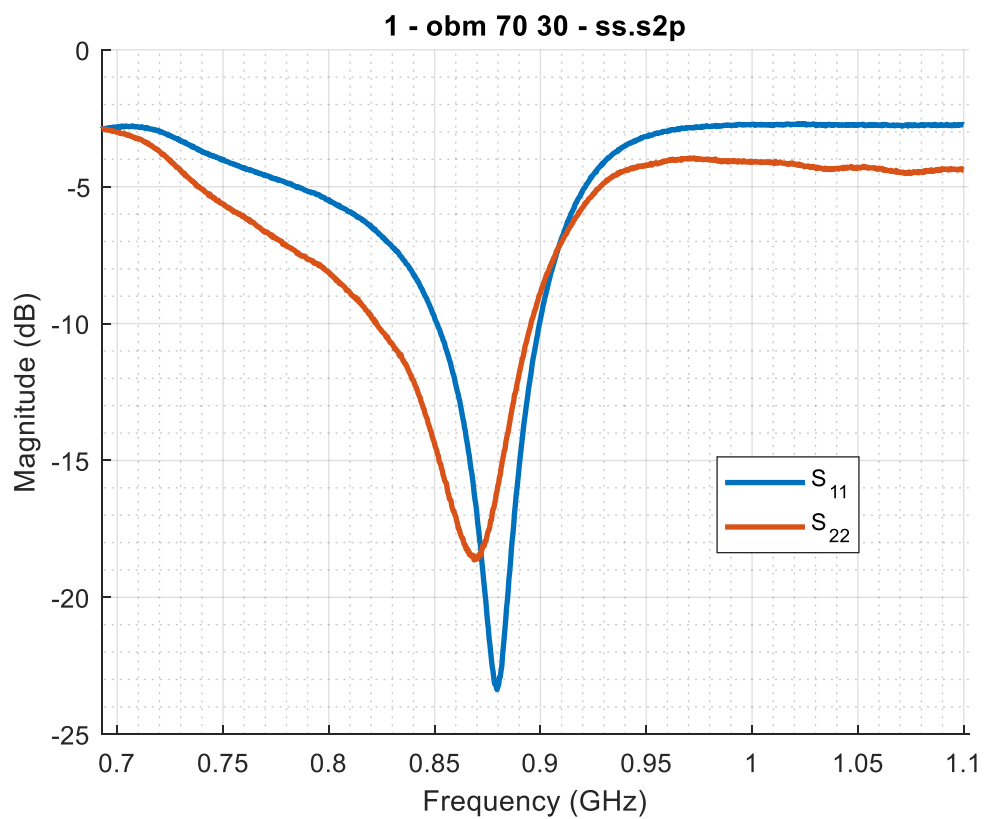
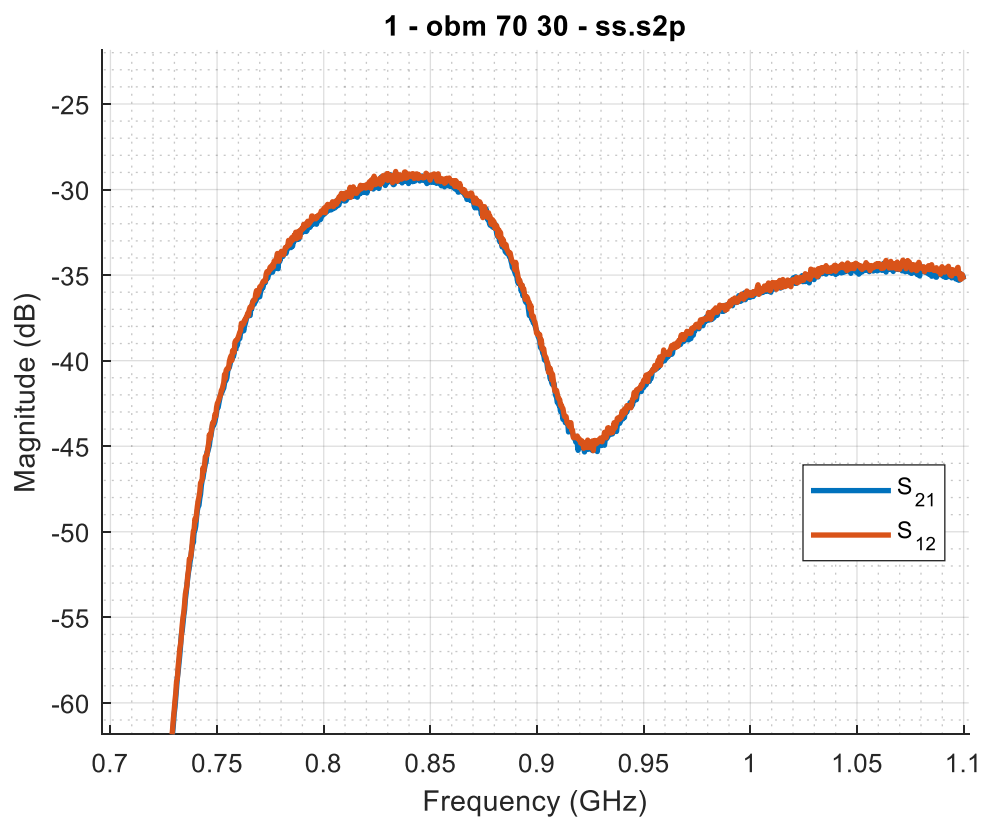


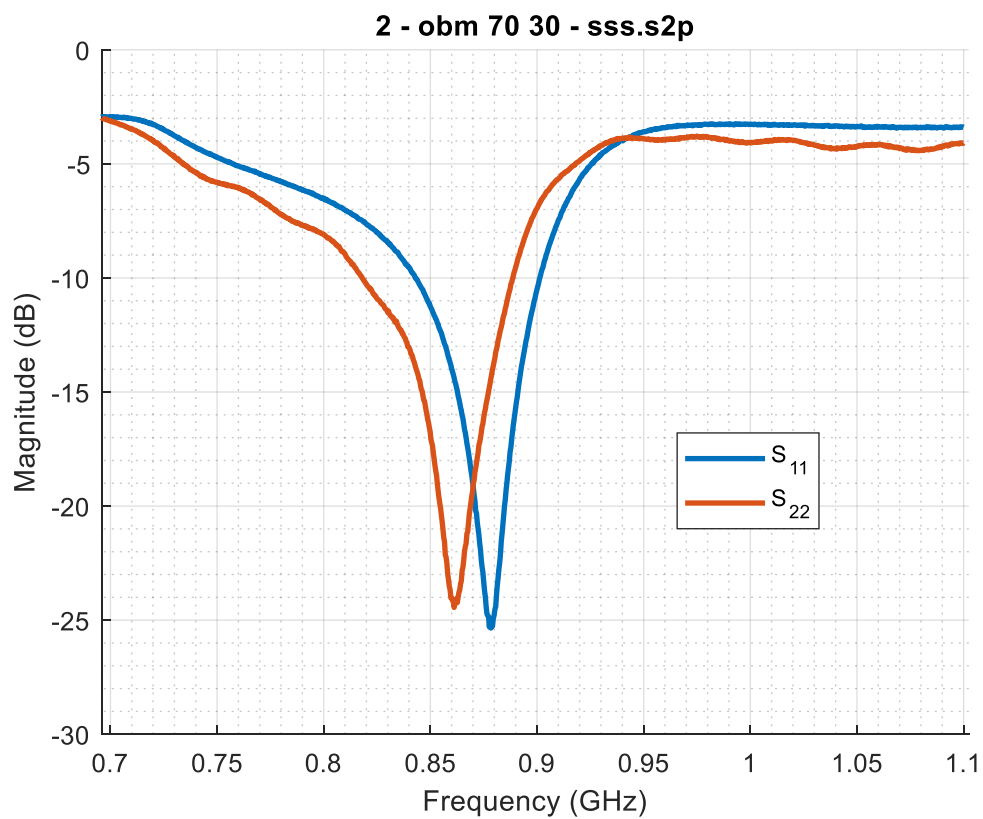
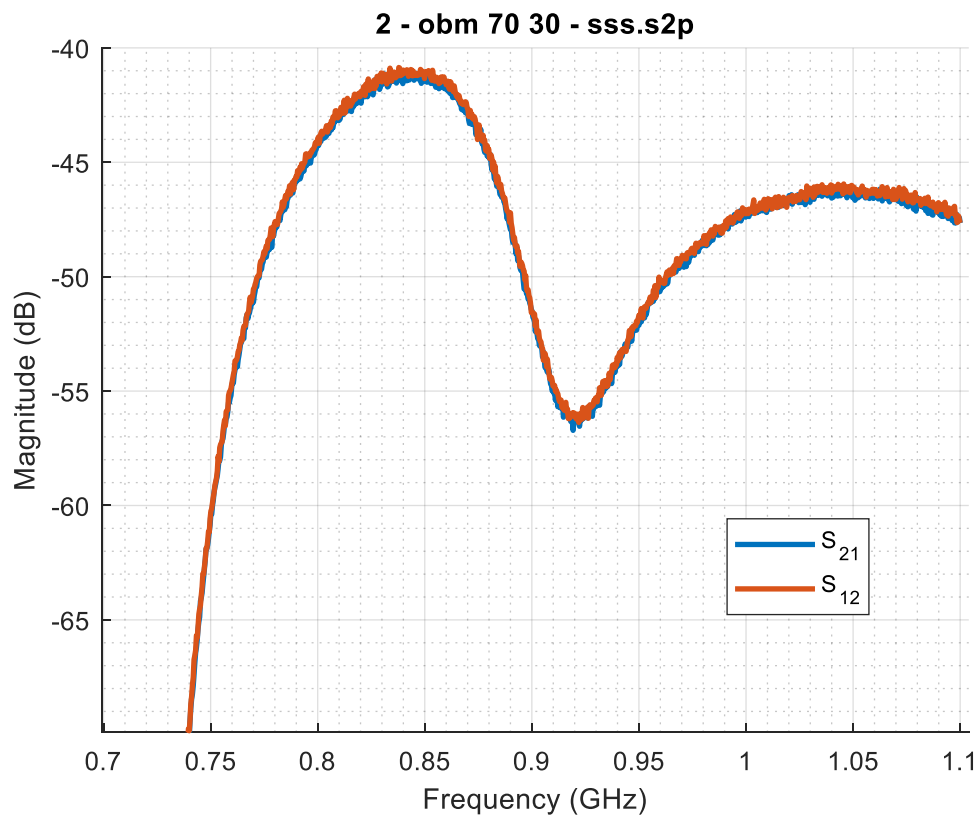




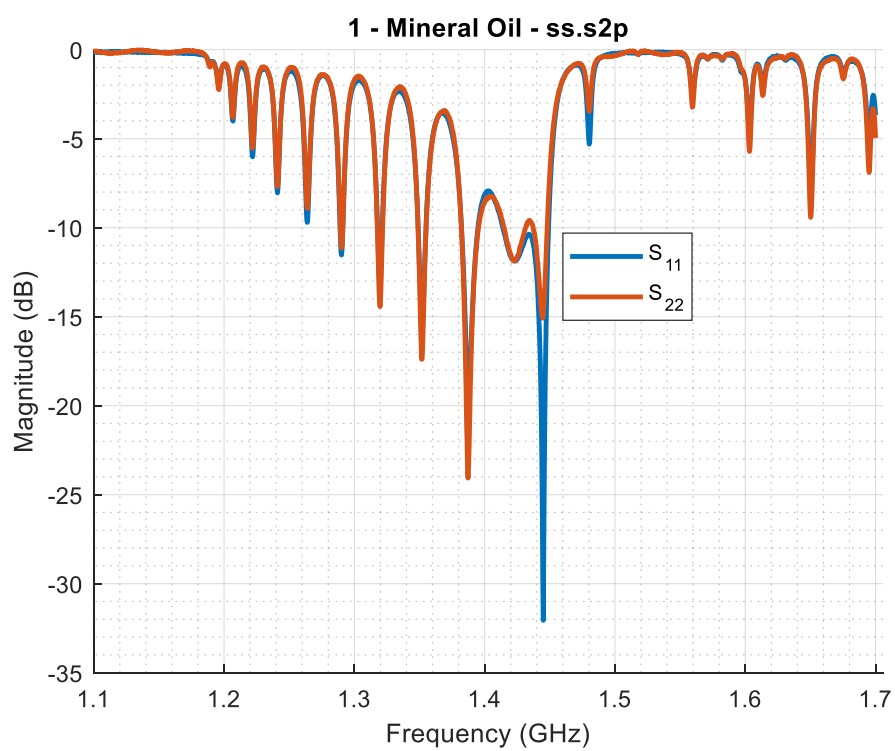
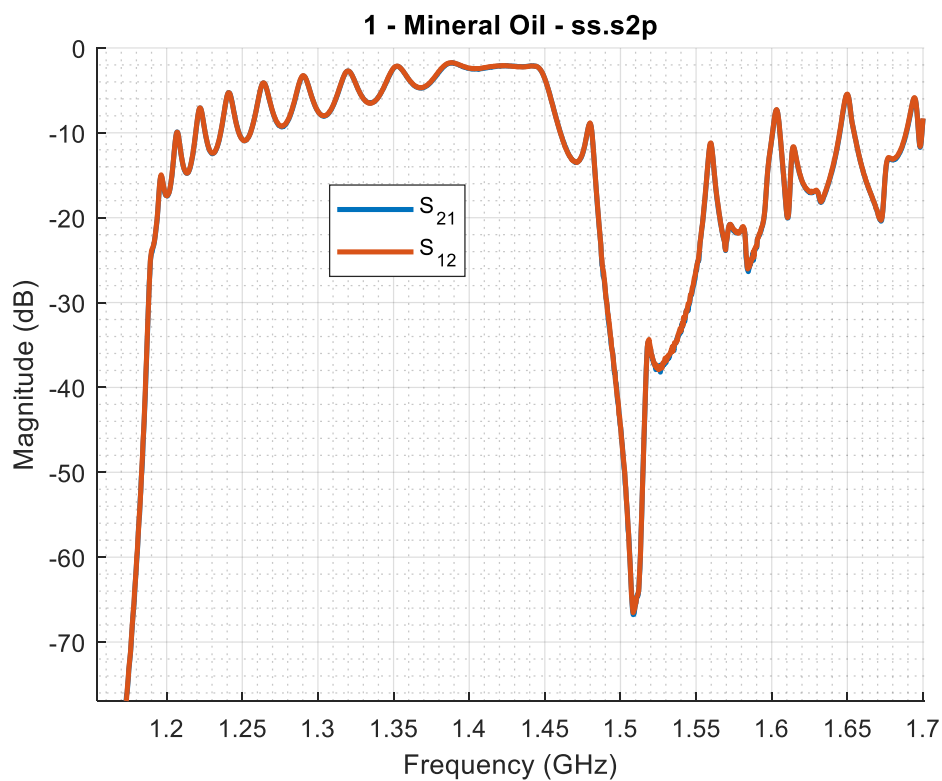


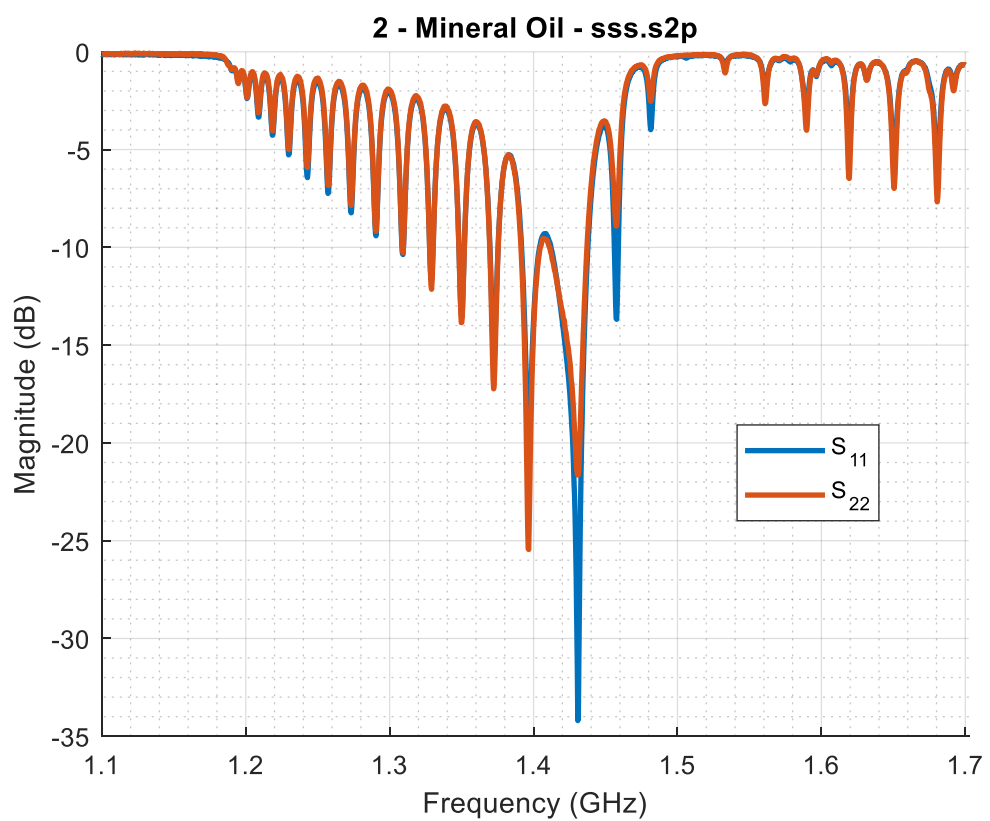
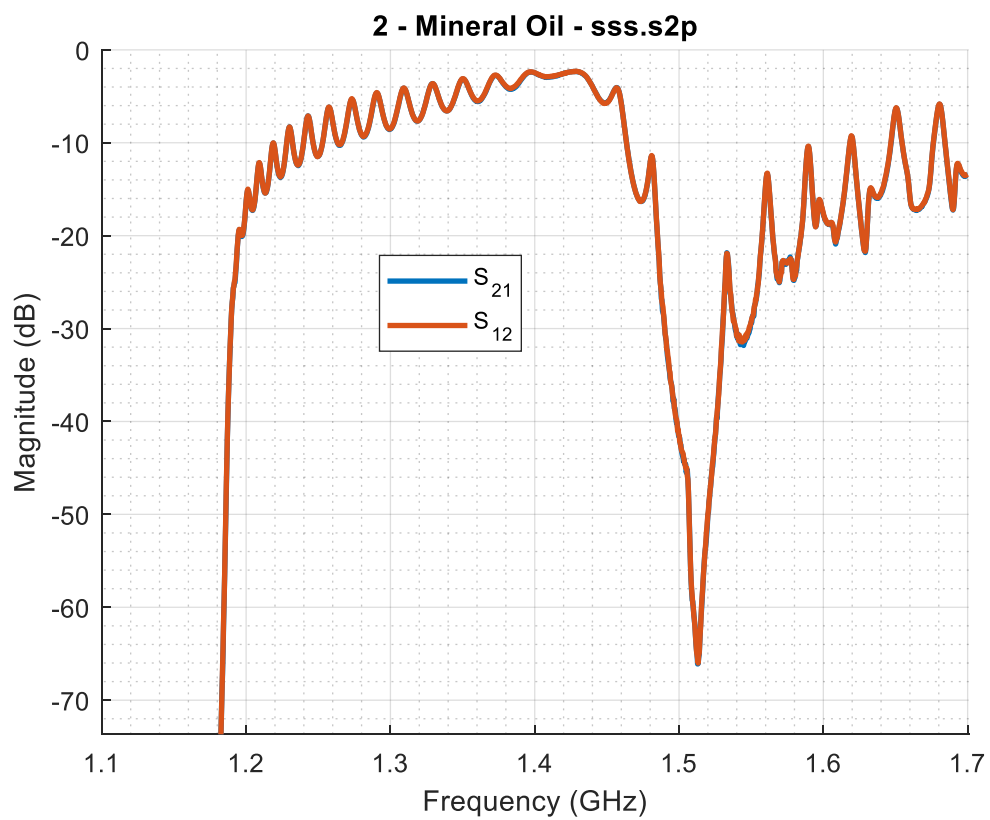


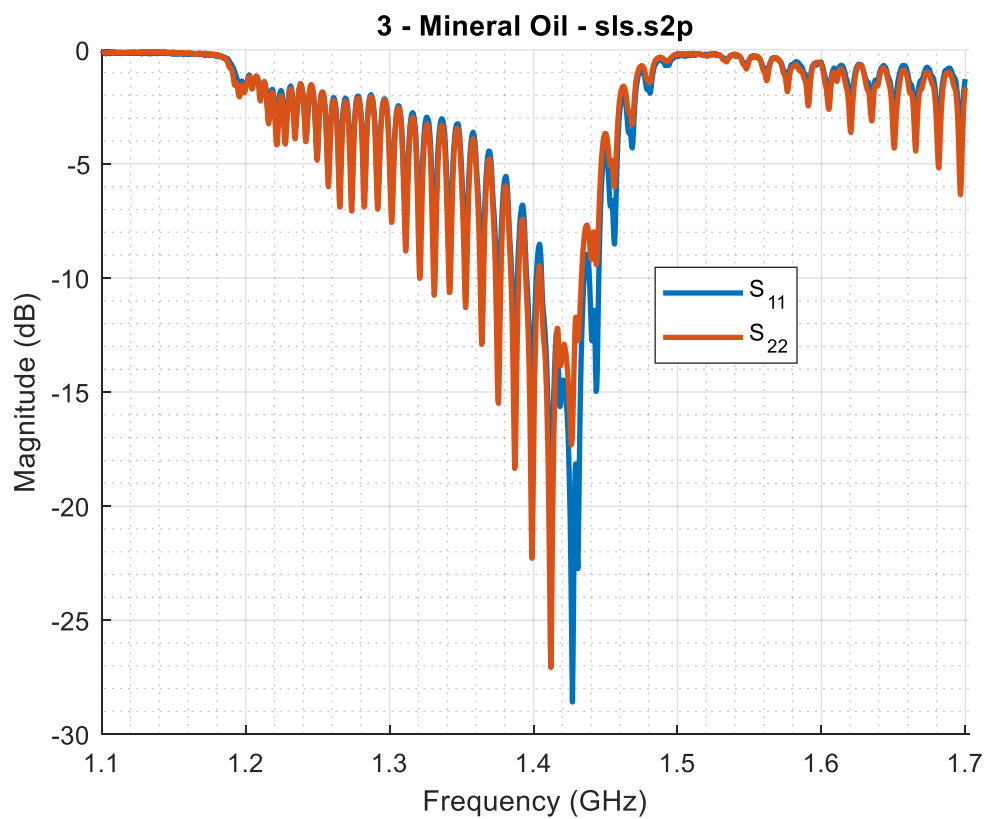
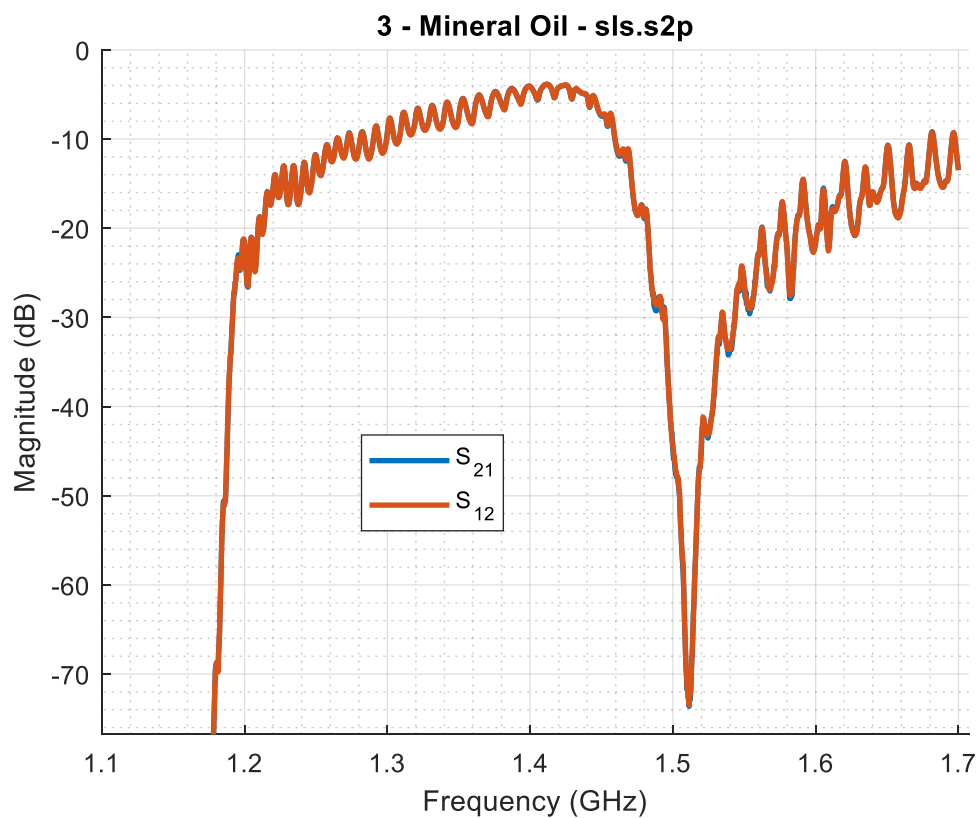




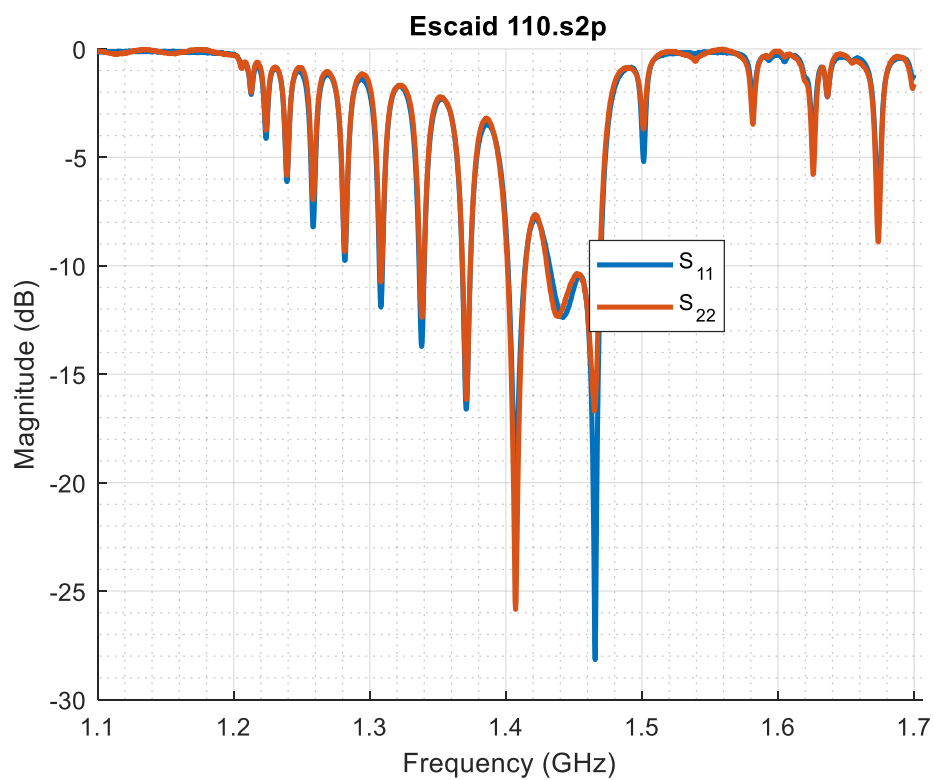
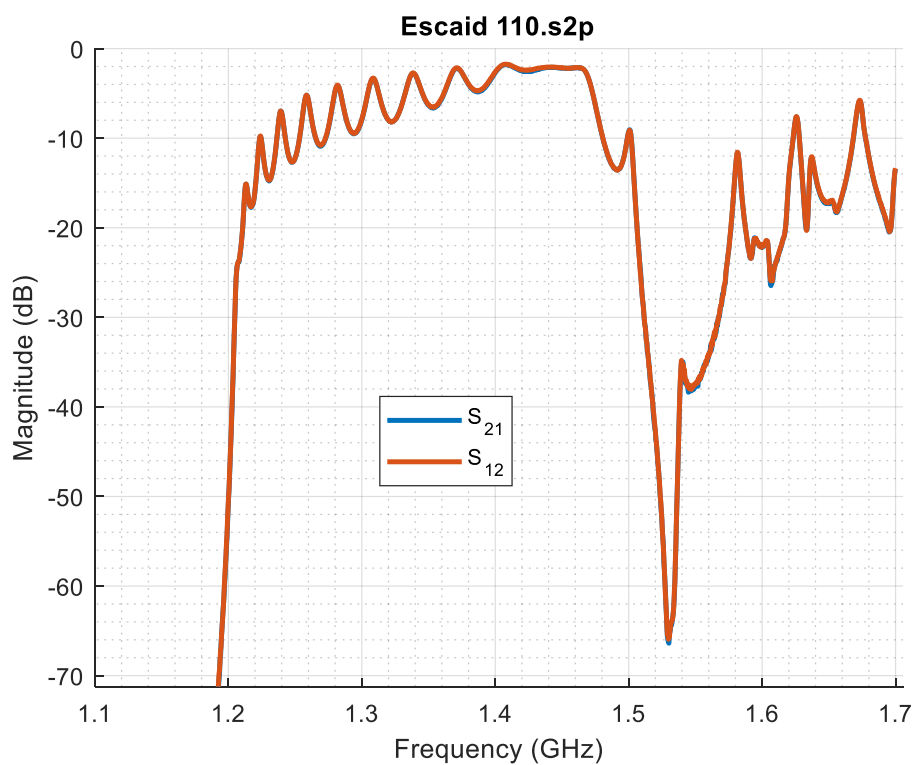
Appendix G: Mineral Oil S-Parameter Plots







Appendix H: Escaid™ 110 S-Parameter Plots



Appendix I: MATLAB Scripts

```

% attenuationCalcs.m
% 2019 - Patrick Cote
% Montana Tech - Masters Research
% Calculate the attenuation constants from measurements
format compact;
clear; close all; clc;
addpath('functions');

%% Params
% Electrical Properties
ur = 72.7; % permeability of pipe
sigma = 4.15e6; % conductivity [1e6]
% Pipe Geometry
r = 0.0512; % pipe radius [m]
short = 0.803; % short pipe length [m]
long = 3.210; % long pipe length [m]
probe_depth = 0.1; % Probe distance from end of pipe [m]
% Calculation Parameters
avg_length = 10; % Moving average tap length to smooth MAG
magNormFlag = 0; % Normalize MAG plot to Fc (dBDown)
dBdown = 50; % dB Down from Max MAG to use for Fc calc
fscale = 1.165; % Fc multiplier to get operating Frequency

LINK_BUDGET = 100; % Link Budget
% Plots
PLOTS = [1 1]; % [ Plot Mag Flag, Plot Regression Flag]

%% Prompt user for Files
[file,path] = uigetfile('s2p\*.s2p',...
    'Select Two or More Touchstone Files', ...t
    'MultiSelect', 'on');
if ~iscell(file)
    error('Must select more than one file');
end
Nfiles = size(file,2);

% Parse file name to get fluid type for plot titles
strSplT = split(file{1},'-');
fluidStr = strSplT{2};

% Build Pipe Sections based on number of files selected
% Assumes shortest to longest with the pattern: ss, sss, sls, slls, ...
pipeSections = [0 short long*(1:Nfiles-2)];

lengthVec = pipeSections + 2*short - probe_depth*2;

%% Calculate Dielectric Constant, Cutoff Frequency, and Operating Freq.
[er, fc] = calcEr(r,dBdown,file,path)
f = fc*fscale

%% Find Loss
b = 1/avg_length*ones(avg_length,1);
magVec = zeros(Nfiles,1);
for k = 1:Nfiles
    S = sparameters([path,file{k}]);
    sma_linear = filter(b,1,powergain(S, 'Gmag'));
    Gmag = 10*log10(sma_linear);
    n = find(S.Frequencies >= f,1);
    magVec(k) = Gmag(n);
end

```

```

end

%% Linear Least-Squares Fit
% Calculate Poly Fit
[p, S] = polyfit(lengthVec',magVec,1);
% Isolate Fit values
db_per_m = p(1)
db_per_probe = p(2)/2
% Calculate regression metric
rsquared = 1 - (S.normr/norm(magVec - mean(magVec)))^2

%% Repeater Distance
dmax = -LINK_BUDGET/db_per_m
dmax_joints = floor(dmax/9)
dmax_stands = floor(dmax/27)

%% Calculate Loss Tangent
losstan = calcLossTan(r,f/1e9,er,sigma,ur,-db_per_m)

%% Plots
if PLOTS(1)
    % Plot Normalized MAG
    s2pMagPlot(avg_length,magNormFlag,file,path);
    title(['MAG of ',fluidStr]);
end

if PLOTS(2)
    % Plot Regression
    % Distance Vector
    m = 0:.1:lengthVec(end)*1.5;
    % Total Loss
    loss = db_per_m*m + db_per_probe*2;

    figure;
    hold on
    plot(m,-loss,'Color',[0.9290, 0.6940, 0.1250],'Linewidth',1.25)
    plot(lengthVec,-magVec,'Color',[1 0
0], 'Marker','x', 'Linewidth',1, 'LineStyle','none')
    grid on;grid minor;
    title(['Losses in ',fluidStr]);
    legend( ...
        ['Curve fit: y=',num2str(-db_per_m),'x + ',num2str(-db_per_probe*2),' (R^2=
',num2str(rsquared),')'],...
        'Measured', ...
        'Location','best');
    xlabel('Pipe Length (m)');
    ylabel('Attenuation (dB)');
end

% %% Air UR
% W = circWaveguide(r,f,l,sigma,1,0);
% Xmn = 1.8412;
% er = 1;
% eta = 377/sqrt(er);
% fc = W.fc;
% Rs = (-db_per_m/8.686) * (r*eta*sqrt(1-(fc/f)^2)) / ((fc/f)^2 + (1/(Xmn^2 -1)));
% ur = Rs^2 * (2*sigma) / ((2*pi*f)*(pi*4e-7))

%% Calculate H2O Permittivity
% h2oPermittivity

%% Clean up

```

```

clear sma_linear S Gmag n k b dBdown file path loss m Nfiles fluidStr
clear long short probe_depth p r pipeSections magNormFlag

function [er,fc] = calcEr(r,dBdown,file,path)
%% calcEr.m
%
% Calculate the dielectric constant from measured data based on the cutoff
% frequency. Fc is determined by when the maximum available gain crosses
% the dB down threshold. Assumes TE11 propagation in circular waveguide.
% If multiple files are supplied the calculated er
% and fc are an average all files supplied.
%
% INPUT:
%   r           Circular Waveguide Radius [m]
%   dBdown      Decibels down
%   file        file name
%   path        file directory path
% OUTPUT:
%   er          Dielectric Constant
%
% 2019 - Patrick Cote
% Montana Tech - Graduate Research

%% Input Check and Set Defaults
% Default radius to 4.03" ID
if ~exist('r','var')
    r = 0.0512;
end
% default to -60 dB cutoff frequency threshold
if ~exist('dBdown','var')
    dBdown = 50;
end
% If no file(s) supplied, prompt the user.
if ~exist('file','var')
    % Select Files
    [file,path] = uigetfile('*.s2p',...
        'Select Touchstone Files', 'MultiSelect', 'on');
end

%% Count number of files
Nfiles = size(file,2);

%% Find Cutoff Frequency
if ~iscell(file) % If, Single File
    % Load S-Parameters
    S = sparameters([path,file]);
    % Calculate MAG in dB
    Gmag = 10*log10(powergain(S,'Gmag'));
    % Find the ndx of the first frequency where mag is above threshold
    Nf = find(Gmag>-dBdown,1);
    % Save the frequency
    fc = S.Frequencies(Nf);
else % Else, multiple files
    fcVec = zeros(Nfiles,1);
    % For each file
    for n = 1:Nfiles
        % Load S-Parameters
        S = sparameters([path,file{n}]);
        % Calculate MAG in dB
        Gmag = 10*log10(powergain(S,'Gmag'));
        % Find the ndx of the first frequency where mag is above threshold
    end
end

```

```

        Nf = find(Gmag>max(Gmag)-dBdown,1);
        % Save the frequency to a vector
        fcVec(n) = S.Frequencies(Nf)
    end
    % Average the frequency vector
    fc = mean(fcVec);
end

%% Calculate Er from cutoff frequency equation
% Bessel Solution for TE11 mode
Xmn = 1.8412;
% Free-space velocity (m/s)
c = 3e8;
% Solve fc function (Balanis) for er
er = (Xmn*c./(2*pi*r*fc)).^2;

end

function [lossTan] = calcLossTan(r,f,er,sigma,ur,alpha)
%circWaveguide Calculates Waveguide Characteristics for given specs
% Assumes TE11 Mode, Supports a vector of operating frequencies
% INPUT:
%   r      = Waveguide Radius           [m]
%   f      = Operating Frequency       [GHz]
%   er     = Relative Permittivity of Waveguide Fill
%   sigma  = Conductivity of Waveguide [S/m]
%   ur     = Relative Permeability of Waveguide Structure
%   alpha  = Attenuation constant (ac+ad) [dB/m]
% OUTPUT
%   lossTan = Loss Tangent of Waveguide Fill
%
% 2018 - Patrick Cote
% Masters Research
% 20181214 - v1.0
% 20190507 - v1.1

%% Variable Check
if ~exist('er','var')
    er = 1;
end
if ~exist('ur','var')
    ur = 1;
end
if ~exist('sigma','var')
    sigma = 1e7;
end

%% Propagation Mode Constant and frequency scaling
Xmn = 1.8412;
f = f*1e9;

%% Attenuation Constant
% Calculate theoretical attenuation due to conduction in dB/m
% Equations from Pozar and Balanis
eta = 377/sqrt(er);
k = 2*pi*f*sqrt(er)/(3e8);
kc = Xmn./r;
beta = sqrt(k.^2 - (Xmn./r).^2);
Rs = sqrt((2*pi*f)*(pi*4e-7)*ur/(2*sigma));

```

```

alpha_c = Rs./(r.*k.*eta.*beta) .* (kc.^2 + k.^2/(Xmn^2-1))*8.686
% Calculate dielectric atten. assuming exact theoretical conduction losses
alpha_d = alpha - alpha_c
% Calculate loss tangent
lossTan = alpha_d/8.686*(2*beta)/k.^2;

```

```
end
```

```

function [W] = circWaveguide(r,f,er,sigma,ur,lossTan,TM)
%circWaveguide Calculates Waveguide Characteristics for given specs
% Assumes TE11 Mode, Supports a vector of operating frequencies
% INPUT:
%   r      = Waveguide Radius          [m]
%   f      = Operating Frequency       [GHz]
%   er     = Relative Permittivity of Waveguide Fill
%   sigma  = Conductivity of Waveguide [S/m]
%   lossTan = Loss Tangent of Waveguide Fill
%   TM     = TM01 flag
% OUTPUT
%   W      = Containing Structure
%   W.fc   = Cutoff Frequency          [Hz]
%   W.lambda_g = Guided Wavelength    [m]
%   W.alpha_d = Dielectric Loss constant [dB/m]
%   W.alpha_c = Conduction Loss constant [dB/m]
%   W.alpha = Total Loss constant      [dB/m]
%   W.Z    = Wave impedance            [ohms]
%
% 2018 - Patrick Cote
% Masters Research
% 20181214 - v1.0

%% Variable Check
if ~exist('er','var')
    er = 1;
end
if ~exist('ur','var')
    ur = 1;
end
if ~exist('sigma','var')
    sigma = 1e7;
end
if ~exist('lossTan','var')
    lossTan = 0;
end
if ~exist('TM','var')
    TM = 0;
end
%% Propagation Mode Constants
if TM
    Xmn = 2.4049;
else
    Xmn = 1.8412;
%   Xmn = 3.8318;
    m = 1;
    n = 1;
end
f = f*1e9;

%% Cutoff Frequency Calculation

```

```

W.fc = Xmn*(3e8)./(2*pi*r*sqrt(er));

%% Guided Wavelengths Calculations
lcut = 3e8./W.fc;
lfree = 3e8./f;
W.lambda_g = lfree./(sqrt(1-(lfree./lcut).^2));

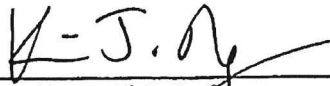
%% Attenuation Constant
eta = 377/sqrt(er);
k = 2*pi*f*sqrt(er)/(3e8);
kc = Xmn./r;
beta = sqrt(k.^2 - (Xmn./r).^2);
alpha_d = k.^2*lossTan./(2*beta)*8.686;
Rs = sqrt((2*pi*f)*(pi*4e-7)*ur/(2*sigma));
if TM
    alpha_c = Rs./(r.*eta.*sqrt(1-(W.fc./f).^2))*8.686;
else
    alpha_c = Rs./(r.*eta.*sqrt(1-(W.fc./f).^2)).* ((W.fc./f)^2 + m^2/(Xmn^2 -
m^2))*8.686;
end
W.alpha = (alpha_c + alpha_d);
W.alpha_c = alpha_c;
W.alpha_d = alpha_d;
%% Wave Impedance
W.Z = k.*eta./beta;

end

```

SIGNATURE PAGE

This is to certify that the thesis prepared by Patrick Cote entitled "Downhole RF Communication: Characterization and Modeling of Waveguide Propagation In Fluid-filled Drill Pipe" has been examined and approved for acceptance by the Department of Electrical Engineering, Montana Technological University, on this 24th day of July, 2019.



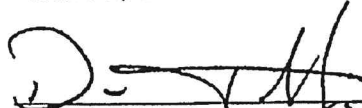
Kevin Negus, PhD, Professor
Department of Electrical Engineering
Chair, Examination Committee

Digitally signed by Lee Richards

DN: cn=Lee Richards, o=Montana Tech, ou=Petroleum Engineering,
email=lrichards@mtech.edu, c=US

Date: 2019.08.05 17:21:54 -06'00'

Lee Richards, PhD, Professor
Department of Petroleum Engineering
Member, Examination Committee



Dan Trudnowski, PhD, Dean
School of Mines and Engineering
Member, Examination Committee



Bryce Hill, PhD, Professor
Department of Electrical Engineering
Member, Examination Committee